

Understanding Bcl-2 family interactions through  
computational modelling

Benjamin James Lansdell

Submitted in total fulfilment of the requirements  
of the degree of Master of Philosophy

June 2012

Department of Mathematics and Statistics  
The University of Melbourne



# Abstract

The Bcl-2 family of 15 or more proteins are key regulators of the intrinsic apoptosis pathway. Elucidating the mechanisms of two of these proteins (Bak and Bax) used to control mitochondrial outer membrane permeabilisation and subsequent cytochrome *c* release is therefore the focus of significant research. The role played by the ‘direct’ and ‘indirect’ Bak activation mechanisms is yet to be fully elucidated. Insights can be gained, however, by studying a reduced experimental system in which only a subset of Bcl-2 family proteins are present. A mouse liver mitochondria (MLM) assay to monitor Bak-mediated permeabilisation provides such a system.

This thesis develops a deterministic mass-action model of the relevant Bcl-2 family protein interactions in order to better understand the reduced mitochondrial system *in vitro* and therefore the intrinsic apoptosis pathway *in vivo*. By focusing on a simplified experimental system, a relatively complete, realistic model is constructed which is also tractable in terms of the number of unknown parameters and experimental verifiability. Issues in constructing a relevant and realistic model are discussed.

The ‘direct’ and ‘indirect’ activation hypotheses are compared. The ‘direct’ activation mechanism is shown to be a required component of the model in matching with available experimental data. Previous studies have investigated the role bistability plays in apoptosis regulation. The models determined here do not exhibit any bistable phenomena while still being able to mimic the MLM experimental system and provide a mechanism for the regulation of cytochrome *c* release, calling into doubt the need for a Bcl-2 ‘bistable-switch’ mechanism. A related model of Bcl-2 interactions *in vivo* is investigated and demonstrated to be capable of bistability. In this case the direct activation model is found to act as a more *robust* bistable switch, compared with an indirect activation model, in line with previous studies.

Other properties of the models are investigated, such as their parametric robustness, which reveals the components of the models which are most sensitive to variation.

# Declaration

This is to certify that:

1. the thesis comprises only my original work towards the MPhil except where indicated in the preface,
2. due acknowledgement has been made in the text to all other material used,
3. the thesis is less than 50 000 words in length, exclusive of tables, maps, bibliographies and appendices.

Benjamin James Lansdell



# Preface

This thesis was written under the joint supervision of Professor Kerry Landman in the Department of Mathematics and Statistics at the University of Melbourne and Professor Terence Speed in the Bioinformatics Division at the Walter and Eliza Hall Institute for Medical Research (WEHI).

This project is a collaboration with Dr Ruth Kluck, at the WEHI, who performed the mouse liver mitochondria experiments.

The protein binding data was made available by Dr Douglas Fairlie and Dr Erinna Lee, WEHI.

Dr Martin O'Hely, at the WEHI, provided feedback on the modelling and proof-reading of this thesis. Dr Federico Frascoli, at the University of Melbourne, provided assistance with the numerical continuation methods and implementation.



# Acknowledgements

I would like to thank the following people:

Professor Kerry Landman and Professor Terry Speed for their supervision. I am very grateful for their support and guidance throughout this project and for encouraging me to push myself. I am also grateful for their understanding while I completed my candidature part-time.

Dr Martin O’Hely for his always insightful feedback throughout the entire project.

Dr Federico Frascoli for very generously spending a month teaching me how to study bifurcations with AUTO.

Dr Ruth Kluck for her role in instigating this project; for her patience in answering my many questions about proteins, mitochondria and experimental procedures; for spending her time showing me the complicated process by which a live mouse turns into data points on a computer; and for repeating difficult timing experiments to provide us with more data.

Dr Doug Fairlie and Dr Erinna Lee for generously allowing us to make use of their protein binding data of the Bcl-2 family interactions – the cumulative result of many years of work.

Stephanie Fennell for her work on the experiments on which this thesis is based and for showing me the details of laboratory work – observing biological research first-hand was a very valuable experience.

The Department of Mathematics and Statistics and the Walter and Eliza Hall faculty and staff for providing a supportive environment to conduct research.

I am grateful for having received an Australian Postgraduate Award to support me during my candidature.

Finally, for their continual love and support my parents and brother, Andrew, thanks for always being there.



# Contents

<b>Abstract</b>	<b>i</b>
<b>Declaration</b>	<b>iii</b>
<b>Preface</b>	<b>v</b>
<b>Acknowledgments</b>	<b>vii</b>
<b>1 Cells and cell-death</b>	<b>1</b>
1.1 Life inside a cell . . . . .	1
1.2 Apoptosis . . . . .	3
1.2.1 Bcl-2 family proteins . . . . .	5
1.2.2 Activation of Bak and Bax . . . . .	7
1.3 Understanding a simplified mitochondrial system of ‘apoptosis’ . . . . .	9
1.3.1 Experimental Methodology . . . . .	11
1.4 Thesis aims . . . . .	14
1.5 Thesis outline . . . . .	15
<b>2 Mathematical formulation</b>	<b>17</b>
2.1 Dynamical systems . . . . .	17
2.1.1 Long-term behaviour . . . . .	19
2.1.2 Hysteresis and bistability . . . . .	20
2.1.3 Conservative systems . . . . .	22
2.2 Biochemical modelling . . . . .	23
2.2.1 Kinetics . . . . .	24
2.2.2 Stoichiometry . . . . .	28

2.2.3	Sensitivity analysis . . . . .	30
2.3	Numerics . . . . .	32
2.3.1	Numerical Simulation . . . . .	32
2.3.2	Numerical Continuation . . . . .	34
2.4	Conclusion . . . . .	37
<b>3</b>	<b>Developing a model of Bcl-2 family interactions</b>	<b>39</b>
3.1	Previous work . . . . .	39
3.2	Biological considerations . . . . .	41
3.2.1	Bak activation . . . . .	41
3.2.2	Bak homo-dimerisation and auto-activation . . . . .	43
3.2.3	Bak multimerisation and pore formation . . . . .	43
3.2.4	Reversibility . . . . .	43
3.2.5	Model equations . . . . .	44
3.3	Physical considerations . . . . .	47
3.3.1	Previous work . . . . .	47
3.3.2	MLM geometry . . . . .	48
3.3.3	On diffusion-limited processes . . . . .	50
3.4	Conclusion . . . . .	54
<b>4</b>	<b>Model calibration</b>	<b>55</b>
4.1	An experiment to observe Bak:Mcl-1 disruption . . . . .	55
4.1.1	Quantifying experimental data . . . . .	57
4.1.2	BH3-only stimulus . . . . .	59
4.2	Parameter Estimation from Experiment . . . . .	60
4.2.1	Non-linear least squares estimation . . . . .	60
4.2.2	Optimisation . . . . .	62
4.2.3	Simulations . . . . .	63
4.3	Binding data . . . . .	64
4.4	Model selection . . . . .	65
4.4.1	Naive use of binding data . . . . .	65
4.4.2	Scaled use of binding data . . . . .	68
4.4.3	Relative use of binding data . . . . .	69

4.4.4	Molecular transport . . . . .	76
4.4.5	Discussion . . . . .	79
4.5	Conclusion . . . . .	82
<b>5</b>	<b>Exploring apoptosis <i>in silico</i></b>	<b>83</b>
5.1	On the role of auto-activation . . . . .	83
5.2	On the role of bistability . . . . .	84
5.2.1	Bifurcation analysis of a reduced fitted model . . . . .	86
5.2.2	Robustness of bistability . . . . .	88
5.2.3	Discussion . . . . .	90
5.3	Sensitivity analysis . . . . .	92
5.3.1	Local analysis . . . . .	92
5.3.2	Global analysis . . . . .	95
5.4	Modelling other experiments . . . . .	97
5.5	Conclusion . . . . .	99
<b>6</b>	<b>Conclusion</b>	<b>101</b>
6.1	Principal findings . . . . .	101
6.2	Significance . . . . .	102
6.3	Challenges . . . . .	103
6.4	Future work . . . . .	104
6.5	Concluding comments . . . . .	105
	<b>Bibliography</b>	<b>115</b>

# List of Figures

1.1	Diagram of a eukaryotic cell . . . . .	2
1.2	Views of apoptosis . . . . .	4
1.3	The intrinsic and extrinsic apoptotic pathways . . . . .	5
1.4	BH3 family of proteins . . . . .	6
1.5	Mechanisms of Bak activation . . . . .	10
1.6	Western blot of an experiment performed in the MLM system . . . . .	12
1.7	Schematic of SPR-based instrument . . . . .	13
2.1	Smallest bistable chemical reaction system . . . . .	21
3.1	Schematic of Bcl-2 family interactions . . . . .	47
3.2	Schematic of Bcl-2 family interactions on mitochondrial membrane . . . . .	50
4.1	MLM experiment demonstrating Bak:Mcl-1 formation . . . . .	56
4.2	Scaled densitometry data under assumptions in the MLM system . . . . .	58
4.3	Spike-in BH3-only protein function . . . . .	60
4.4	Simulation of direct activation model using available Biacore data (tBIM) . . . . .	66
4.5	Simulation of direct activation model using available Biacore data (tBid) . . . . .	67
4.6	Simulation of direct activation model using scaled Biacore data (tBIM) . . . . .	70
4.7	Simulation of direct activation model using scaled Biacore data (tBid) . . . . .	71
4.8	Simulation of direct activation model using ‘relative’ Biacore data (tBIM) . . . . .	72
4.9	Simulation of direct activation model using ‘relative’ Biacore data (tBid) . . . . .	73

4.10	Simulation of indirect activation model using ‘relative’ Biacore data (tBIM) . . . . .	74
4.11	Simulation of indirect activation model using ‘relative’ Biacore data (tBid) . . . . .	75
4.12	Effect of diffusion-limited mass-transport on direct activation model . . . . .	77
5.1	Alternative direct activation model, including endogenous Bcl-x <sub>L</sub> . . . . .	85
5.2	Bifurcation analysis of reduced kinetic model with fitted parameters . . . . .	88
5.3	Bifurcation analysis of reduced kinetic model with simplified parameters . . . . .	89
5.4	Two parameter continuation of simplified model . . . . .	90
5.5	Distribution of bifurcation points . . . . .	91
5.6	Local sensitivity analysis of hybrid model . . . . .	94
5.7	Global sensitivity analysis for hybrid model . . . . .	96
5.8	3 hour MLM incubation experiments . . . . .	97
5.9	Direct model prediction of alternative MLM experiment . . . . .	100
5.10	Indirect model prediction of alternative MLM experiment . . . . .	100



# Chapter 1

## Cells and cell-death

Before introducing the project and its aims, the relevant biology, experiments and methodology will be described. Important and unfamiliar words are *emphasised* with their first use. Footnotes are provided to elucidate concepts which may be unfamiliar to readers with little biological background.

### 1.1 Life inside a cell

Cells are the fundamental building blocks of all life. The human body consists of approximately 100 trillion cells of approximately 200 distinct cell types. A typical cell weighs 1 ng and has a radius of 10  $\mu\text{m}$ . Like larger organisms that are composed of many cells, an individual cell grows, reproduces (divides), absorbs nutrients, moves and dies. Cells of multicellular organisms contain various subcomponents known as organelles. These include the *nucleus*, housing a copy of the organism's genetic material within chromosomes, and *mitochondria*, which use oxygen to produce a source of chemical energy for the rest of the cell.<sup>1</sup> The solution in which organelles are situated is known as the *cytosol*.<sup>2</sup> The cytosol and organelles (except the nucleus) are collectively referred to as the *cytoplasm*. The cytoplasm is enclosed in the *cell membrane* (Figure 1.1).

---

<sup>1</sup>Mitochondria contain their own genome in a single, circular chromosome. They share many properties with bacteria and it is hypothesised mitochondria were once separate organisms which were taken in by the host cell – a key example of endosymbiosis.

<sup>2</sup>Cyte- (Greek): container, body, cell.

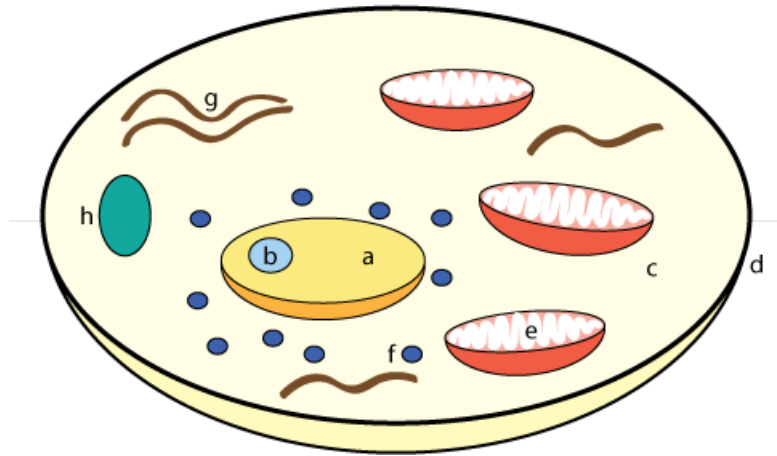


Figure 1.1: Diagram of a eukaryotic cell (a cell possessing organelles). The organism's DNA is housed in the nucleus (a) along with smaller structures known as nucleoli (b). Organelles are situated in a solution known as the cytosol (c) and are enclosed in the cell membrane (d). Other components include mitochondria (e), protein translating machines known as ribosomes (f), a cytoskeleton (g) and others (h).

Underlying this broad structure a cell is a hive of chemical activity – an astoundingly complex system of closely regulated biochemical reactions. The key macromolecules regulating, or catalysing, these reactions are *proteins*. A protein is a chain of amino acids linked by peptide bonds. Each of the 20 possible amino acids have different properties (*e.g.* size, hydrophobicity, charge) which determine a unique shape, or *conformation*, the protein can fold itself into. The structure of a protein determines what it can interact with and therefore its function. Smaller functional units of amino acids which may be common to more than one protein are known as *protein domains*.

The complement of proteins found within each cell is determined by instructions ‘written’ in the organism’s chromosomal DNA. In this context a *gene* is defined as a sequence of DNA nucleotides which correspond to a sequence of amino acids – a set of instructions for building a protein. Sometimes, the distinction between a gene and the protein it encodes is not made explicitly and needs to be inferred from the given context. The human genome consists of approximately 23,000 genes, which in turn encode an even larger number of proteins. A good introduction to these

preliminaries is found in Gonick and Wheelis [1].

The connection between a cell's response to both external and internal stimuli and the underlying biochemical reactions is understandably a very complex one. This thesis intends to help unravel the mechanism behind one cell response – that of apoptotic cell death. In this chapter we delve into what is known about apoptosis and how we intend to improve its understanding.

## 1.2 Apoptosis

Apoptosis<sup>3</sup> is a cellular process of ‘programmed’ cell death occurring in multicellular organisms [2]. A number of reasons may necessitate a cell committing itself to death. These include the removal of superfluous cells in the development of organs or digits, and the maintenance of homeostasis in which apoptosis provides a complementary but opposite function to cell division, or *mitosis*. A stressed or damaged cell may undergo apoptosis to prevent damaged cells developing into cancer or perhaps to prevent the spread of a virus. Examples of such stresses include infection, starvation and DNA damage from ionising radiation. Developing immune cells, known as lymphocytes, which are ineffective or potentially damaging to the organism are removed via apoptosis on a daily basis [3].

Morphological features of apoptosis include the condensation of the nucleus and cytoplasm, fragmentation of the nucleus and the separation of protuberances on the cell surface. These protuberances form membrane-bound cell remnants, known as apoptotic bodies, containing mostly intact cell components and organelles (Figure 1.2). Apoptotic bodies are phagocytised by neighbouring cells thereby recycling cell material.<sup>4</sup> This is in contrast to premature cell death, or necrosis, in which cells simply break open to release damaging contents into the surrounding tissue, and often resulting in inflammation. Necrosis occurs to the detriment of the organism while apoptosis occurs to the benefit – in general.

A number of diseases are associated with the malfunctioning of apoptotic pathways. These include autoimmune diseases such as lupus and rheumatoid arthritis [5] and cancer [6]. The tumour suppressor protein p53 is so-named because it is up-

---

<sup>3</sup>Apoptosis (Greek): the dropping off of petals from a flower or leaves from a tree.

<sup>4</sup>Phago- (Greek): akin to devour or eat.

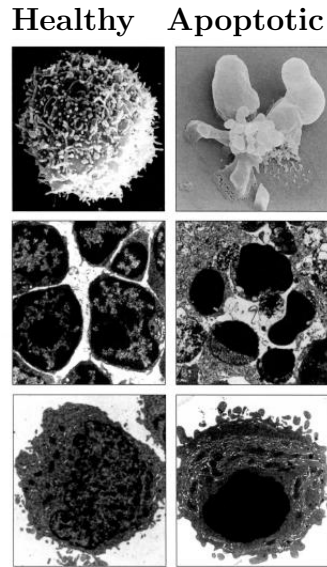


Figure 1.2: Changes resulting from apoptosis. Healthy cells are shown on left, apoptotic cells are shown on right. Upper right frame shows condensation of plasma membrane into ‘blebs’. Reproduced from Green [4].

regulated following DNA damage and induces apoptosis to prevent tumourigenesis [7]. Any disruption in the function of p53 can therefore result in tumour growth. Many viruses have the ability to inhibit apoptosis, for example by encoding viral homologues of Bcl-2 family pro-survival genes which are described below [8].

Two largely independent pathways operate to instigate apoptosis: the ‘intrinsic’ or ‘mitochondrial’ or stress-induced and the ‘extrinsic’ pathway. The intrinsic pathway is the more evolutionary conserved, ancient pathway. It is activated by a diverse range of intra-cellular stresses resulting in a complex series of interactions between proteins in the Bcl-2 family which act as an ‘on/off’ switch in deciding whether the cell commits to apoptosis. The intrinsic pathway initiates apoptosis through the release of the protein cytochrome c (and other proteins) from mitochondria and is hence also termed the ‘mitochondrial’ pathway. This process is known as mitochondrial outer membrane permeabilisation (MOMP). The extrinsic pathway is induced when death receptors on the cell surface bind to ligands from the Tumour Necrosis Factor (TNF) family of cytokines<sup>5</sup>. Both pathways result in the activation of pro-

---

<sup>5</sup>A cytokine is a signalling protein used for intercellular communication in the immune system – similar to a hormone but generally held at lower concentrations except in specific circumstances,

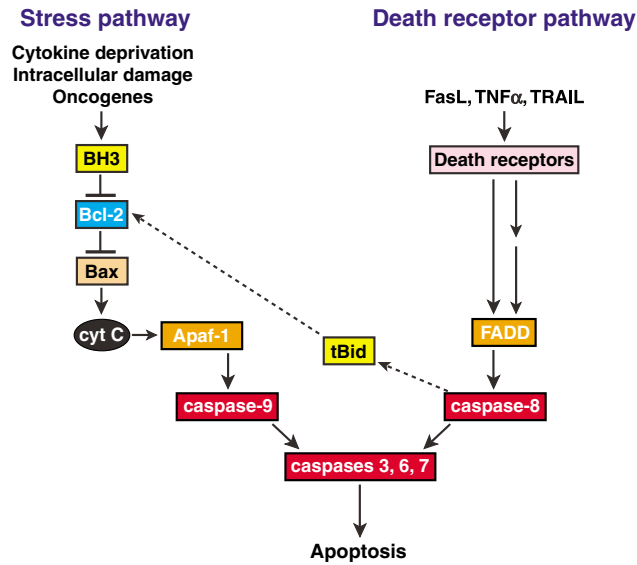


Figure 1.3: The ‘intrinsic’ and ‘extrinsic’ pathways operate largely independently of each other to induce apoptosis via the activation of caspases. The stress pathway is activated as a result of various intracellular stresses. The death receptor pathway is activated by extracellular TNF ligands binding to their receptors on the cell surface (adapted from [9]).

teases named caspases which cleave multiple proteins to mediate cell deconstruction (Figure 1.3 and [9]). A nice overview of apoptosis and cell death more generally can be found in Green [4].

### 1.2.1 Bcl-2 family proteins

The Bcl-2<sup>6</sup> gene which is activated by a chromosome translocation in human follicular lymphoma was first discovered in 1984 [10], and was identified as a regulator of apoptosis in 1988 [11]. Bcl-2 family proteins share one or more of four so-called Bcl-2 homology (BH) domains named BH1, BH2, BH3 and BH4. (Figure 1.4.) Depending on their function and BH domains Bcl-2 family genes can be categorised as either pro-survival, pro-apoptotic BH3-only or pro-apoptotic Bak and Bax (and possibly Bok but this will not be discussed).

*i.e.* infection.

<sup>6</sup>Bcl-2: short for B-cell lymphoma 2.

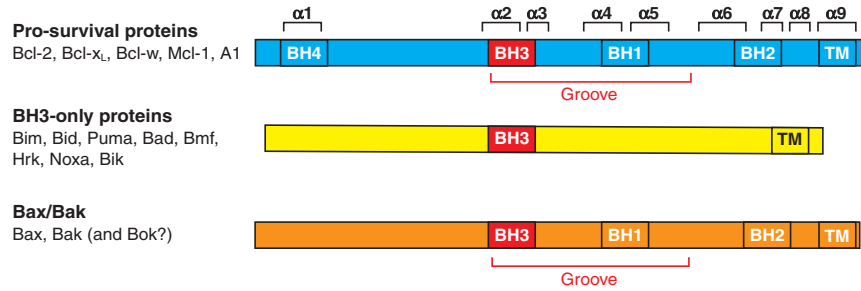


Figure 1.4: Bcl-2 family genes are divided into three categories. Members which form a hydrophobic groove are able to bind the BH3 domain of other Bcl-2 members. Some have a transmembrane (TM) domain attaching the protein to the mitochondrial outer membrane [12].

The BH3-only proteins are largely unrelated in peptide sequence to both themselves and to other Bcl-2 family members, with the exception of the BH3 domain, and act as damage sensors in the cell. The BH3 domain is an amphipathic<sup>7</sup> alpha helix<sup>8</sup> of approximately 24 amino acids.

The pro-survival proteins are so named because they protect the cell when exposed to cytotoxic stresses and do so by engaging with the pro-apoptotic proteins. The BH1, BH2 and BH3 domains in pro-survival proteins as well as in Bak and Bax fold into globular proteins containing a hydrophobic groove on its surface. A protein with an exposed BH3 domain is able to bind to this groove, allowing for interaction between Bcl-2 family members. Thus, the pro-survival proteins and Bak and Bax are very similar in sequence, particularly in the conserved BH domains, and also in their molecular structure.

Bak and Bax are mostly redundant in function with the removal of only one having little effect in many cell types. Removal of both genes however, results in a number of developmental abnormalities, as Bak<sup>-/-</sup> Bax<sup>-/-</sup> mice die around birth [13]. Bak is an integral membrane protein found on the cytosolic face of mitochondria (MT), whilst Bax is cytosolic and migrates to the mitochondria on receiving cytotoxic signals. For this reason Bak is more open to study and will be the focus of this thesis. To distinguish pro-apoptotic Bax and Bak from the

<sup>7</sup>Amphipathic: possessing both hydrophobic and hydrophilic domains.

<sup>8</sup>Alpha helix ( $\alpha$ -helix): a coiled secondary protein structure, like a spring.

pro-apoptotic BH3-only proteins both Bax and Bak will be described as *effector* molecules.

During apoptosis, Bak and Bax undergo a major conformation change – to the *activated* forms – that then oligomerise to form a pore in the outer membrane and release proteins from the intra-membrane space [14]. In particular, cytochrome c is released which subsequently binds to Apaf-1 and results in the construction of the ‘apoptosome’. The apoptosome activates cysteine proteases known as caspases which cleave hundreds of cellular proteins ensuring the destruction of the cell. Disruption of the mitochondrial outer membrane is considered the ‘point-of-no-return’.

Due to the Bcl-2 family’s intimate role in the regulation of apoptosis, a full understanding of its members is important in developing effective cancer therapies. Many tumours have defective apoptosis pathways due to defects in the upstream p53 pathway mentioned in Section 1.2, and many have excessive levels of Bcl-2 or related pro-survival proteins. Provided the remaining apoptotic machinery remains operational, however, proteins that mimic the action of BH3-only proteins should be able to induce apoptosis in such tumour cells. The selectivity with which BH3-only proteins bind to pro-survival proteins raises the possibility of creating anti-cancer drugs which target the specific Bcl-2 family members most responsible for specific tumour types, thereby reducing the effect of such drugs on normal cells. One promising ‘BH3 mimetic’ is ABT-737 which binds strongly to Bcl-2 family members Bcl-2, Bcl-x<sub>L</sub> and Bcl-w [15], analogues of which are in clinical trials.

### 1.2.2 Activation of Bak and Bax

How effector proteins are activated to induce MOMP is a controversial issue – reviews can be found in [16, 17]. Research has been complicated by the size of the Bcl-2 family and the differing affinities with which they bind to each other. However, it is known that early in apoptosis Bax removes its transmembrane (TM) domain from its hydrophobic surface groove, migrates from the cytosol to the mitochondrial membrane and inserts its TM domain into the OM. Bak, on the other hand, is already found attached to the OM and its surface groove is vacant.

Dewson *et al* [14] propose that a key step in the activation of Bak is the exposure of the BH3 domains. This allows each activated Bak molecule to form symmetric

homo-dimers – in which each molecule’s BH3 domain binds to another’s hydrophobic surface groove. Indeed, blocking exposure of the domain prevented MOMP, as did addition of an antibody against the Bak BH3 domain. As the hydrophobic surface groove in pro-survival proteins is known to be the binding site of BH3-only proteins, there is mounting evidence that all interactions between Bcl-2 family members occur via a similar BH3:groove interaction.

The nature and role of the interactions between effector molecules with both pro-survival and BH3-only proteins has yet to be fully elucidated. In particular two important hypotheses have been proposed:

- The **indirect** model posits that activated effector molecules are suppressed by continuously binding to pro-survival proteins, preventing homo-dimerisation (of Bak or Bax) which would otherwise occur ‘by default’. BH3-only proteins induce apoptosis by binding competitively to pro-survival proteins, displacing Bak or Bax. As interactions of varying affinities are observed between different BH3-only and pro-survival proteins, it is hypothesised that a combination of BH3-only proteins are required to neutralise all pro-survival proteins and encourage Bak/Bax homo-dimerisation. A key problem with the indirect hypothesis is the small amount of evidence that endogenous Bak and Bax are sequestered by pro-survival proteins prior to the onset of apoptosis.
- The **direct** model proposes that BH3-only proteins engage effector molecules directly to induce their activation, homo-oligomerisation, and pore formation. The role of pro-survival Bcl-2 members in the direct model is to sequester BH3-only proteins, ensuring a reasonable level of BH3-only molecules are required for apoptosis to occur. Bim and Bid have been shown to induce conformational changes in Bak and Bax and are thus termed *direct activators*. Other BH3-only proteins are termed *sensitisers* for their ability bind and occupy the pro-survival proteins and so to increase sensitivity to Bim and Bid. Direct interactions between BH3-only proteins and effector molecules has been difficult to observe so the direct model has remained somewhat controversial. More recently however evidence has supported the direct activation hypothesis [18, 19] (Figure 1.5). The focus of this study is on the relative importance of each model in apoptosis.

With recent evidence in mind, a **unified** model was the focus of the study by Llambi *et al* [20]. In a unified model two roles or *modes* for pro-survival proteins can be identified. When acting under **mode 1** the pro-survival proteins complex with BH3-only protein, inhibiting their direct activation of Bak or Bax. When acting under **mode 2** the pro-survival proteins complex with active Bak or Bax, preventing their homodimerisation. The importance of each mode in a given situation is yet to be determined.

It is important to note that the bulk of the work presented here was performed when the direct and indirect terminology was standard and a unified model had not been fully considered – different ‘modes’ of pro-survival action had not been introduced. Whether a particular Bcl-2 interaction is labelled as being direct or indirect or, mode 1 or mode 2, is semantic and is not as important as the interactions themselves. That said, given the changing terminology, exactly what is meant by direct and indirect model in this thesis and how it relates to recent unified models is made explicit in later chapters.

In addition to indirect and direct activation of effector molecules there is evidence that Bak and Bax can spontaneously activate under certain conditions, *e.g.* under heat [21]. Auto-activation, where activated Bak or Bax molecules engage with inactivated Bak or Bax, is also possible [22].

### 1.3 Understanding a simplified mitochondrial system of ‘apoptosis’

As mentioned above, two difficulties in elucidating the precise mechanisms by which the Bcl-2 family regulates apoptosis are the number of Bcl-2 family members and the differing affinities these members have for one another. Given these difficulties, it is helpful to study a reduced system in which only a few Bcl-2 family members are present, so as to limit the interactions between individual members. Experiments with isolated mouse liver mitochondria (MLM) provide such an assay. The MLM system is well suited since it contains significant endogenous levels of Bak, a low level of Bcl-x<sub>L</sub> and no detectable levels of any other Bcl-2 family members [23]. In this assay, MOMP is dependent on Bak, and can be regulated by addition of purified

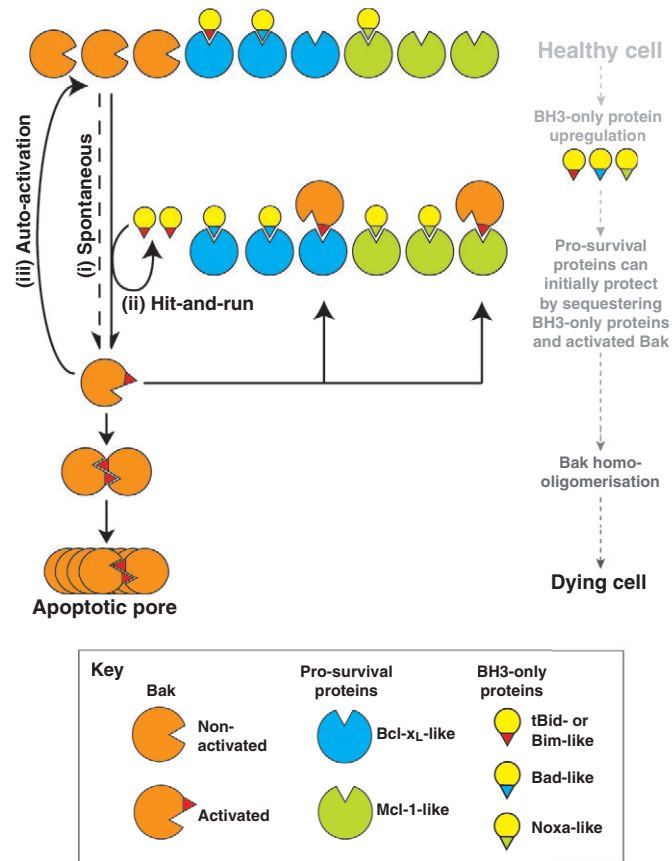


Figure 1.5: Mechanisms of Bak activation. A conformational change in Bak protein to expose the BH3 domain (red triangle) allows Bak homo-oligomerisation. Sufficient levels of activated Bak and subsequent Bak homo-oligomerisation form an apoptotic pore on the mitochondrial membrane. The role of BH3-only proteins are to either (indirect) disrupt the Bak:pro-survival complex or to (direct, ii) interact with Bak directly in a hit-and-run activation step. Spontaneous and auto-activation (i and iii) have also been observed [12].

recombinant<sup>9</sup> BH3-only proteins (*e.g.* tBid) and prosurvival proteins (*e.g.* Mcl-1).

The assay has been used extensively to investigate the role complexes between effector and pro-survival proteins (*e.g.* Bak bound to Mcl-1) play in apoptosis regulation. Which BH3-only proteins can create and/or disrupt these complexes and how?

### 1.3.1 Experimental Methodology

Experimental data used to develop the models comes from mouse liver mitochondria experiments and protein binding measurements (surface plasmon resonance instruments) which are described briefly here.

#### MLM experiments

Mouse liver mitochondria are extracted from hepatocytes (liver cells) and are added to a physiological buffer. Mitochondria are diluted to 1mg of total protein per millilitre of solution. In this dilute solution approximately 10nM of the pro-apoptotic Bak and approximately 3nM of the pro-survival Bcl-x<sub>L</sub> are estimated to be present. Other Bcl-2 members are added during experiments: one of the BH3-only proteins tBid or tBIM; and the pro-survival protein Mcl-1. Samples taken are subject to a *western blot* analysis which determines the presence or absence of proteins or protein complexes of interest. An example is presented in Figure 1.6. The details of the particular experiments modelled are described on pages 55 and 97.

Some recombinant proteins added to the MLM incubations are not ‘native’ proteins but are modified. In particular, tBIM is a chimera, in which the BH3 domain of the wild-type<sup>10</sup> tBid has been replaced by the Bim BH3 domain. In addition, Mcl-1 does not possess a transmembrane domain which would allow it to anchor in the mitochondrial membrane.

---

<sup>9</sup>A recombinant protein is one which has been artificially synthesised by introducing ‘recombinant’ DNA into a suitable host cell which translates the DNA to protein. Recombinant protein may be modified from their wild-type counterparts.

<sup>10</sup>the genotype(s) which occurs in nature with highest frequency

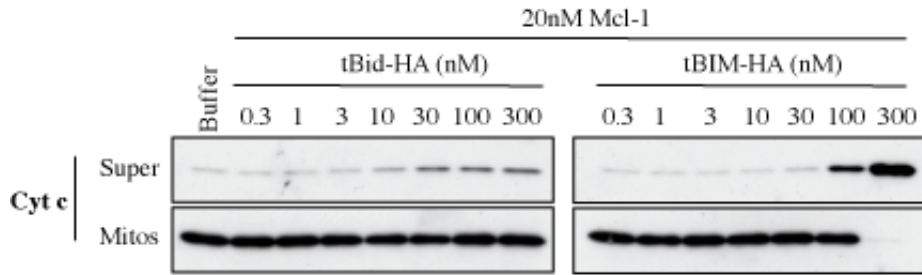


Figure 1.6: Western blot of an experiment performed in the MLM system. The top rows indicate the initial concentration (nM) of recombinant Bcl-2 family members spiked into the system (pro-survival Mcl-1 with the BH3-only protein tBid or tBIM) for each experiment. Following a two hour incubation, samples are analysed by western blot. The dark bands indicate the presence cytochrome c (Cyt c). Here cyt c mitos indicates the cytochrome c present within the mitochondrial membrane, cyt c super indicates the cytochrome c which has been released into solution following MOMP. Unpublished experiment by Dr. Ruth Kluck, WEHI.

### Protein binding between Bcl-2 family members

Protein association and dissociation rates can be determined using surface plasmon resonance (SPR) technology (Biacore AB corporation [www.biacore.com](http://www.biacore.com)). Biosensor technologies measure protein-protein interactions and protein binding affinities. Uses of such SPR technology include the evaluation of macromolecules, for example, ensuring recombinant proteins have similar structure to their native counterpart by testing their affinity for their natural ligands. More relevant here, SPR-based technology can measure equilibrium constants, as well as measuring kinetic on and off rates between two species (*e.g.* BH3 peptides and Mcl-1 protein).

An SPR-based instrument consists of a small flow cell (approximately 20-60 nL in volume) in which one molecule (*e.g.* Mcl-1) being studied is immobilised on a sensor surface. An analyte (*e.g.* Bim BH3) is introduced in solution (the sample buffer) which flows through the cell ( $1-100 \mu\text{L}\cdot\text{min}^{-1}$ ). The analyte binds the ligand attached to the sensor surface. The resulting increase in protein on the surface affects the refractive index. This optical effect is detected by the SPR instrument and can be used to quantify the extent of binding in real-time.<sup>11</sup> The resulting *sensorgram*

<sup>11</sup>Light incident on a noble metal (*i.e.* gold)-glass interface at a critical angle,  $\theta_{spr}$ , excites surface plasmons (mobile electrons on the metal surface) causing them to resonate. At  $\theta_{spr}$  the

measures resonance units (RU), where one RU corresponds roughly the binding of 1 pg protein/mm<sup>2</sup>. Following sufficient time for the analyte to have reached a steady-state at the surface, a running buffer is introduced containing no analyte. In this way the rate at which ligand and analyte dissociate is also observed (Figure 1.7).

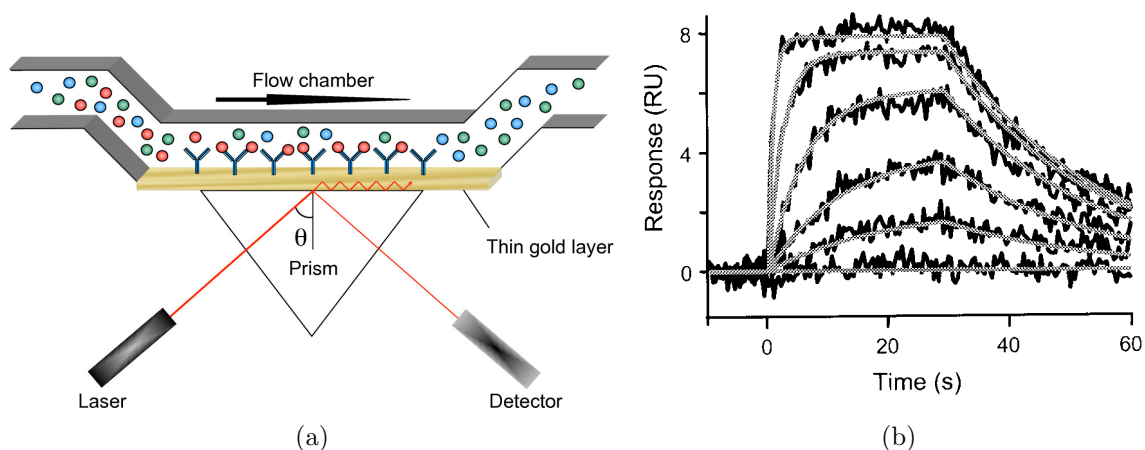


Figure 1.7: (a) Schematic diagram of SPR-based instrument. Changes in the refractive index of the the gold-glass interface are detected and used to infer total protein bound to surface (Image reproduced from [24]). (b) Example sensorgram showing both the association and dissociation of protein complex in response units. Black curves represent the average of four repeat injections for six different analyte concentrations. Grey curves represent a best fit of the data using a simple bimolecular reaction model ( $A + B = AB$ ) (Image reproduced from [25]).

---

reflected beam of light reduces in intensity since energy is transferred to the plasmons. Thus  $\theta_{spr}$  can be detected by a dip in reflected intensity. Since  $\theta_{spr}$  depends on the refractive index of the surface, which in turn depends on the amount of protein bound to the surface, measurements of this critical angle can be used to infer the amount of protein bound to the surface.

## 1.4 Thesis aims

Having outlined the necessary biology and the experimental methodology, the aims of this thesis can now be described.

---

### Key Aim

---

*In this thesis, mathematical modelling, in combination with Bcl-2 family binding data and MLM experimental data, will be used to investigate the feasibility of proposed mechanisms of apoptosis regulation via Bcl-2 family interactions, thereby providing a well-defined framework with which to understand and propose future experiments. By focusing on a simplified experimental system we are able to construct a relatively complete, realistic model which is also tractable in terms of the number of unknown parameters and experimental verifiability. This work is in collaboration with biologists at the Walter and Eliza Hall Institute of Medical Research, ensuring the modelling assumptions are biologically realistic.*

---

In particular they are to:

1. Develop a representative kinetic model of a subset of Bcl-2 family interactions in order to perform *in silico*<sup>12</sup> experiments in the MLM system. This will involve determining how kinetic binding measurements provided by the Biacore machine are best integrated with information obtained from MLM experiments.
2. Investigate proposed mechanisms of Bak activation. This involves comparing both the direct and indirect activation mechanisms. The most *explanatory* model in terms of understanding MLM experiments can be identified and thereby provide information about the relative importance of each mechanism in a given apoptotic setting.
3. Investigate the role of Bak auto-activation in MLM experiments. By comparing how well kinetic models both with and without a Bak auto-activation mechanism fit the above experiments, we can determine the importance of

---

<sup>12</sup>Almost Latin for ‘in silicon’, meaning to perform on computer. Compare with *in vivo* (‘in the living’) meaning an experiment performed within a living organism and *in vitro* (‘in the glass’) meaning an experiment performed within a controlled environment like a test-tube.

auto-activation in the simplified MLM assay. The role of *bistability* in an experimentally determined kinetic model, as well in models more generally, can also be investigated. The concept of robustness will be investigated both in terms of parameter variation and the model's capacity for bistability.

## 1.5 Thesis outline

With these aims in mind the remainder of this thesis proceeds as follows:

**Chapter 2** provides the necessary mathematical background and context of models for systems of biochemical reactions. The theory behind kinetic modelling is reviewed.

**Chapter 3** develops a kinetic model of Bcl-2 family members relevant for understanding experiments performed in the MLM assay.

**Chapter 4** investigates the use of Biacore data in simulating experiments. The physical transport of protein in the MLM experiments is studied. Kinetic parameters are estimated from experimental data. The role direct and indirect activation mechanisms play in understanding MLM experiments is compared.

**Chapter 5** investigates the mathematical properties of the kinetic model built, including the stability of steady states and the potential for bistability in the model. The sensitivity of the model to parameters is investigated and the role of auto-activation in the fitted models is studied. Parametric robustness is investigated. Both the fitted direct and indirect models are used to predict a disruption experiment in the MLM system.

**Chapter 6** draws conclusions about the present body of work and proposes directions in which the project can continue.



# Chapter 2

## Mathematical formulation

The purpose of this chapter is to provide the necessary mathematical background required to describe a system of biochemical reactions, such as a set of Bcl-2 family interactions, in a deterministic fashion. Simple examples are developed and the mathematics necessary to model a biochemical system of arbitrary size and topology is described.

### 2.1 Dynamical systems

A dynamical system is a system which changes, or evolves, with time. Many physical processes can be modelled as dynamical systems, including the motion of planets, the swinging of a pendulum and the competing populations of foxes and rabbits. This chapter will only consider *deterministic*<sup>1</sup> models, in which the evolution of the system is determined entirely by its present state and a set of rules. By specifying how a system changes with time we hope to gain an understanding of its long-term behaviour and the range of phenomena it can exhibit. For our purposes these rules

---

<sup>1</sup>In contrast to a *stochastic* model.

take the form of ordinary differential equations (ODEs). Let:

$$\begin{aligned}\frac{dx_1}{dt} &= f_1(x_1, x_2, \dots, x_n), \\ \frac{dx_2}{dt} &= f_2(x_1, x_2, \dots, x_n), \\ &\vdots \\ \frac{dx_n}{dt} &= f_n(x_1, x_2, \dots, x_n),\end{aligned}\tag{2.1.1}$$

be a system of ordinary differential equations describing the time evolution of  $\mathbf{x} = (x_1, x_2, \dots, x_n)$ . This is also written  $\frac{d\mathbf{x}}{dt} = \mathbf{f}(\mathbf{x})$  where  $\mathbf{x}(t) : \mathbb{R} \rightarrow \mathbb{R}^n$  and  $\mathbf{f}(\mathbf{x}) : \mathbb{R}^n \rightarrow \mathbb{R}^n$ .<sup>2</sup> In the present context each  $x_i$  may represent the concentration of a chemical within a cell. By also specifying the initial conditions,  $\mathbf{x}_0 = (x_1(0), x_2(0), \dots, x_n(0))$ , we are describing an *initial value problem* (IVP). Solutions to a specified initial value problem can be called trajectories. Provided  $\mathbf{f}(\mathbf{x})$  is Lipschitz continuous these solutions exist and are unique [26].

This formulation is more general than it may seem. For instance, time dependence in  $\mathbf{f}(\mathbf{x})$  is included by simply adding  $x_{n+1} = t$  and  $\frac{dx_{n+1}}{dt} = 1$  to the system. Higher order ordinary differential equations can also be written in the form (2.1.1). For instance, the equation of motion for the simple harmonic oscillator is:

$$\frac{d^2x}{dt^2} = -k^2x,$$

and can also be written as:

$$\begin{aligned}\frac{dx_1}{dt} &= x_2, \\ \frac{dx_2}{dt} &= -k^2x_1.\end{aligned}$$

A system is described as *linear* if each  $f_i(\mathbf{x})$  is a linear function of  $\mathbf{x}$ . Otherwise it is a *non-linear* system. A key feature of linear ODEs is that the sum of any set of solutions is itself a solution. This allows us to break the problem into pieces, solve the pieces separately and recombine each solution to obtain a final answer. Solutions

---

<sup>2</sup>Where  $\mathbb{R}$  denotes the set of real numbers.

of linear ODEs are therefore limited in form and hence in dynamic behaviour. Non-linear ODEs do not share this property and as a result allow for the possibility of more complex and interesting behaviour. A linear system is exactly equal to the sum of its parts. A non-linear system is in some way more than the sum of its parts.

### 2.1.1 Long-term behaviour

For the general system described in (2.1.1), a key question is what characterises the long-term behaviour? Does it reach equilibrium, diverge or oscillate indefinitely? By classifying the fixed points of the system we can begin to understand how it will behave. A fixed point, or steady state is any  $\mathbf{x}^*$  which satisfies  $\left[ \frac{d\mathbf{x}}{dt} \right]_{\mathbf{x}=\mathbf{x}^*} = \mathbf{f}(\mathbf{x}^*) = \mathbf{0}$ .

In order to determine the *stability* of a steady state,  $\mathbf{x}^*$ , we ask what happens when the system is perturbed by a small amount,  $\mathbf{x} = \mathbf{x}^* + \mathbf{u}$ . Does the perturbation grow or diminish with time? Expanding a Taylor series about the steady state we obtain:

$$\begin{aligned} \frac{d\mathbf{x}}{dt} &= \frac{d\mathbf{u}}{dt} = \mathbf{f}(\mathbf{x}^* + \mathbf{u}) \\ &= \mathbf{f}(\mathbf{x}^*) + \mathbf{Df}(\mathbf{x}^*)\mathbf{u} + \dots \\ &\approx \mathbf{Df}(\mathbf{x}^*)\mathbf{u}. \end{aligned} \tag{2.1.2}$$

The fact that  $\mathbf{f}(\mathbf{x}^*) = \mathbf{0}$  is used to obtain a linear approximation for the system. The term  $\mathbf{Df}(\mathbf{x}^*)$  is the Jacobian matrix of  $\mathbf{f}$  evaluated at  $\mathbf{x}^*$  and is given by:

$$\mathbf{Df}(\mathbf{x}^*) = \left[ \begin{array}{ccc} \frac{df_1}{dx_1} & \frac{df_1}{dx_2} & \dots & \frac{df_1}{dx_n} \\ \frac{df_2}{dx_1} & \frac{df_2}{dx_2} & \dots & \frac{df_2}{dx_n} \\ \vdots & & & \\ \frac{df_n}{dx_1} & \frac{df_n}{dx_2} & \dots & \frac{df_n}{dx_n} \end{array} \right]_{\mathbf{x}=\mathbf{x}^*}. \tag{2.1.3}$$

This approximation is valid provided the steady-state is suitably well-behaved. In the context of systems of interacting animal populations, the Jacobian matrix is known as the community matrix [27]. Henceforth we will simply write  $A = \mathbf{Df}(\mathbf{x}^*)$ . For a linear dynamical system  $\mathbf{f}(\mathbf{x}) = A\mathbf{x}$  for all  $\mathbf{x}$ . We propose the evolution of the

perturbation,  $\mathbf{u}$ , with time has the general solution:

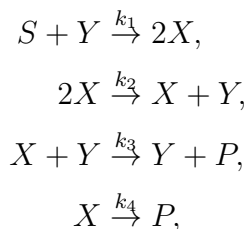
$$\mathbf{u} = \mathbf{v}_1 \exp(\lambda_1 t) + \mathbf{v}_2 \exp(\lambda_2 t) + \dots \quad (2.1.4)$$

where  $\lambda_1, \lambda_2, \dots, \lambda_n$  are distinct eigenvalues and respective eigenvectors  $\mathbf{v}_1, \mathbf{v}_2, \dots, \mathbf{v}_n$  of  $n \times n$  matrix  $A$ . The solution (2.1.4) can be verified by direct substitution into  $\frac{d\mathbf{u}}{dt} = A\mathbf{u}$ . For non-distinct eigenvalues, the solution also includes  $t^k \exp(\lambda t)$  terms which will not affect our conclusions. The distinct eigenvalue case is presented for clarity. The form of (2.1.4) makes it clear that  $|\mathbf{u}|$  will diminish if all eigenvalues have negative real part and will grow if at least one eigenvalue has positive real part. The former and latter cases correspond to *stable* and *unstable* steady states respectively. The borderline case in which all eigenvalues have non-positive real part requires more care. A more detailed classification of steady-states based on linearisation and inspection of eigenvalues can be achieved for 2-dimensional systems [27, p. 504]. For higher dimensional systems, however, no such theory exists.

The classification of steady-states is an important step in analysing the behaviour of a dynamical system: to do this one must identify the steady-states by solving  $\mathbf{f}(\mathbf{x}) = \mathbf{0}$  and compute the eigenvalues of the Jacobian matrix at each steady-state solution.

## 2.1.2 Hysteresis and bistability

Dynamical systems may have more than one stable steady-state and it is possible that the number of steady-states depends on the model parameters. To demonstrate how this can manifest itself we consider the chemical reaction model of [28]. A set of chemical reactions between species  $S, X, Y$  and  $P$  occur in a container of fixed volume:



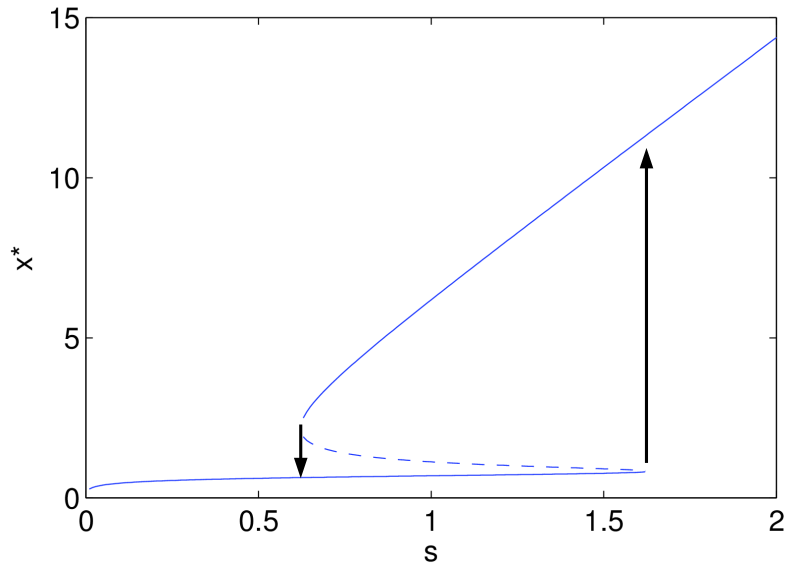


Figure 2.1: Steady-state concentration,  $x^*$ , of system (2.1.5) as a function of substrate concentration,  $s$ . Solid lines represent stable steady-states while dotted lines represent unstable steady-states. The up and down arrows represent *jumps* in concentration that occur when  $s$  is increased/decreased beyond a threshold value. Here  $k_1 = 8s$ ,  $k_2 = 1$ ,  $k_3 = 1$ ,  $k_4 = 1.5$  and  $k_5 = 0.6$ . Model and parameters taken from [28].

where  $S$  and  $P$  denote substrate and product respectively and their concentrations are kept constant. The ODEs governing the system are:

$$\begin{aligned} \frac{dx}{dt} &= 2k_1y - k_2x^2 - k_3xy - k_4x + k_5, \\ \frac{dy}{dt} &= k_2x^2 - k_1y, \end{aligned} \tag{2.1.5}$$

for concentrations  $x$  and  $y$  of species  $X$  and  $Y$  respectively. Note there is a production rate  $k_5$  for species  $X$  which is not listed in the above set of question. There exists at most three steady-states, depending on parameters, whose stability can be computed as described in Section 2.1.1 and which are illustrated in Figure 2.1 for a particular set of parameters  $\{k_i\}$ .

These parameters have been chosen so that the system has one stable steady state for extreme values of substrate concentration (here considered a parameter) while

for an intermediate range of values the system has *two* stable steady states. This phenomenon is called *bistability*. In the bistable range of parameters, the steady-state which the system approaches will depend on which state the system is ‘closest to’ initially. Here, the unstable steady-state acts as a *separatrix*, delineating regions which tend towards one stable state or the other. Therefore, when the substrate concentration is gently perturbed, such that the steady-states are gently changed, the new steady-state that the system approaches will depend on which steady-state it was ‘closest to’ previously. In this sense the system remembers where it was. This memory is known as *hysteresis*.

When the substrate concentration is perturbed beyond the bistable region the system will suddenly shift to the only steady-state remaining. This ‘switching’ behaviour which results in a sudden jump between an ‘on’ and an ‘off’ state after a sufficiently large perturbation in some model parameter has been investigated in a number of biological systems.

### 2.1.3 Conservative systems

Dynamical systems can conserve certain quantities which can affect the behaviour of the system.

**Definition 2.1.1.** A system,  $\frac{d\mathbf{x}}{dt} = \mathbf{f}(\mathbf{x})$ , is called *conservative* if there exists a *conservative* quantity,  $E(\mathbf{x})$ , such that on trajectories of  $\mathbf{x}$  we have  $\frac{dE}{dt} = 0$ .  $E(\mathbf{x})$  is required to be non-constant on every open set.

The requirement that  $E(\mathbf{x})$  be non-constant on every open set removes trivial conservative quantities which would render every system a ‘conservative’ system. The  $E$  here is chosen to correspond to ‘energy’ as total energy is often a conserved quantity in physical systems.

**Lemma 2.1.1.** *A conservative system has no stable steady-states.*

*Proof.* The following argument is from [29, p. 160]. Suppose such a fixed point,  $\mathbf{x}^*$ , did exist. Then there exists a ‘basin of attraction’: the set of points,  $B$ , such that  $\mathbf{x} \in B$  implies  $\mathbf{x} \rightarrow \mathbf{x}^*$  as  $t \rightarrow \infty$ . All points in  $B$  must have the same energy since they all end at the same point. This contradicts our definition of  $E(\mathbf{x})$  being non-constant on all open sets. We must conclude that  $\mathbf{x}^*$  is not *stable*.  $\square$

Within the framework modelling systems of biochemical reaction the existence of conservation relations implies the Jacobian matrix,  $A$ , is degenerate and has a zero eigenvalue. The steady-states of these systems therefore correspond to the borderline case mentioned in Section 2.1.1 in which the steady state is either non-isolated or requires analysing higher order terms of (2.1.2).

We have only touched on a few aspects in the study of dynamical systems which are relevant in our later analysis. The preceding sections are in no way meant to represent a comprehensive overview of the field of dynamical systems (refer to [29] for an introduction).

## 2.2 Biochemical modelling

This section details how to model a system of biochemical equations. The primary focus is on describing the concentration of a set of reacting species and the rate or velocity at which each reaction occurs. The notation and structure of this overview follows predominantly [30].

Let  $\mathbf{x}(\mathbf{r}, t) \in \mathbb{R}_{\geq 0}^n$  represent the vector of  $n$  species' concentrations in Molar at time  $t$  and position  $\mathbf{r} = (x, y, z)$  within the volume, where  $\mathbb{R}_{\geq 0}^n$  represents the non-negativity of each chemical concentration. It is convenient to assume that the volume being modelled is fixed and spatially homogeneous such that  $\mathbf{x}(\mathbf{r}, t) = \mathbf{x}(t)$ . 'Bulk' spatial inhomogeneities can be considered, maintaining this simplification, by compartmentalising the space. Species are transported between compartments, each of which is considered to be well-mixed. For compartments of different volume, this can only be adopted by either using units of moles or by dividing the reaction rates in each compartment by their volume.

The stoichiometry<sup>3</sup> of a reaction is the ratio at which reactants combine to form products. For elementary reactions, the stoichiometry corresponds to the molecularity of the reactants and products and is therefore always an integer. This is not necessarily the case for larger, 'composite' reactions. In the reaction:




---

<sup>3</sup>Stoichiometric (Greek): from *stoicheion*, meaning element, and *metric*, meaning measure.

the substances  $\text{H}_2$ ,  $\text{O}_2$  and  $\text{H}_2\text{O}$  have stoichiometric coefficients  $-2$ ,  $-1$  and  $2$ , respectively, since reactants are assigned negative coefficients and products positive. It is convenient to write down the vector stoichiometric coefficients of each species such that, for (2.2.1):

$$S = \begin{bmatrix} -2 \\ -1 \\ 2 \end{bmatrix}. \quad (2.2.2)$$

When considering a set of  $r$  reactions, the set of corresponding columns form the  $n \times r$  *stoichiometric matrix*,  $S$ . The element  $s_{ij}$  then represents the stoichiometric coefficient of species  $i$  in reaction  $j$ .

The reaction rate, in Molar per second, can be defined in terms of the reaction extent:

$$v(t) = \frac{1}{V} \frac{d\xi}{dt},$$

where  $\xi$  is defined as:

$$\xi(t) = \frac{1}{s_i} [N_i(t) - N_i(t_0)],$$

which represents the change in moles of species  $i$  between time  $t$  and a reference time  $t_0$ . The variable  $s_i$  is the stoichiometric coefficient of species  $i$  in the specified reaction and  $N_i(t)$  is the amount in mole of species  $i$  at time  $t$ . Let  $\mathbf{v}(t) \in \mathbb{R}^r$  represent the reaction rate vector. The rate of change of a substance,  $x_i$ , is given by:

$$\frac{dx_i}{dt} = \sum_{j=1}^r s_{ij} v_j,$$

so that the system dynamics are therefore represented compactly as:

$$\frac{d\mathbf{x}}{dt} = S\mathbf{v}.$$

### 2.2.1 Kinetics

The reaction rate vector,  $\mathbf{v}(\mathbf{x}, \mathbf{k})$ , is a function of the concentrations and a set of kinetic rate parameters  $\mathbf{k}$ . The study of the rates of chemical reactions is known as kinetics.

## Mass-action

The law of mass action states that the rate of a bimolecular reaction is linearly proportional to concentration of both species. Given this assumption we derive a simplified form ([31]). Consider the following irreversible reaction:



Over a short period  $\Delta t$ , let  $\Delta C$  represent the increase in concentration of C. We claim that  $\Delta C$  is proportional to the number of relevant molecular collisions that occur within  $\Delta t$  multiplied by the probability the reactants have sufficient kinetic energy to overcome the activation energy of the reaction. An approximation for the number of collisions which occur is  $r_1 AB \Delta t$  for some constant of proportionality  $r_1$  and  $A$  and  $B$  are the concentration of species A and B in Molar, respectively. Denote by  $r_2$  the probability a collision has enough energy to initiate a reaction, giving:

$$\Delta C = r_2 \cdot r_1 AB \Delta t,$$

and therefore:

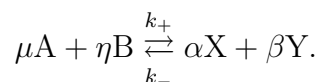
$$\frac{\Delta C}{\Delta t} = k AB,$$

where constant  $k$  is identified as the rate constant,  $r_1 r_2$ , and has units  $M^{-1} s^{-1}$ . As  $\Delta t \rightarrow 0$  we obtain the reaction rate:

$$\frac{dC}{dt} = k AB$$

which corresponds to the form expected from (2.2.4).

Slightly more generally, the law, as proposed in [32], considers the reaction between reactants A and B and products X and Y:



Constants  $k_+$  and  $k_-$  are the forward and reverse reaction rates. The law states that

the reaction proceeds in the forward direction<sup>4</sup> with rate  $v$ :

$$v = k_+ A^\mu B^\eta - k_- X^\alpha Y^\beta. \quad (2.2.4)$$

The system reaches dynamic equilibrium – the point at which the forward and reverse reaction occur at the same rate – when  $J_1 = 0$ . Substituting this into (2.2.4) we obtain:

$$K_D = \frac{k_d}{k_a} = \frac{A^\mu B^\eta}{X^\alpha Y^\beta}, \quad (2.2.5)$$

where  $K_D$  is known as the equilibrium constant.

For elementary reactions, mass-action kinetics are accurate. For larger, ‘composite’ reactions whose mechanism is unknown, mass action provides only an approximation. In this case the association of the exponents  $\mu$ ,  $\eta$ ,  $\alpha$  and  $\beta$  to the stoichiometric coefficients is an empirical one – some reactions do not observe this rule and the exponents must be measured experimentally.

### Generalised mass-action kinetics

For a system of  $r$  reactions, the mass-action kinetics for reaction  $j$  can be expressed as:

$$v_j(\mathbf{x}) = k_{j+} \prod_{i=1}^n x_i^{s_{ij}^-} - k_{j-} \prod_{i=1}^n x_i^{s_{ij}^+}, \quad (2.2.6)$$

where  $k_{j+}$  and  $k_{j-}$  are the forward and reverse rate constants. The exponents  $s_{ij}^-$  and  $s_{ij}^+$  are the *orders* for the forward and reverse reaction and, for mass-action, are the stoichiometric coefficient of the reactants and products respectively. Let:

$$s_{ij}^- = \begin{cases} -s_{ij}, & s_{ij} < 0; \\ 0, & s_{ij} \geq 0. \end{cases}, \quad s_{ij}^+ = \begin{cases} s_{ij}, & s_{ij} > 0; \\ 0, & s_{ij} \leq 0. \end{cases},$$

---

<sup>4</sup>The left to right reaction. Which reaction constitutes the forward reaction is merely a matter of convenience since all reactions technically are reversible to some extent.

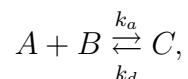
such that  $s_{ij} = s_{ij}^+ - s_{ij}^-$ . This is the general law of mass action kinetics [33]. Throughout this thesis the  $r \times 2$  matrix  $\mathbf{k}$  will denote the kinetic parameter matrix:

$$\mathbf{k} = \begin{bmatrix} k_{1a} & k_{1d} \\ k_{2a} & k_{2d} \\ \vdots & \vdots \\ k_{ra} & k_{rd} \end{bmatrix}.$$

Here,  $k_{ja}$  and  $k_{jd}$  are chosen instead of  $k_{j+}$  and  $k_{j-}$  to reflect the association and dissociation occurring between the Bcl-2 family members later being considered.

### Protein-protein interaction kinetics

The preceding sections have dealt with chemical and biochemical reactions in general. This thesis is concerned primarily with protein-protein complex association and dissociation. For proteins  $A$  and  $B$  forming complex  $C$ :



where parameters  $k_a$  and  $k_d$  are the association and dissociation rate, or the on and off rate, respectively. The theory of protein-protein interaction kinetics is less complete; for reviews refer to [34] and [35]. Most of the preceding arguments apply to protein-protein interaction kinetics. Though protein association is not an ‘elementary’ chemical reaction, the law of mass action still provides a useful description.<sup>5</sup> Also, protein-protein interactions can be affected by restriction to membranes (*e.g.* [36]). This thesis will use the generalised mass-action framework to model the system of protein association and dissociation between Bcl-2 family members.

### Limitations

Mass-action kinetics assume that certain environmental factors are fixed such that the rate parameters are indeed constants and that the system remains well mixed

---

<sup>5</sup>Indeed, just as for chemical reactions, *activation energies* or *enthalpies* can be measured for protein-protein associations. The heuristic derivation of the law of mass action presented in Section 2.2.1 can be therefore be applied.

such that concentrations can be considered spatially homogeneous. Diffusion can affect not just the validity of the well-mixed assumption but can also impact how ligands bind to receptors. Depending on the association and dissociation rates, low diffusivity allows for the rebinding of ligand to receptor before the ligand has the chance to escape into solution, which can affect the apparent kinetic rates [37].

It is also important to note that the use of differential equations has limits. By modelling kinetics with differential equations we assume that concentration is a continuous quantity when of course it is not. Molecules are not indefinitely divisible objects and at particularly low concentrations stochastic effects may become significant. Assuming the volume of a human cell is  $10^{-12}$ L then a concentration of 0.1nM corresponds to approximately 60 molecules per cell.<sup>6</sup> At such concentrations it is therefore reasonable that a continuous model may fail in some respects and that a stochastic model is more appropriate. This can be achieved using either a cellular automata approach (*e.g.* [38]) or a stochastic modelling approach (*e.g.* [39, 40]).

## 2.2.2 Stoichiometry

Independent of the reaction kinetics, the stoichiometric matrix provides information about the behaviour of a reaction network. Typically, the stoichiometric matrix is better characterised than the set of kinetic parameters. It is therefore worthwhile discussing what can be inferred about the dynamics from the stoichiometric matrix alone.

### Conservation relations

During the evolution of the system, it is possible the total concentration of a collection of substances will not change with time as a result of the reaction stoichiometry. Consequently, a linear combination of some of the species will remain constant. This provides a set of conservation relations,  $\mathbf{e}_i \in \mathbb{R}^n$ , each of which can be written as:

$$\mathbf{g}_i^T \mathbf{x} = T_i = \text{const.}$$

---

<sup>6</sup>Let  $V$  denote volume,  $c$  concentration in Molar,  $n$  number of moles,  $N$  number of particles and  $N_A$  as Avagadro's constant. If  $V = 10^{-12}$ L and  $c = 0.1$ nM then  $n = c \times V = 10^{-22}$ mol hence  $N = N_A \times n = 6.02 \times 10^{23} \times 10^{-22} \approx 60$ .

Since  $\mathbf{g}_i^T \mathbf{x}$  is a constant for all time it is true that:

$$\mathbf{g}_i^T S = \mathbf{0}^T. \quad (2.2.7)$$

The *conservation matrix*,  $G$ , is formed by a complete set of linearly independent row vectors satisfying (2.2.7) and therefore itself satisfies:

$$GS = \mathbf{0},$$

and:

$$G\mathbf{x} = \mathbf{T}. \quad (2.2.8)$$

The rows of  $G$  provide a basis for the nullspace of  $S^T$  and using the fundamental theorem of algebra:  $\text{rank}(G) = n - \text{rank}(S)$ . When solving the system of differential equations  $\text{rank}(G)$  concentrations can therefore be eliminated from the system.

Section 2.1.3 highlighted a problem in analysing the steady-states of conservative systems – they are always non-stable. This can be circumvented by considering the stability of a reduced biochemical reaction system. Rearrange the stoichiometric matrix,  $\mathbf{S}$ , so that the top  $\text{rank}(\mathbf{S})$  rows are linearly independent. The  $\mathbf{S}$  can be written as:

$$\mathbf{S} = \begin{bmatrix} \mathbf{S}^0 \\ \mathbf{S}' \end{bmatrix},$$

and since the rows of  $\mathbf{S}'$  are linearly dependent  $\mathbf{S}$  can be written:

$$\mathbf{S} = \mathbf{L}\mathbf{S}^0 = \begin{bmatrix} \mathbf{I} \\ \mathbf{L}' \end{bmatrix} \mathbf{S}^0,$$

for *link* matrix  $\mathbf{L}$ . The dynamical system becomes:

$$\frac{d}{dt} \begin{bmatrix} \mathbf{x}_a \\ \mathbf{x}_b \end{bmatrix} = \begin{bmatrix} \mathbf{I} \\ \mathbf{L}' \end{bmatrix} \mathbf{S}^0 \mathbf{v}.$$

The evolution of  $\mathbf{x}_b$  is:

$$\frac{d\mathbf{x}_b}{dt} = \mathbf{L}' \frac{d\mathbf{x}_a}{dt},$$

and therefore the trajectory  $\mathbf{x}_b$  is:

$$\mathbf{x}_b = \mathbf{L}'\mathbf{x}_a + \mathbf{c}.$$

The dynamics is therefore completely determined by the  $\mathbf{x}_a$ . Since  $\mathbf{S}^0$  is full-rank with no conservation relations, Lemma 2.1.1 no longer necessarily applies and the stability of any steady-states can be determined by analysing the reduced system:

$$\frac{d\mathbf{x}_a}{dt} = \mathbf{S}^0\mathbf{v}. \quad (2.2.9)$$

### 2.2.3 Sensitivity analysis

Determining which parameters are most sensitive to changes can provide some insight into the ‘robustness’ of the model to parameter variation. This section derives metrics that will later be used to quantify this general idea of ‘robustness’. For a given parameter set  $\mathbf{k}$  and a given time  $t$  during a simulation, we compute the relative change in concentration  $x_i(t)$  per relative change in reaction rate  $v_j$  as a result of a perturbation in parameter  $k_j$ :

$$c_{ij}(t) = \frac{v_j}{x_i(t)} \frac{\partial x_i / \partial k_j}{\partial v_j / \partial k_j}.$$

In metabolic control analysis (MCA) [30] the  $c_{ij}$  are termed concentration control coefficients and are typically computed at the steady-state concentrations and fluxes. The necessary extensions of MCA to non-steady states is considered in detail in [41]. Here  $v_j$  denotes the reaction for which  $k_j$  is a part. Adapting the sensitivity analysis from [42], we compute the 1-norm of each function  $c_{ij}$  over a simulation of  $T$  seconds:

$$C_{ij} = \|c_{ij}\|_1 = \int_0^T |c_{ij}(t)| dt. \quad (2.2.10)$$

Each  $C_{ij}$  gives some measure of how sensitive the evolution of species  $x_i$  is to changes in parameter  $k_j$  *near* a given set of parameters  $\mathbf{k}$ . This is therefore a *local* sensitivity analysis.

This measure is extended to quantify the overall robustness of each species  $x_i$

and the robustness of the system for a specific set of kinetic parameters ([43]). Let:

$$\bar{\mathbf{x}}(t) = \begin{pmatrix} \Delta x_1(t)/x_1(t) \\ \vdots \\ \Delta x_n(t)/x_n(t) \end{pmatrix}, \quad \mathbf{C}(t) = \begin{pmatrix} c_{11}(t) & \dots & c_{1r}(t) \\ \vdots & \ddots & \vdots \\ c_{1n}(t) & \dots & c_{nr}(t) \end{pmatrix}, \quad \bar{\mathbf{v}}(t) = \begin{pmatrix} \Delta v_1(t)/v_1(t) \\ \vdots \\ \Delta v_n(t)/v_n(t) \end{pmatrix},$$

and therefore  $\bar{\mathbf{x}} = \mathbf{C}\bar{\mathbf{v}}$ . For clarity,  $\bar{\mathbf{x}}(t)$ ,  $c_{ij}(t)$ ,  $\mathbf{C}(t)$  and  $\bar{\mathbf{v}}$  will be abbreviated to  $\bar{\mathbf{x}}$ ,  $c_{ij}$ ,  $\mathbf{C}$  and  $\bar{\mathbf{v}}$ , respectively. Assuming that the perturbations in kinetic parameters are independently distributed with zero mean, the expected values  $\langle \Delta x_i/x_i \rangle$  and  $\langle \Delta v_j/v_j \rangle$  are both zero. The variances and covariances of  $\bar{\mathbf{x}}$  are:

$$\langle \bar{\mathbf{x}}\bar{\mathbf{x}}^T \rangle = \langle (\mathbf{C}\bar{\mathbf{v}})(\mathbf{C}\bar{\mathbf{v}})^T \rangle = \langle \mathbf{C}(\bar{\mathbf{v}}\bar{\mathbf{v}}^T)\mathbf{C}^T \rangle.$$

The reaction rates fluctuate independently so non-diagonal elements of  $\bar{\mathbf{v}}\bar{\mathbf{v}}^T$  do not contribute to  $\langle \bar{\mathbf{x}}\bar{\mathbf{x}}^T \rangle$ . Assume a common parameter variance  $v^2 = \langle v_j^2 \rangle$  for all  $j$ . Therefore:

$$\begin{aligned} \frac{\langle \bar{\mathbf{x}}\bar{\mathbf{x}}^T \rangle}{v^2} &= \mathbf{C}\mathbf{C}^T \\ &= \begin{pmatrix} (c_{1,1})^2 + \dots + (c_{1,r})^2 & \dots & c_{1,1}c_{n,1} + \dots + c_{1,r}c_{n,r} \\ \vdots & \ddots & \vdots \\ c_{1,1}c_{n,1} + \dots + c_{1,r}c_{n,r} & \dots & (c_{n,1})^2 + \dots + (c_{n,r})^2 \end{pmatrix} \end{aligned}$$

The diagonal elements of  $\mathbf{C}\mathbf{C}^T$  can be interpreted as the normalised variance of species  $x_i$  caused by perturbations in the reaction rates. From this we can quantify the average effect a perturbation in kinetic parameter has on a species as:

$$\sigma_i^2(t) = \frac{1}{r} \sum_{j=1}^r [c_{i,j}(t)]^2$$

The overall variance can be defined as the sum of the individual variances:

$$\sigma^2(t) = \frac{1}{nr} \text{Tr}(\mathbf{C}\mathbf{C}^T)$$

As in (2.2.10) this is summarised over a simulation of  $T$  seconds by computing:

$$\sigma_i^2 = \int_0^T |\sigma_i^2(t)| dt, \quad (2.2.11)$$

and:

$$\sigma^2 = \int_0^T |\sigma^2(t)| dt. \quad (2.2.12)$$

The metrics (2.2.11) and (2.2.12), in addition to (2.2.10), will be used to quantify the robustness of the reaction systems for a given set of kinetic parameters.

## 2.3 Numerics

The majority of mathematical models are too difficult or are impossible to solve ‘exactly’ (solutions having a closed form in terms of known functions), and must be studied either through asymptotic approximations or numerical approximations. This thesis uses the latter, which are discussed here.

### 2.3.1 Numerical Simulation

The bulk of the analysis of Chapter 4 is based on the simulation of dynamical systems in the form of chemical reaction systems described above. Here we outline the basics of the numerical methods used in this thesis. The interested reader is directed to LeVeque [44] for a more comprehensive introduction.

We are interested in solutions to the initial value problem (IVP) of the form:

$$y' = f(y, t), \quad y(t_0) = y_0,$$

where  $' = d/dt$  and  $y$  can be a vector or scalar. Recall that the IVP will have a unique solution if the function  $f(y, t)$  is Lipschitz continuous in  $y$  over our domain of interest. If the solution at time  $t > t_0$  cannot be determined exactly then we can imagine approximating it with the following scheme:

$$y_{n+1} = y_n + hf(y_n, t_n),$$

for some sufficiently small step-size  $h > 0$  such that  $t_n = t_0 + nh$ . The notation  $y_n$  represents our approximation of  $y(t_n)$ . This is known as the *Forward Euler* method. We have replaced the derivative  $y'$  by a *finite difference* approximation which can be iterated over efficiently by computer. This is an *explicit* method since the unknown term  $y_{n+1}$  appears only on the left hand side. The error introduced by making this finite approximation is known as the *local truncation error* (LTE) and in this case is defined as:

$$\tau^n = \frac{y(t_{n+1}) - y(t_n)}{h} - f(y(t_n), t_n),$$

which, using the definition of our scheme, is  $O(h)$  (first order accurate). A method is called *consistent* if the LTE goes to zero as  $h \rightarrow 0$ . Of course, we also want to know that the *global* error goes to zero in this same limit. Loosely, a method is said to be *convergent* if the error  $y_N - y(T), T = t_0 + Nh$  at some generic, later time  $T > t_0$  goes to zero as  $h \rightarrow 0$ . We might expect this to be so when a method is both consistent and when the errors introduced over successive time steps do not get amplified – when the method is suitably *stable*. A number of different definitions of stability lend themselves to different purposes. It is the case that an IVP method is convergent if it is both consistent and *zero-stable*.<sup>7</sup>

The Forward Euler method has a number of drawbacks so is rarely used in practice. Firstly, it is only first order accurate. And secondly, it is unstable for a wide range of test problems of the form  $y' = \lambda y$  for some complex parameter  $\lambda$ . For a fixed  $\lambda$  a method which is stable to the corresponding test problem is known as *absolutely stable*. Forward Euler's *region of absolute stability* can be calculated to be  $|1 + h\lambda| \leq 1$  – a disk of radius 1 centered at  $(-1, 0)$  on the complex  $h\lambda$  plane. With such a method not only is it unstable for exponentially growing test problems, if  $\text{Re}(\lambda) > 0$ , it is also unstable for exponentially decaying test problems, if  $\text{Re}(h\lambda)$  is *too* negative. This can greatly reduce the allowed step-size if  $\lambda$  itself has a large negative real part, in which case  $h$  must be chosen to ensure stability and not to obtain the desired accuracy. This makes the method inefficient. Problems which may exhibit this rapidly decaying transient behaviour often arise when modelling

---

<sup>7</sup>Strictly only true for Linear Multi-step Methods, of which Forward Euler is an example. A method is zero-stable if it is stable to perturbations in the solution to the trivial test problem  $y' = 0$ , which is true provided the method satisfies a certain *root condition*.

a process acting over two or more different time-scales. Such problems are called *stiff*. Knowing if this is the case for the problem being modelled is an important consideration when choosing which numerical method to use.

A method which does much better on stiff problems is the *Backward Euler* method:

$$y_{n+1} = y_n + hf(y_{n+1}, t_{n+1}),$$

an *implicit* method of first order whose region of absolute stability is the region  $|1 - h\lambda| > 1$  – the *complement* of the disk of radius 1, centered at the point  $(1, 0)$  on the complex  $h\lambda$  plane. Backward Euler will fair better on stiff problems because the region of absolute stability now includes the entire left half plane, so there is no concern about taking time-steps that are too large to sufficiently resolve any rapidly decaying transient behaviour. Since the unknown term  $y_{n+1}$  appears now on both the left and right hand sides of the equation it must be solved for, using Newton’s root-finding method, for example.

An example of another method is the trapezoidal method, obtained by averaging the above two methods:

$$y_{n+1} = y_n + \frac{h}{2}(f(y_n, t_n) + f(t_{n+1}, t_{n+1})),$$

which is implicit and second-order accurate. Its region of absolute stability is the entire left half-plane, making it a suitable method for stiff problems also.<sup>8</sup> A trapezoidal method is used by MATLAB’s `ode23t` function.

These three examples serve to introduce the basic concepts and issues involved in employing a numerical method. A vast array of other methods of different error and stability behaviour exist. Choosing the ‘right’ one depends on knowledge of the problem at hand and the methods available.

### 2.3.2 Numerical Continuation

In Section 5.2, analysis performed with the numerical continuation package AUTO [45] will be discussed. This section introduces briefly what is meant by numerical continuation. A more detailed overview can be found in [46]. Dynamical systems

---

<sup>8</sup>Ignoring for this discussion the fact that the trapezoidal method is not L-stable.

are typically non-linear and unless they have a specific, well-studied form (such as a Hamiltonian system), there is typically a limited amount we can infer about the system without resorting to numerics. For a general dynamical system

$$\dot{\mathbf{u}} = \mathbf{f}(\mathbf{u}, \lambda),$$

for  $\mathbf{u} \in \mathbb{R}^n$  and a parameter  $\lambda \in \mathbb{R}$ , we are typically interested in the fixed points

$$0 = \mathbf{f}(\mathbf{u}, \lambda).$$

Of particular interest is how the set of fixed points changes as we vary  $\lambda$ . Continuation methods can help answer this question.

Note that  $\mathbf{f} : \mathbb{R}^{n+1} \rightarrow \mathbb{R}^n$  and the aim is to find the set of points  $\gamma \in \mathbb{R}^{n+1}$  such that

$$\mathbf{f}(\gamma) = 0.$$

Application of the implicit function theorem tells us that for points  $(\mathbf{u}, \lambda)$  where the Jacobian  $\frac{\partial \mathbf{f}}{\partial \mathbf{u}}$  is invertible then locally the set  $\gamma$  is unique and is one-dimensional – it is a smooth curve  $\gamma = \gamma(s), s \in \mathbb{R}$ . Such points are referred to as regular points. Points where the Jacobian is not invertible are known as singular points and can represent bifurcations of the corresponding dynamical system. Curves of regular points are known as branches. Numerical continuation characterises these curves.

### Predictor-corrector methods

Starting from a known fixed point  $\mathbf{x}_0 = (\mathbf{u}_0, \lambda_0) = \gamma(s_0)$ , most numerical continuation packages use predictor-corrector methods to extend the curve  $\gamma(s)$ . As the name suggests this is broken down into the steps: (i) predict a new point,  $\mathbf{x}_0 \rightarrow \mathbf{x}_0^p$  and (ii) correct the prediction  $\mathbf{x}_0^p \rightarrow \mathbf{x}_1$  to ensure  $\mathbf{f}(\mathbf{x}_1) = 0$ .

#### (i) Prediction

One can take as the prediction

$$\mathbf{x}_0^p = \mathbf{x}_0 + h\mathbf{v}_0,$$

where  $h$  is some step size and  $\mathbf{v}_0$  is a vector satisfying

$$\frac{\partial \mathbf{f}}{\partial \mathbf{x}}(\mathbf{x}_0)\mathbf{v}_0 = 0,$$

such that  $\mathbf{v}_0$  is pointing in a direction which produces (linear terms considered) the least change in  $\mathbf{f}(\mathbf{x})$ .

## (ii) Correction

To correct the prediction set

$$\mathbf{f}(\mathbf{x}_1) = 0,$$

which can be taken as a root-finding problem using the prediction  $\mathbf{x}_0^p$  as an initial guess. This can be solved using Newton iterations, for example. The form of the iteration would then be

$$\mathbf{x}_0^{n+1} = \mathbf{x}_0^n + \mathbf{J}(\mathbf{x}_0^n)^{-1}\mathbf{F}(\mathbf{x}_0^n),$$

where  $\mathbf{J}$  is the Jacobian of  $\mathbf{F}$ . The problem with this scheme is that if we set  $\mathbf{F} = \mathbf{f}$  then  $\mathbf{J}$  is not a square matrix and so its inverse is not defined. The system can be augmented to place constraints on how the continuation is to be performed. For example, take

$$\mathbf{F} = \begin{bmatrix} \mathbf{f} \\ g \end{bmatrix}, \quad \mathbf{J} = \begin{bmatrix} \mathbf{f}_u & \mathbf{f}_\lambda \\ g_u & g_\lambda \end{bmatrix}.$$

One choice for the function  $g$  would be

$$g = \lambda - \lambda_n,$$

where  $\lambda_n$  is the desired parameter value, such that  $\lambda_n = \lambda_{n+1} + \Delta\lambda$ . This simply increases the parameter  $\lambda$  by a fixed amount with each step; this is called natural parameter continuation. This is the simplest continuation scheme however it runs in to trouble if  $1/\mathbf{f}_\lambda$  goes to zero. The continuation package AUTO uses a type of pseudo-arclength continuation instead.

## Identifying bifurcations

The continuation procedure outlined above applies to any curve defined by  $\mathbf{f}(\mathbf{u}, \lambda) = 0$  and does not consider the fact that  $\mathbf{f}$  describes a dynamical system. Therefore, in order to identify properties of the dynamical system, such as bifurcations, more tools are required. For different types of bifurcations different *test* functions are used which will return zero at a given bifurcation point. That is, for test function  $\phi : \mathbb{R}^{n+1} \rightarrow \mathbb{R}$  we solve the system

$$\mathbf{f}(\mathbf{u}, \lambda) = 0, \quad \phi(\mathbf{u}, \lambda) = 0.$$

So, for example, when a saddle node bifurcation occurs one eigenvalue of the Jacobian goes through zero. A possible test function for these bifurcations is then

$$\Psi_{SN} = \det(\mathbf{f}_u) = \prod_{i=1}^N \lambda_i,$$

where  $\det(\mathbf{f}_u)$  denotes the determinant of the Jacobian matrix  $\mathbf{f}_u$ . Other bifurcations require other test functions.

Packages such as AUTO also contain routines for other problems such as branch switching when two solution branches intersect, characterising periodic orbits and homoclinic orbits. The purpose of this section is to convey the idea of numerical continuation so these tasks are not discussed here.

## 2.4 Conclusion

The purpose of this chapter was to provide an overview of the mathematics used in subsequent chapters. An introduction to the dynamical systems relevant to this thesis was provided. The formalism for modelling systems of biochemical reactions was described and issues such as the existence of conservation relations and the choice of kinetics were discussed. A metric to quantify the concepts of robustness was developed and the basic concepts behind numerical continuation were introduced.



# Chapter 3

## Developing a model of Bcl-2 family interactions

This chapter describes the process of developing a model of the Bcl-2 family interactions. For this we require consideration of the biological and physical aspects of the system.

### 3.1 Previous work

A number of studies have developed ODE models of very comprehensive or very specific aspects of both the intrinsic and extrinsic death pathways.

The studies in [47, 48, 49] provide a dynamical systems analysis of ODE models of the ‘Bcl-2 switch’. In these, emphasis is placed on the capability of such models to exhibit bistable behaviour. The possibility of such hysteresis phenomena is proposed as an explanation for the switch-like behaviour of the mitochondrial apoptosis pathway. Studies into bistability in apoptosis more broadly have also been performed. For example, the study in [50] examines the possibility of bistability caused by receptor clustering in initiating the extrinsic cell death pathway. The study in [51] investigates bistability in the intrinsic apoptotic pathway in the presence of nitric oxide. An alternative to typical numerical continuation analysis, the study uses chemical reaction network theory to identify the capability for bistability in the model. The work of Feinburg (*e.g.* [52, 53]) constructs a *species-reaction*

graph with which the potential for *multistationarity* (and therefore bistability) can be investigated.

The absence of applicable rate constants and concentrations *in vivo* makes it difficult to build detailed, comprehensive and biologically realistic models of the apoptosis pathways. Instead, the function of the pathway under parametric variation can be investigated (*e.g.* [54, 55]). Indeed, the robustness of cellular functions is a well-recognised feature of living systems. The chaotic, crowded environment inside a cell does indeed suggest that for any signal transduction pathway to operate reliably it must be able to work over a wide range of model parameters.<sup>1</sup>

Albeck *et al* [58] constructs a comprehensive model of the extrinsic cell death pathway in an attempt to understand the pathway's 'snap-action' response. Bcl-2 family interactions are a subset of the interactions included. The model is able to make a number of testable predictions, for instance, proposing that mitochondrial outer membrane permeabilisation (MOMP) is complete following the assembly of relatively few pores. Furthermore, the model finds that feedback loops are unnecessary to produce a 'snap-action' response in the induction of MOMP.

The model of Huber *et al* [59] considered a spatial-temporal model of MOMP induced apoptosis which can explicitly model diffusive processes. This model does not require the assumption that the medium is spatially homogeneous or that mass-transport effects are irrelevant. The study found that anisotropies which may be present in cytochrome c concentration are damped and do not affect the subsequent caspase signalling cascade.

Beyond deterministic models, both stochastic and cellular automata models have been implemented to model Bcl-2 family interactions [38, 54, 49]. These papers address similar questions of bistability and robustness to those addressed in deterministic models.

Huber *et al* [60] and Spencer and Sorger [61] both provide reviews of the mathematical studies into apoptosis.

Though there are a number of studies which have constructed Bcl-2 family models similar to those that will be developed here, to date none of these have been developed in close collaboration with experiment. In any modelling exercises there

---

<sup>1</sup>The idea of robustness has been used to successfully guide searches for plausible and experimentally verifiable ranges of parameters in other pathways [56, 57].

exists a trade-off between the need for sufficient scope and the need for sufficient detail and experimental data required to build a relevant and realistic model. The present work represents a good compromise in both of these aspects.

## 3.2 Biological considerations

An important consideration in constructing a kinetic model is which interactions to include and in how much detail. This section discusses a *base* model which will be developed and later modified to investigate the MLM system. Only a few Bcl-2 family members are present so we only need consider a handful of interactions.

### 3.2.1 Bak activation

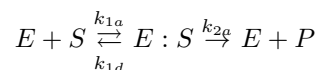
In the MLM system, there are two suggested mechanisms by which Bak can be activated to induce MOMP following BH3-only stimulus. The ‘direct’ activation model proposes that spiked-in tBid or tBIM interact with Bak directly, possibly via a ‘hit-and-run’ mechanism:



Throughout this thesis Act denotes the activator protein, either tBid or tBIM, and Bak\* is used to denote Bak in an active conformation. The interaction is in essence a catalysing reaction and may be more accurately represented by a Michaelis-Menton enzymatic model.<sup>2</sup> Indeed, some kinetic models do explicitly use the Michaelis-Menton model for similar ‘enzymatic’ reactions (*e.g.* [63]). Given the known difficulty in observing a transient tBid : Bak complex, however, this level of detail is unnecessary.

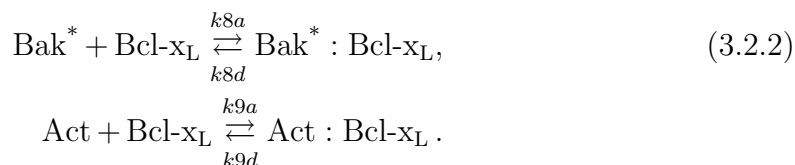
---

<sup>2</sup>The Michaelis-Menton model ([62]) describes catalytic reactions in which a substrate,  $S$ , binds temporarily to an enzyme,  $E$ , thereby catalysing the formation of product,  $P$ . That is, it models the following reactions:



## Direct vs indirect activation

The ‘indirect’ activation model supposes that Bak does not interact with Act. However, since MOMP does not occur ‘by default’, it can be inferred that most endogenous Bak must be inactive. Therefore, the activation step must occur when small amounts of active Bak bound to endogenous Bcl-x<sub>L</sub> are disrupted by BH3-only stimulation. The unbound active Bak is then able to activate the remaining endogenous Bak via auto-activation. This step requires the following interactions:



The indirect activation model therefore requires some endogenous Bak to be active and bound to Bcl-x<sub>L</sub>, which has not been established experimentally in the MLM system. In fact there is some evidence that Bak is not prebound to Bcl-x<sub>L</sub> in the MLM system<sup>3</sup> but due to its role in an indirect activation mechanism we include these interactions regardless.

The phrase ‘direct model’ has the particular meaning that BH3-only proteins *can* interact with Bak to induce a conformation change, while the ‘indirect model’ means simply that BH3-only proteins *cannot* interact with Bak. This differs to the typical definition of direct and indirect activation provided in Chapter 1, page 7.

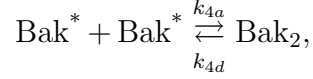
As outlined in Section 1.4, an aim of this project is to determine which activation hypothesis plays a more significant role in experiments of the MLM system. In practice, a model including both the ‘direct’ and ‘indirect’ mechanisms is developed. Each mechanism is tested by setting the necessary kinetic parameters to zero: the direct activation model does not use endogenous Bak complexed to Bcl-x<sub>L</sub> so interactions (3.2.2) are not included. Similarly, the indirect activation model does not include the (3.2.1) interaction.

---

<sup>3</sup>Dr. Ruth Kluck, WEHI, personal communication.

### 3.2.2 Bak homo-dimerisation and auto-activation

Bak homo-dimerisation is assumed to occur via the bimolecular interaction:



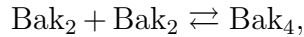
and Bak is assumed to be able to activate itself via the interaction:



Though there is also evidence that spontaneous activation can occur in some circumstances. It was decided that this process is unimportant on the timescale being considered.

### 3.2.3 Bak multimerisation and pore formation

The presence of Bak homo-dimers on the mitochondrial membrane is assumed insufficient to induce MOMP. It is hypothesised that these dimers form a larger cluster which is able to induce permeability of the membrane [64]. This is represented by a ‘multimerisation’ step. Two Bak dimers (or four Bak molecules) affect the mitochondrial membrane allowing for the release of intra-membrane cytochrome c into the cytosol [65]:



This mechanism is similar to that used in [47, 58]. [49] provides an alternative mechanism.

### 3.2.4 Reversibility

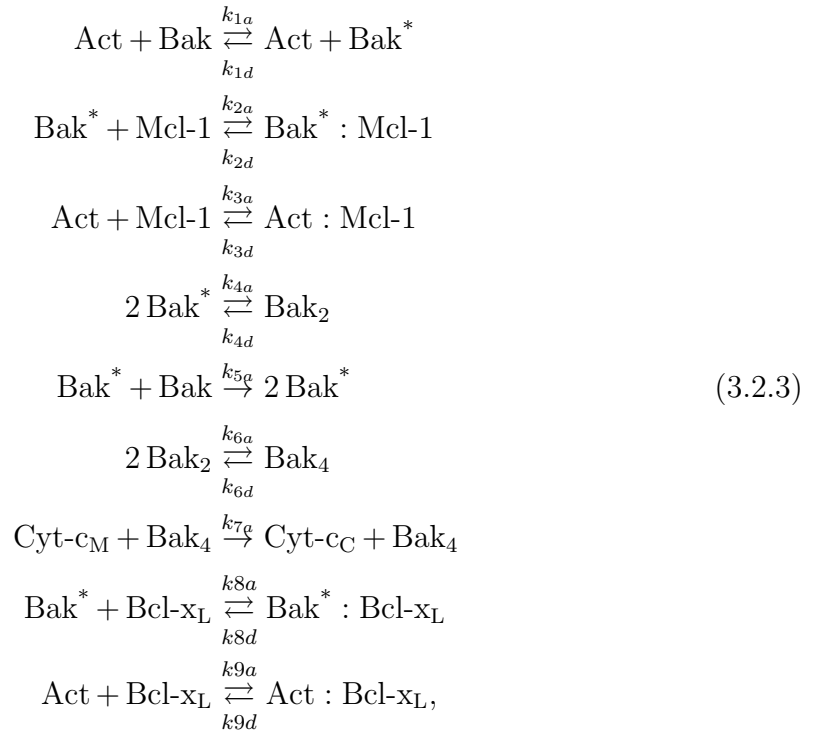
Some changes and interactions between Bcl-2 members are considered essentially irreversible: Bak activation and homo-dimerisation, for instance. Whether the Bak:Mcl-1 complex is a ‘dead-end’ complex which does not release Bak once it

has formed is also a question of some interest – both for providing interpretations to the present MLM experiments and more generally.

However, by making some processes reversible and some irreversible, the outcome of our simulations becomes predetermined. For example, if Bak homo-dimerisation is irreversible and Bak:Mcl-1 complex formation is reversible then Bak homo-dimerisation and therefore cytochrome c release is inevitable, regardless of kinetic parameters. For this reason a completely reversible model will be built. By making each reaction reversible the system remains in ‘dynamic’ equilibrium, rather than static equilibrium, so that complexes are constantly forming and unforming.

### 3.2.5 Model equations

The complete set of equations describing interactions in the MLM system is:



and is represented in Figure 3.1. Let  $\mathbf{x} = (B, A, M, C, X, \hat{B}, \hat{B}_2, \hat{B}_4, \hat{A}_M, \hat{A}_X, \hat{M}, \hat{C}, \hat{X})$  be the state vector. The variables are:  $B = \text{Bak}$ ,  $A = \text{Act}$ ,  $M = \text{Mcl-1}$ ,  $C = \text{Cyt-c}_M$ ,  $X = \text{Bcl-x}_L$ ,  $\hat{B} = \text{Bak}^*$ ,  $\hat{B}_2 = \text{Bak}_2$ ,  $\hat{B}_4 = \text{Bak}_4$ ,  $\hat{A}_M = \text{Act} : \text{Mcl-1}$ ,  $\hat{A}_X =$



By applying the law of mass action, the reaction-rate vector is given by:

$$\mathbf{J}_{bcd2} = \begin{pmatrix} k_{1a}BA - k_{1d}\hat{B} \\ k_{2a}M\hat{B} - k_{2d}\hat{M} \\ k_{3a}AM - k_{3d}\hat{A}_M \\ k_{4a}\hat{B}^2 - k_{4d}\hat{B}_2 \\ k_{5a}\hat{B}B \\ k_{6a}\hat{B}_2^2 - k_{6d}\hat{B}_4 \\ k_{7a}\hat{B}_4C \\ k_{8a}X\hat{B} - k_{8d}\hat{X} \\ k_{9a}AX - k_{9d}A_X \end{pmatrix}. \quad (3.2.6)$$

The initial conditions are

$$\begin{aligned} B(0) &= B_0, & A(0) &= A_0, & M(0) &= M_0, & \hat{X}(0) &= X_0, \\ \hat{B}(0) &= \hat{A}_M(0) = \hat{M}(0) = X(0) = \hat{A}_X = 0, \\ C(0) &= \hat{C}(0) = \hat{B}_2(0) = \hat{B}_4(0) = 0. \end{aligned} \quad (3.2.7)$$

Equations 3.2.4-3.2.7 fully specify the model.

Recall the conservation matrix, (2.2.8), defines which species' concentrations are conserved and that  $\text{rank}(G) = n - \text{rank}(S)$ . In the present case,  $n = 13$  and  $\text{rank}(S) = 8$  therefore 5 concentrations can be eliminated from the system. At any time  $t$  the following relations apply:

$$\begin{aligned} A_0 + \int_0^t f(t') dt' &= A + \hat{A}_M + \hat{A}_X, \\ C_0 &= C + \hat{C}, \\ M_0 &= M + \hat{M} + \hat{A}_M, \\ B_0 &= B + \hat{B} + 2\hat{B}_2 + 4\hat{B}_4 + \hat{M} + \hat{X}, \\ X_0 &= X + \hat{X} + \hat{A}_X. \end{aligned} \quad (3.2.8)$$

These can be verified by showing  $\mathbf{g}^T S = \mathbf{0}^T$  for each relation. They correspond to the conservation of activator, cytochrome c, Mcl-1, Bak and Bcl-x<sub>L</sub> in the system,

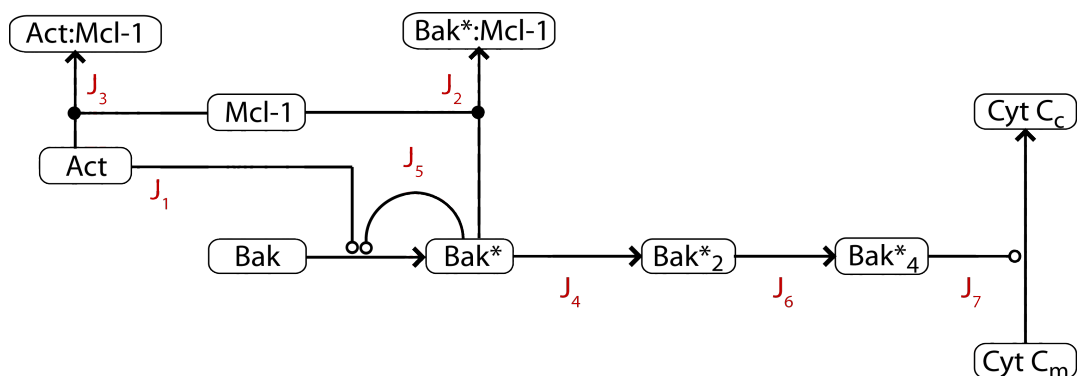


Figure 3.1: Schematic of Bcl-2 family interactions.  $Bak^*$  indicates the ‘active’ conformation of Bak. Act is used to indicated either tBid or tBIM. The arrows represent the forward direction of each reaction and do not indicate (ir)reversibility. The corresponding model equations assume that all interactions occur within a well-mixed solution. Arrowheads indicate product of reaction, species connected with an empty dot play a catalysing role, while species connected with filled dots indicate complex formation.

respectively.

The initial conditions are assumed to be known and the kinetic parameters will be estimated both from Biacore binding data and by fitting to MLM experiments.

### 3.3 Physical considerations

Determining how Biacore binding data can be incorporated into the mass-action kinetic models requires some consideration of the physical aspects of the MLM experimental system. These considerations suggest a framework to include Biacore binding data into a model of MLM experiments.

#### 3.3.1 Previous work

Before considering the MLM system we describe the following three examples incorporating experimental binding data (SPR), or similar, into kinetic models.

The extrinsic cell death pathway model of [58] is trained on experimental data based on live-cell imaging, flow cytometry and immunoblotting of cells perturbed by protein depletion and overexpression. Where available, experimental values for ini-

tial concentrations and kinetic parameters are used. Kinetic parameters come from a variety of sources, including SPR experiments. Rates of interactions occurring on the mitochondrial membrane are scaled by the ratio of cell volume to mitochondria volume – to reflect to increased chance of molecular collisions occurring on the membrane. Unknown rates are set at an intermediate value within a biologically realistic range and are fit to experiments ( $k_a = 10^5 \text{ M}^{-1}\text{s}^{-1}$  and  $k_d = 10^{-3} \text{ s}^{-1}$ ).

[63] develops a deterministic model of the eukaryotic mitogen-activated protein kinase signalling pathway. The model uses diffusion-limited kinetic models for ligand-receptor interactions occurring on the membrane and for interactions occurring between membrane-associated and cytosolic associated species. Units for rate constants of these intra-membrane interactions were scaled appropriately [66].

A relatively simple kinetic model is implemented in [67] to investigate the role rebinding plays in T-cell responses to antigen.<sup>4</sup> An explicit mechanism for diffusion is included to investigate the effect of rebinding in the efficient recognition of antigenic molecules. By allowing for brief unbinding, the T cell receptors are able to discriminate antigens based on both their association and dissociation rates. SPR measurements are utilised in the model. The units of the SPR measurements are adjusted from the three-dimensional  $\text{M}^{-1}\text{s}^{-1}$  to the two-dimensional  $\text{m}^2\text{s}^{-1}$  by dividing by a confinement length factor – the membrane thickness – here 0.262nm. The resulting rates are compatible with experimentally determined membrane associated rates. However the authors state the accuracy of this method is unknown.

### 3.3.2 MLM geometry

Bak and Bcl-x<sub>L</sub> are membrane associated proteins and any interaction they have with themselves or other proteins occurs on the mitochondrial membrane. This consideration can affect the form of the mass-action equations described in Section 2.2.1. Though primarily concerned with ligand-receptor complex association, [66] addresses this issue. This section follows their derivations, where appropriate.

Section 2.2.1 describes protein complex formation as a one-step, reversible pro-

---

<sup>4</sup>T cells are part of the cell-mediated immune response, they recognise antigens presented by the major histocompatibility complexes of host cells and are able to kill or co-ordinate the killing of the responsible pathogen.

cess in which two proteins,  $A$  and  $B$  form a complex,  $C$ :



where  $k_a$  and  $k_d$  are the effective association and dissociation rates, respectively. A more realistic model is the two-step binding model in which proteins  $A$  and  $B$  first must ‘encounter’ one another – via molecular transport – before forming complex  $C$ :



where  $A..B$  denotes the ‘encounter complex’,  $k_+$  represents the transport rate which is influenced by diffusion and geometry,  $k_{\text{on}}$  and  $k_{\text{off}}$  represent the *intrinsic* association and dissociation rates respectively. The rates  $k_{\text{on}}$  and  $k_{\text{off}}$  are determined via kinetic experiments such as those a Biacore machine performs. Three possibilities present themselves in the MLM system:

1. Both  $A$  and  $B$  are free in solution
2.  $A$  and  $C$  are membrane associated and  $B$  is free in solution
3.  $A$ ,  $B$  and  $C$  are membrane associated.

When both  $A$  and  $B$  are free in solution we will assume that the interaction is *reaction-limited* such that (3.3.1) is a sufficient representation of the interaction.

When  $A$  is membrane associated and  $B$  is free in solution, we will assume that molecular transport of  $B$  may not be neglected such that (3.3.2) is a required representation of the interaction. This requires an expression for the effective forward and reversible reaction rates,  $k_a$  and  $k_d$ , in terms of  $k_+$  and  $k_{\text{on}}$  and  $k_{\text{off}}$ .

When both  $A$  and  $B$  are membrane associated, we will neglect surface diffusion of proteins required to encounter each other such that, again, (3.3.1) is sufficient. In a sense we are considering the interactions divided into two compartments, both of which are sufficiently well-mixed that they can be modelled by simple mass-action kinetics. Interactions occurring ‘on the boundary’ of the compartments need more care.

Since Mcl-1 lacks a transmembrane domain we assume that it is predominantly situated in solution; similarly with tBid and tBIM. Therefore, we suppose that

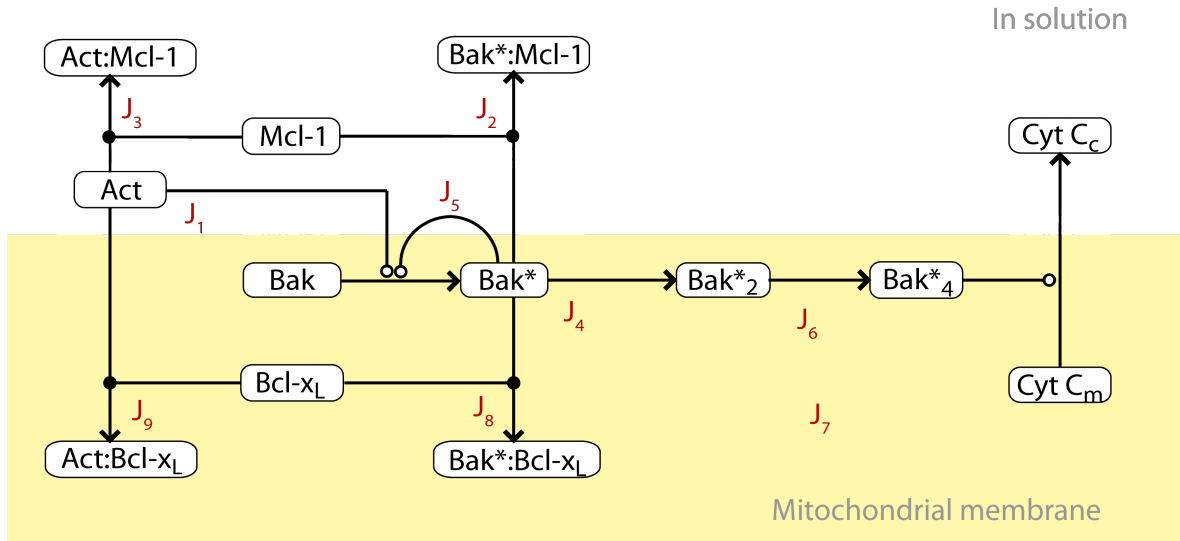


Figure 3.2: Schematic of Bcl-2 family interactions. Some interactions occur on the mitochondrial membrane, some occur in solution. The arrows represent the forward direction of each reaction and do not indicate (ir)reversibility.

transport between ‘compartments’ is transient – only occurring when a solution and membrane-associated protein complex – when they dissociate the proteins return to their respective compartments. For this reason we do not develop an explicit compartmental model as implemented in [58], although in future modelling efforts this is definitely an addition to consider.

Figure 3.2 illustrates the compartmentalisation of the Bcl-2 family interactions.

### 3.3.3 On diffusion-limited processes

In order to incorporate transport effects which may affect solution proteins associating with membrane associated protein, here we derive an effective forward and reverse rate for reactions in which diffusion of protein to and from the membrane is non-negligible. The derivation of  $k_f$  is presented in detail with the derivation of  $k_r$  following a similar process.

To begin with, consider the rate at which the free protein  $B$  associates with the mitochondrion surface as a whole. Later we divide the rates we obtain by the number of  $A$  molecules present on the surface to obtain a per ‘receptor’ rate. Assuming the concentration of  $B$  molecules is significantly higher than that of mitochondria

in solution, we assert that around a single mitochondrion,  $M$ , the concentration of  $B(r)$  as a function of distance from  $M$  is given by the steady-state diffusion equation in radially symmetric spherical coordinates:

$$D \frac{d}{dr} \left( r^2 \frac{dB}{dr} \right) = 0, \quad (3.3.3)$$

for diffusivity,  $D$  in units  $\text{cm}^2 \text{s}^{-1}$ . In this derivation it is most natural to use the units  $\text{cm}^{-3}$  for  $B(r)$  and  $\text{cm}^{-2}$  for  $A$  and  $C$ . Molar and  $\text{cm}^{-3}$  can be interchanged as follows:

$$1 \text{ cm}^{-3} = 10^3 N_A^{-1} \text{ M}, \quad (3.3.4)$$

where  $N_A$  is Avagadro's constant and is  $N_A \approx 6.02 \times 10^{23}$ .<sup>5</sup>

The concentration 'very far' from  $M$  is assumed to equal the *bulk* concentration,  $B$ :

$$B(r) \rightarrow B, \quad r \rightarrow \infty. \quad (3.3.5)$$

The other boundary condition, at the *encounter radius*  $r = s$  (the radius of the mitochondrion), in which the influx of  $B$  molecules is given by the intrinsic 'mitochondria' on-rate multiplied by the local concentration  $B(s)$  and, at steady-state, also by the diffusion rate multiplied by the 'encounter' surface area. Therefore, the second boundary condition is:

$$4\pi s^2 D \left. \frac{dB}{dr} \right|_{r=s} = (k_{\text{on}})_{MT} B(s). \quad (3.3.6)$$

Let  $(k_{\text{on}})_{MT}$  denote the intrinsic mitochondria on-rate and let  $(k_f)_{MT}$  denote the effective forward rate of protein  $B$  binding with mitochondria surface. These are related to  $k_{\text{on}}$  and  $k_f$ , our known and target quantities respectively, by:

$$(k_{\text{on}})_{MT} = [A]k_{\text{on}}, \quad (k_f)_{MT} = [A]k_f,$$

where  $[A]$  denotes the number of free  $A$  molecules per mitochondrion. The solution

---


$${}^5 1 \text{ cm}^{-3} = 1 \left( \frac{\#}{\text{cm}^3} \right) = 10^3 \left( \frac{\#}{L} \right) = \frac{10^3}{N_A} \left( \frac{\text{moles}}{L} \right) = 10^3 N_A^{-1} \text{ M}$$

of (3.3.3) with boundary conditions (3.3.5) and (3.3.6) is:

$$B(r) = \frac{-(k_{\text{on}})_{MT} s B}{4\pi D s + (k_{\text{on}})_{MT} r} \frac{1}{r} + B_0.$$

Recalling that our overall flux of molecules associating with  $M$  is given by  $(k_f)_{MT} B$  and is equal to:

$$(k_f)_{MT} B = 4\pi s^2 D \left. \frac{dB}{dr} \right|_{r=s},$$

we obtain:

$$(k_f)_{MT} = B^{-1} 4\pi s^2 D \left. \frac{db}{dr} \right|_{r=s} = (k_{\text{on}})_{MT} B(s) B^{-1},$$

and thus:

$$\begin{aligned} (k_f)_{MT} &= \frac{4\pi s D (k_{\text{on}})_{MT}}{4\pi s D + (k_{\text{on}})_{MT}} \\ &= \left( \frac{1}{4\pi s D} + \frac{1}{(k_{\text{on}})_{MT}} \right)^{-1}. \end{aligned} \quad (3.3.7)$$

When the quantity  $4\pi s D$  is much smaller than  $(k_{\text{on}})_{MT}$ , the binding is termed *diffusion-limited*. When  $(k_{\text{on}})_{MT}$  is much smaller than  $4\pi s D$ , the binding is termed *reaction-limited*. We identify  $4\pi s D$  with the transport rate mentioned above  $k_{\pm}$ . In terms of  $k_{\text{on}}$ :

$$k_f = \frac{4\pi s D k_{\text{on}}}{4\pi s D + [A] k_{\text{on}}},$$

and since  $[A] = 4\pi s^2 A$ , then:

$$k_f = \frac{D k_{\text{on}}}{D + s A k_{\text{on}}}. \quad (3.3.8)$$

The effective forward association rate is no longer a constant. Interestingly, it becomes less efficient the higher the concentration of free  $A$  molecules. This is a result of increased competition between  $A$  molecules for unbound  $B$ .

The dissociation rate is derived using a similar approach and is given by:

$$(k_r)_{MT} = \frac{4\pi s D (k_{\text{off}})_{MT}}{4\pi s D + (k_{\text{on}})_{MT}},$$

and therefore:

$$k_r = \frac{D k_{\text{off}}}{D + s A k_{\text{on}}}. \quad (3.3.9)$$

As with  $k_f$ , the effective dissociation rate becomes less efficient the higher the concentration of free  $A$  molecules, since rebinding is more likely to occur. Equations (3.3.8) and (3.3.9) account for the effect of diffusion on both the association and dissociation rates mentioned in Section 2.2.1. Evaluation of  $k_f$  and  $k_r$  requires knowing  $A$  in units of  $\text{cm}^{-2}$  and  $k_{\text{on}}$  in units of  $\text{cm}^3 \text{s}^{-1}$ . Let  $\bar{A}$  be the level of protein  $A$  in nanomolar and  $\bar{k}_{\text{on}}$  and  $\bar{k}_{\text{off}}$  be  $k_{\text{on}}$  and  $k_{\text{off}}$  in units of  $\text{nM}^{-1} \text{s}^{-1}$ , respectively. Using (3.3.4) gives:

$$k_{\text{on}} = \frac{10^{12} \bar{k}_{\text{on}}}{N_A}. \quad (3.3.10)$$

The number of  $A$  molecules per millilitre is given by  $N = 10^{-12} \bar{A} N_A$ . The number of mitochondria per millilitre is  $N_{MT} = \rho_{MT} / m_{MT}$ , where  $\rho_{MT}$  (g/ml) is density of mitochondria in solution and  $m_{MT}$  (g) is the mass of one mitochondrion. Therefore the number of  $A$  molecules per mitochondria is:

$$N_{A/MT} = \frac{N}{N_{MT}} = \frac{\bar{A} N_A m_{MT}}{10^{12} \rho_{MT}},$$

and the density per square centimetre is:

$$A = \frac{N_{A/MT}}{4\pi a^2} = \frac{\bar{A} N_A m_{MT}}{4\pi a^2 10^{12} \rho_{MT}}, \quad (3.3.11)$$

for mitochondria radius  $a$  (cm). Using the following estimates:

$$a = 10^{-4} \text{ (cm)}, \quad m_{MT} = 10^{-12} \text{ (g)}, \quad \rho_{MT} = 10^{-3} \text{ (g/ml)},$$

and using (3.3.11) and (3.3.10) we obtain:

$$k_f = \frac{10^6 D \bar{k}_{\text{on}}}{10^6 D + \bar{A} \bar{k}_{\text{on}}}, \quad k_r = \frac{10^6 D \bar{k}_{\text{off}}}{10^6 D + \bar{A} \bar{k}_{\text{off}}} \quad (3.3.12)$$

where we have left  $D$  as a parameter to be determined, since its magnitude is unknown in the MLM experiments. The system of ODEs is:

$$\frac{d\bar{C}}{dt} = \frac{10^6 D k_{\text{on}} \bar{A} \bar{B}}{10^6 D + \bar{A} k_{\text{on}}} - \frac{10^6 D k_{\text{off}} \bar{C}}{10^6 D + \bar{A} k_{\text{on}}}, \quad \frac{d\bar{A}}{dt} = -\frac{d\bar{C}}{dt}, \quad \frac{d\bar{B}}{dt} = -\frac{d\bar{C}}{dt}$$

The modification to the kinetic rates, (3.3.12), are used later in the context of Bcl-2 family interactions in the MLM experimental system.

### 3.4 Conclusion

This chapter considered both biological and physical issues related to modelling the mitochondrial apoptotic pathway. Previous models were discussed and each Bcl-2 interaction occurring in the MLM system was analysed. The mass-action system was specified. Considerations involving mass-transport were discussed and a correction for diffusion-limited reactions was outlined.

# Chapter 4

## Model calibration

Having outlined the model, this chapter matches the model to timing experiments performed in the MLM system. These experiments are used to determine unknown kinetic parameters which best reproduce the experiment outcomes. Once these have been estimated we can determine the relative importance of the direct and indirect models in modelling the system.

### 4.1 An experiment to observe Bak:Mcl-1 disruption

The following MLM experiments provide data to calibrate our models.

Over an hour, increasing concentrations of tBid or tBIM are added to MLM at 10 minute intervals, along with an initial concentration of 20nM Mcl-1. Approximately 10nM of endogenous Bak is present and initially in the non-activated conformation. Samples are taken every 10 minutes. The increasing tBid or tBIM is used to mimic increasing cellular stresses – the total amount of BH3-only grows exponentially with time so as to force a response from the system at some point. Both tBid and tBIM activate Bak, which then binds to Mcl-1 to form the Bak\*:Mcl-1 complex. The aim of the experiment is to determine which of tBid and tBIM can then disrupt the Bak:Mcl-1 complex to induce apoptosis. Figure 4.1 illustrates a clear Bak:Mcl-1 complex is observed with tBid signalling and a transient Bak:Mcl-1 complex is observed with tBIM signalling. This suggests that tBIM is able to disrupt the

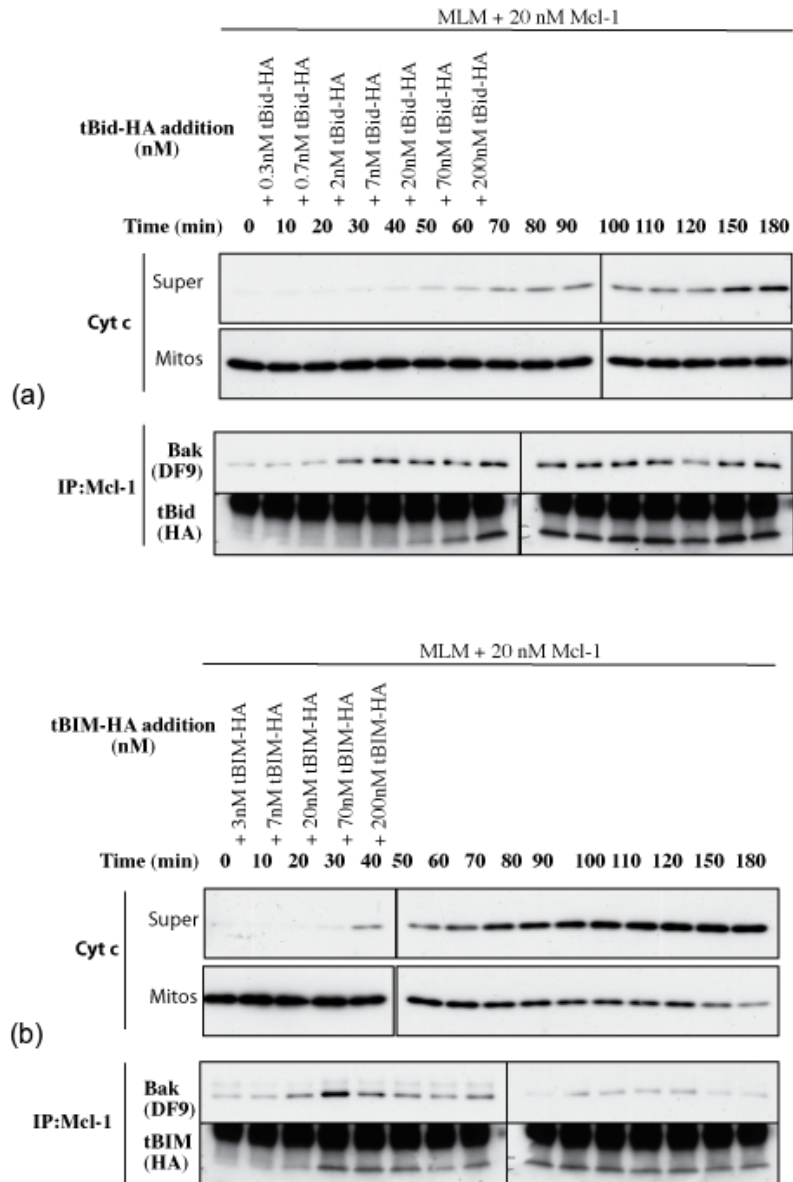


Figure 4.1: Western blots of experiment demonstrating Bak:Mcl-1 complex disruption with tBIM signalling and not with tBid signalling. Initially 20 nM of Mcl-1 and (a) 0.3 nM of tBid or (b) 3nM of tBIM are spiked into the system. Subsequent additions of tBid/tBIM are made every 10 minutes with the quantity of each addition indicated in the top two rows. Cyt c super represents cytochrome c detected in the supernatant – released from mitochondria. Cyt c mito represents cytochrome c in mitochondria. The bottom band in the tBid:Mcl-1 frame indicates the tBid:Mcl-1 complex. Data provided by Dr Ruth Kluck, WEHI, unpublished.

Bak:Mcl-1 complex which forms, but that tBid is not able to. This is consistent with the Biacore binding data present in Table 4.3 which indicates that tBIM binds more strongly to Mcl-1 than Bak does, and that tBid binding to Mcl-1 is weaker than that of Bak.

#### 4.1.1 Quantifying experimental data

The western blots are quantified using a densitometer. At the time of writing calibration data was not available. To convert the densitometry measurements to protein concentrations the following assumptions were therefore necessary:

- In the tBid signalling case: almost all Bak becomes activated and binds to Mcl-1 at the observed peak in signal at  $t = 30$  minutes.
- Almost all Mcl-1 is bound to either Bak or tBIM/tBid at  $t = 180$  min.
- The MLM system contains 5nM of cytochrome *c*. Since cytochrome does not interact with any Bcl-2 members the actual level of protein is of little importance.

Under these assumptions, the proteins level at each sample time point in the experiment can be scaled accordingly from the densitometry data (Figure 4.2).

Prior experimental knowledge<sup>1</sup> of the MLM system also provides the following ‘qualitative’ behaviours we wish to reproduce in any model based on these experiments:

- Low concentrations of monomeric activated Bak at any time point. Bak is expected to dimerise quickly which means that Bak monomers do not accumulate on the mitochondrial membrane.
- Eventual cytochrome *c* release with tBIM stimulation but only minimal cytochrome *c* release with tBid stimulation.
- Low concentrations of Bak homo-dimer. The formation of such dimers is thought to result almost immediately in cytochrome *c* release such that the

---

<sup>1</sup>Dr. Ruth Kluck, WEHI, personal communication

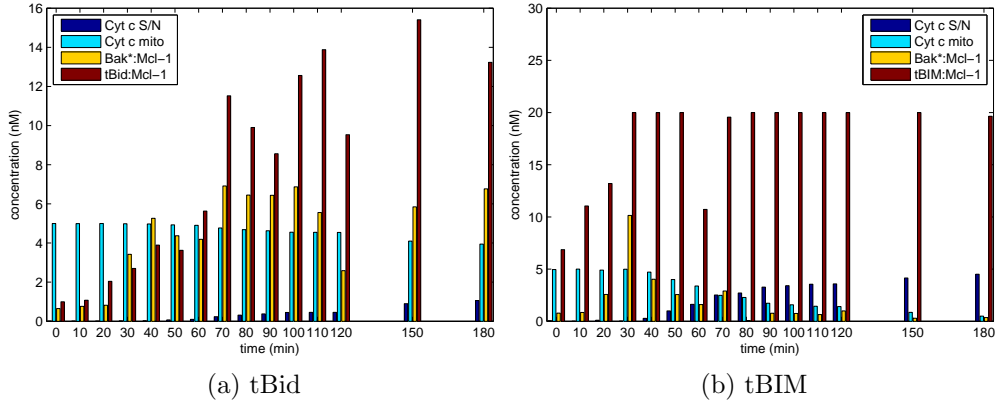


Figure 4.2: Scaled densitometry data under a set of assumptions regarding behaviour in the MLM system. Cyt c S/N represents cytochrome c detected in the supernatant – released from mitochondria. Cyt c mito represents cytochrome c in mitochondria.

observation of cytochrome c is synonymous with Bak dimer formation. Little to no cytochrome c release therefore corresponds to little or no Bak homodimers.

- In indirect model simulations some of the endogenous Bak is assumed to be in an active conformation and prebound to Bcl-x<sub>L</sub> (present at 3nM).

By adding these ‘observations’ as a set of densitometry points these considerations can be included in a non-linear least squares estimation procedure. These ‘concentrations’ are listed in Table 4.1.

The lack of available quantitative data makes these assumptions necessary in order to develop a realistic model which is in accord with known behaviour in the MLM system.

Protein	tBIM	tBid
Bak*	2	0.5
Bak <sub>2</sub>	2	0.5
Bak <sub>4</sub>	2	0.5

Table 4.1: Expected behaviours of unobserved proteins are incorporated into the model by including approximate protein concentrations (nM) in the parameter estimation procedure.

### 4.1.2 BH3-only stimulus

The experiment includes injections of BH3-only protein every ten minutes. In this case the inhomogeneous term of (3.2.4) takes the form:  $\mathbf{f}(t) = (0, f(t), 0, 0, 0, 0, 0, 0, 0)$ . Different availability of BH3-only stock protein meant the amount spiked in was different for tBid and tBIM stimulation. With tBIM stimulation the following piecewise constant function is adopted:

$$f_{tBIM}(t) = \begin{cases} \frac{7}{w}, & 600 - w \leq t < 600, \\ \frac{20}{w}, & 1200 - w \leq t < 1200, \\ \frac{70}{w}, & 1800 - w \leq t < 1800, \\ \frac{200}{w}, & 2400 - w \leq t < 2400, \\ 0, & \text{otherwise} \end{cases} \quad (4.1.1)$$

meaning the total concentration of Act spiked into the system is given by:

$$F(t) = A_0 + \int_0^t f(t') dt'$$

The parameter  $w$  reflects the window of time (in seconds) over which the tBid is spiked into the system every ten minutes. We adopt a relatively large  $w = 60$ s window.  $F(t)$  listed here matches the timing and concentrations of the experiment for tBIM additions (Figure 4.3). In the tBid case, the function  $f(t)$  is described in (4.1.2).

$$f_{tBid}(t) = \begin{cases} \frac{7}{w}, & 600 - w \leq t < 600, \\ \frac{2}{w}, & 1200 - w \leq t < 1200, \\ \frac{7}{w}, & 1800 - w \leq t < 1800, \\ \frac{20}{w}, & 2400 - w \leq t < 2400, \\ \frac{70}{w}, & 3000 - w \leq t < 3000, \\ \frac{200}{w}, & 3600 - w \leq t < 3600, \\ 0, & \text{otherwise} \end{cases} \quad (4.1.2)$$

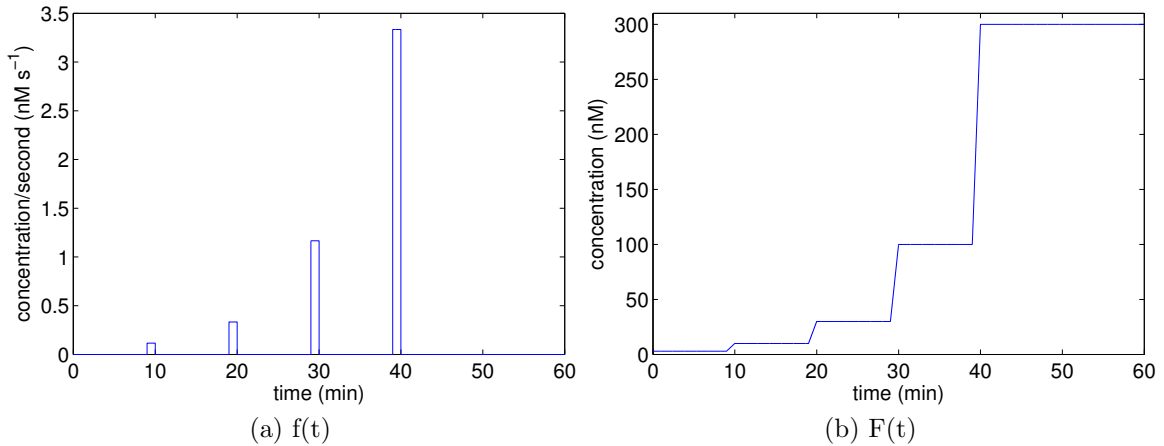


Figure 4.3: Function  $f(t)$  represents rate of tBIM addition into experiment. Function  $F(t)$  represents total amount of tBIM spiked into system in experiment.

## 4.2 Parameter Estimation from Experiment

Kinetic data on some of the protein-protein interactions occurring in our model is available, but not for every interaction. The above described experiments and densitometry data will be used to estimate these kinetic rates for later model analysis. Here we discuss how to estimate these kinetic parameters.

### 4.2.1 Non-linear least squares estimation

Non-linear least squares provides a method for determining parameters which best fit experimental data. The next two sections describe the theory needed for this estimation. Using more general notation adapted from [68], we are analysing systems of the form:

$$\frac{d\mathbf{x}}{dt} = \mathbf{f}(t, \mathbf{x}, \theta),$$

in which  $\mathbf{x}(t, \theta) \in \mathbb{R}^n$  denotes the  $n$ -dimensional state variable,  $\mathbf{f}(t, \mathbf{x}, \theta) \in \mathbb{R}^n$  denotes a Lipschitz continuous rate function, and  $\theta \in \mathbb{R}^p$  denotes a  $p$ -dimensional vector of unknown parameters. At some time,  $t_0$ , the system is subject to a set of  $q$  constraints,  $\mathbf{c} \in \mathbb{R}^q$ , such as initial conditions:

$$\mathbf{c}(\mathbf{x}(t_0, \theta), \theta) = \mathbf{0}.$$

To estimate the parameter vector,  $\theta$ , a number of observations of the state variables at  $N$  time points are available. The measurements,  $\mathbf{y}_i \in \mathbb{R}^n$ , are written:

$$\mathbf{y}_i = \mathbf{x}(t_i, \theta) + \epsilon_i, \quad i = 1, \dots, N,$$

with errors  $\epsilon_i \in \mathbb{R}^n$ . The task is to find parameters,  $\theta^*$ , such that the differences,  $\mathbf{y}_i - \mathbf{x}(t_i, \theta^*)$ , are minimised in some way. The method of least-squares provides the objective function:

$$\theta^* = \operatorname{argmax}_{\theta \in \mathbb{R}^p} \sum_{i=1}^N [\mathbf{y}_i - \mathbf{x}(t_i, \theta)]^T [\mathbf{y}_i - \mathbf{x}(t_i, \theta)], \quad (4.2.1)$$

such that  $\mathbf{x}$  satisfies the initial value problem:

$$\begin{aligned} \frac{d\mathbf{x}}{dt} &= \mathbf{f}(t, \mathbf{x}, \theta), \\ \mathbf{c}(\mathbf{x}(t_0, \theta), \theta) &= \mathbf{0}. \end{aligned}$$

In the context of a linear least-squares fit, the *coefficient of determination*,  $R^2 \in [0, 1]$ , provides a measure of the goodness of fit. It can be interpreted as the proportion of observed variance which can be explained, or accounted for, by the model. Let  $\bar{\mathbf{y}} = \frac{1}{N} \sum_{i=1}^N \mathbf{y}_i$  represent the *average* observation vector. Then we define the following sum of squares:

$$\begin{aligned} SS_{err} &= \sum_{i=1}^N [\mathbf{y}_i - \mathbf{x}(t_i, \theta)]^T [\mathbf{y}_i - \mathbf{x}(t_i, \theta)], \\ SS_{tot} &= \sum_{i=1}^N [\mathbf{y}_i - \bar{\mathbf{y}}]^T [\mathbf{y}_i - \bar{\mathbf{y}}], \end{aligned}$$

and compute  $R^2$  as:

$$R^2 = 1 - \frac{SS_{err}}{SS_{tot}}. \quad (4.2.2)$$

In a non-linear least squares fit  $R^2 \leq 1$  and no longer has a convenient interpretation. It can still be calculated using (4.2.2). In both cases  $R^2 = 1$  indicates a perfect fit and  $R^2 = 0$  indicates a fit as good as would be achieved by fitting with constant

functions.

## 4.2.2 Optimisation

Equation (4.2.1) is a non-linear least squares problem and in general cannot be solved analytically. The problem may contain more than one local minima meaning the ‘optimal’ parameter,  $\theta^*$ , can depend on initial estimates,  $\theta_0$ , and there is no guarantee that a global minimum will be found. A number of methods exist for finding a solution to (4.2.1) [69]. The problem can be seen as a generic optimisation problem for which a wide range of techniques exist.

The Trust-Region algorithm [70] is one such generic optimisation algorithm. The general goal is to find parameters,  $\theta^*$ , which minimise an objective function,  $f(\theta)$ , such as (4.2.1). Beginning at an initial estimate,  $\theta_0$ , we wish to move to a new point,  $\theta_1$ , for which  $f(\theta_1) < f(\theta_0)$ . The standard approach involves approximating the objective function by a quadratic function,  $q(\theta)$ , which is computed from the first two terms of a Taylor series expansion about the point  $\theta_0$ . The region,  $N$ , in which  $q(\theta)$  is presumed to be a good approximation of  $f(\theta)$  is named the *trust-region*. Within  $N$  the approximate objective function can be minimised to produce a trial-step,  $\theta_s$ . If indeed  $f(\theta_s) < f(\theta_0)$  then  $\theta_1 = \theta_s$  and the process is repeated. If however  $f(\theta_s) > f(\theta_0)$  the trust-region is reduced and a new trial-step is attempted.

Some optimisation methods are able to take advantage of the structure of the least-squares objective function, for example, the Gauss-Newton method or the Levenberg-Marquart method [71, 72]. Beyond these so-called *initial value problem* methods, other methods specific to optimising the fit of ODE models exist, such as, the multiple shooting method or the embedding method [73, 74].

The numerical computing package MATLAB<sup>®2</sup> implements both the Trust-Region-Reflective [75] and the Levenberg-Marquart method specifically for solving non-linear least squares problems. Although in theory the values of binding constants are unbounded, in practice definite, physically realistic limits can be set [66]. For this reason the Trust-Region-Reflective algorithm, which is better suited to constrained optimisation problems, will be used to estimate unknown parameters. Further, since the *magnitudes* of the parameters which need to be determined is

---

<sup>2</sup>MATLAB version 7.10.0 (R2010a). Natick, Massachusetts: The Mathworks, Inc., 2010.

unknown, the binding parameters will be fitted as exponents of 10. For parameters,  $\theta$ , the mass-action equations take the form:

$$J_i(\mathbf{x}, \theta) = 10^{\theta_{i,a}} x_1 x_2 - 10^{\theta_{i,d}} x_3.$$

To increase confidence in our estimates,  $\theta^*$ , the optimisation procedure is performed using a range of initial estimates. Beyond one common, intermediate initial guess, all other initial kinetic rate exponents are chosen randomly, uniformly between -1 and -6. It should also be noted that each iteration of the Trust-Region-Reflective algorithm requires evaluating the objective function which in turn requires solving the initial value problem to obtain trajectories  $\mathbf{x}(t, \theta)$ . Each step is therefore computationally very expensive and our exhaustive parameter search becomes infeasible for any more than 8 or 9 free parameters.

### 4.2.3 Simulations

The model equations described in Section 3.2.5 are solved numerically using MATLAB to obtain trajectories for the concentration of each species. Chemical reactions systems have a tendency to be ‘stiff’ in which case the choice of numerical solver can be important. MATLAB’s stiff solver `ode15s` [76] is used on the basis of its solid performance on a stiff and non-stiff test problem (Table 4.2). The solver `ode15s` is a variable order, multi-step solver and is used in [58] and [77] for similar systems.

Solver	<code>ode45</code>	<code>ode23</code>	<code>ode113</code>	<code>ode15s</code>	<code>ode23s</code>	<code>ode23t</code>	<code>ode23tb</code>
Typical	2.54	1.57	2.06	1.34	2.69	0.87	1.11
Extreme	17.36	11.23	16.18	0.82	2.44	0.71	0.89

Table 4.2: Time (s) for different MATLAB ODE solvers to solve two test problems based on the model equations of Section 3.2.5. Test problems are based on the simplified Bcl-2 model presented in 5.2. All kinetic parameters in the ‘typical’ problem are set to intermediate values –  $10^{-4}$ . Three kinetic parameters in the ‘extreme’ problem are set at unrealistic, rapid values –  $10^{-1}$ . In all cases the solution was inspected graphically to ensure convergence to the known solution. The MATLAB ODE suite provides three non-stiff solvers (without suffix) and four stiff solvers (with suffix). The difference between these classes becomes clear in the ‘extreme’ test problem.

### 4.3 Binding data

The Biacore binding data available for Mcl-1 and Bcl-x<sub>L</sub> is contained in Table 4.3.<sup>3</sup> The experimental procedure is as follows: direct binding assays were performed at room temperature using a Biacore S51 biosensor with 10 mM NaH<sub>2</sub>PO<sub>4</sub>, 40 mM Na<sub>2</sub>HPO<sub>4</sub>, 150 mM NaCl, 1 mM EDTA, 0.03% (v/v) Tween-20, 5% (v/v) DMSO, pH 7.4 as the running buffer. Anti-GST was immobilized on a CM5 sensorchip using aminecoupling chemistry. Recombinant GST-tagged Bcl-x<sub>L</sub> or Mcl-1 (100 mg/ml) were then injected at the flow rate of 10 ml/min and captured via the tag. All BH3 domain peptides were prepared in running buffer. Several concentrations of peptide around that peptide's  $K_D$  were injected at a flow rate of 90 ml/min. Weaker-binding ligands ( $K_D > 10$  nM) were allowed to associate with the protein for 60s and dissociation was monitored for 60s, whilst for tighter ligands the association time was 90s and the dissociation time 270s. All sensorgrams were generated using double referencing by subtracting the binding response from a reference spot, followed by corrections for solvent bulk shifts and subtraction of an average of the running buffer bank injections over the immobilized spot.

The proteins tested are similar to those used in MLM experiments, although the Bim and Bak and Bid reagents are BH3 peptides (around 20 residues) rather than full-length proteins (around 150-200 residues). Importantly, many studies from over 10 years of work indicate that these numbers provide an approximation to the relevant binding affinities used in our experiments.

Complex	$K_D$ (nM)	$k_d$ (1/s)	$k_a$ (1/nM/s)
Mcl-1:Bim	0.093	$2.96 \times 10^{-4}$	$3.20 \times 10^{-3}$
Mcl-1:Bak	0.58	$7.98 \times 10^{-4}$	$1.37 \times 10^{-3}$
Mcl-1:Bid	9.3	$7.52 \times 10^{-2}$	$8.10 \times 10^{-3}$
Bcl-x <sub>L</sub> :Bim	0.149	$4.76 \times 10^{-4}$	$3.86 \times 10^{-3}$
Bcl-x <sub>L</sub> :Bak	3.7	$1.02 \times 10^{-2}$	$2.77 \times 10^{-3}$
Bcl-x <sub>L</sub> :Bid	2.53	$3.92 \times 10^{-3}$	$1.55 \times 10^{-3}$

Table 4.3: Kinetic rate constants of Bcl-2 family protein interactions obtained using a Biacore machine.

<sup>3</sup>Experiments and data collection were performed by Dr. Douglas Fairlie and Dr. Erinna Lee, WEHI

## 4.4 Model selection

The applicability of available Biacore binding data and assumptions of mass-transport in the MLM system are not known. The direct and indirect models are therefore compared to experimental data under a number assumptions regarding the use of Biacore data and mass-transport. On the basis of these comparisons a method for incorporating Biacore binding data and MLM experiment data is determined.

### 4.4.1 Naive use of binding data

We first assume the data in Table 4.3 is applicable in the MLM system without adjustment. By using all measured data a non-linear least squares fit is required to determine the parameters  $k_{1a,tbim}$ ,  $k_{1a,tbid}$ ,  $k_{4a}$ ,  $k_{4d}$ ,  $k_{5a}$ ,  $k_{6a}$  and  $k_{6d}$  in the direct model and  $k_{4a}$ ,  $k_{4d}$ ,  $k_{5a}$ ,  $k_{6a}$  and  $k_{6d}$  in the indirect model. Conforming with prior experimental knowledge, the Bak deactivation rate,  $k_{1d}$ , is assumed to be very slow,  $k_{1d} = 10^{-6}$ , and is not a fitted parameter. Every unknown parameter is chosen randomly to obey a log-uniform distribution between  $10^{-6}$  and  $10^{-1}$ .

Figure 4.4 and Figure 4.5 show a simulation of the MLM experiment with tBIM and tBid stimulation, respectively, using these fitted parameters and the **direct activation** model. The non-linear coefficient of determination is  $R^2 = 0.11$ . This figure is provided for later comparison and is, on its own, difficult to interpret. Inspection of the simulations, however, shows the model is not accurate. The most obvious problem being the early formation of tBid:Mcl-1 complex, compared with experiment.

Estimating parameters of the **indirect model** provides a significantly worse fit to the experimental data ( $R^2 = -0.09$ , simulations not shown). The problem lies in the Biacore-measured instability of the Bcl-x<sub>L</sub>:Bak\* complex. The comparatively high dissociation rates used here, without adjustment, result in Bak\* dissociating without any addition of BH3-only protein. The subsequent auto-activation of Bak results in cytochrome c release ‘by default’ – without the addition of any BH3-only protein. This is a significant problem with the indirect model implemented in this fashion and needs to be remedied if the direct and indirect models are to be fairly compared.

### Direct activation model, tBIM stimulation, naive use of binding data

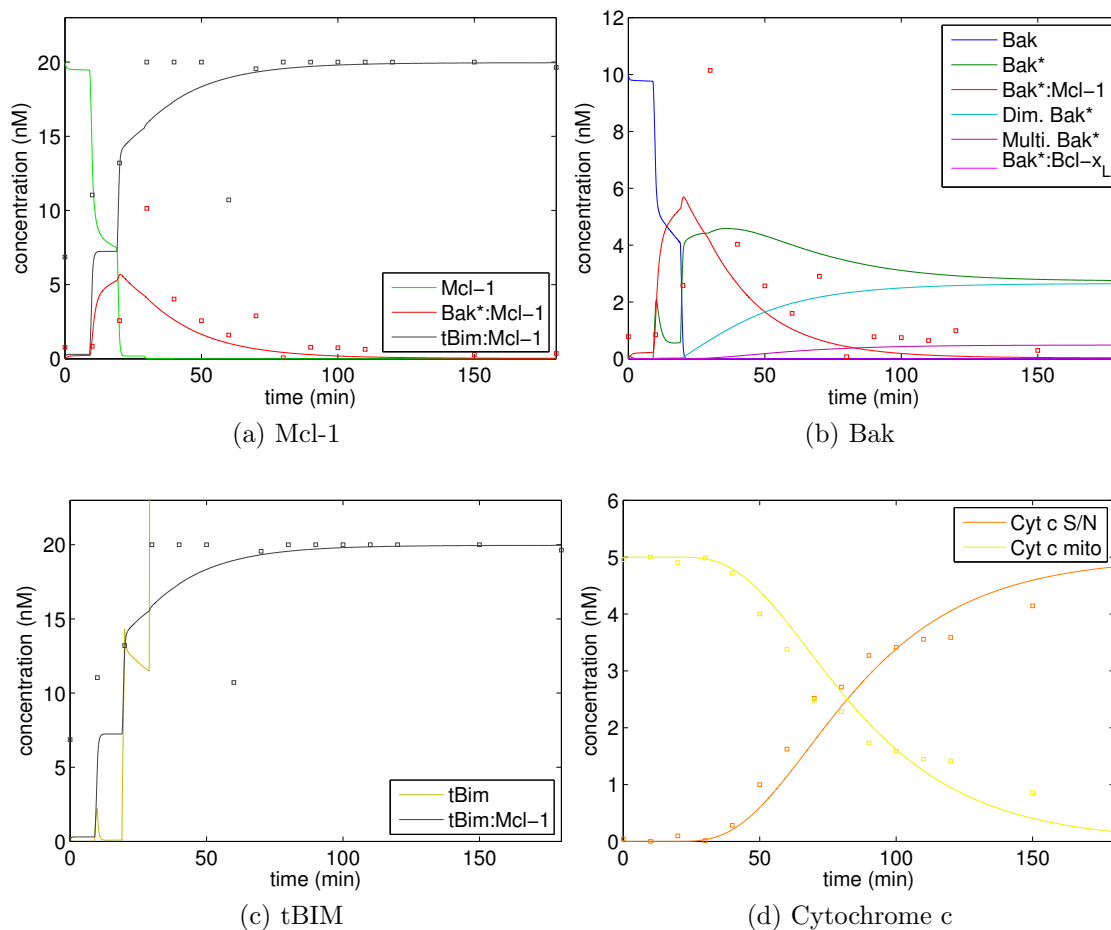


Figure 4.4: Direct activation of Bak via tBIM stimulation. Dynamic simulation of BH3-only spike-in experiment using available Biacore-measured parameters. The remaining unknown parameters are fitted using non-linear least squares ( $R^2 = 0.11$ ). Scale in (c) has been truncated to focus on tBIM:Mcl-1 complex. The curves represent model simulations, the points represent available MLM data points.

### Direct activation model, tBid stimulation, naive use of binding data

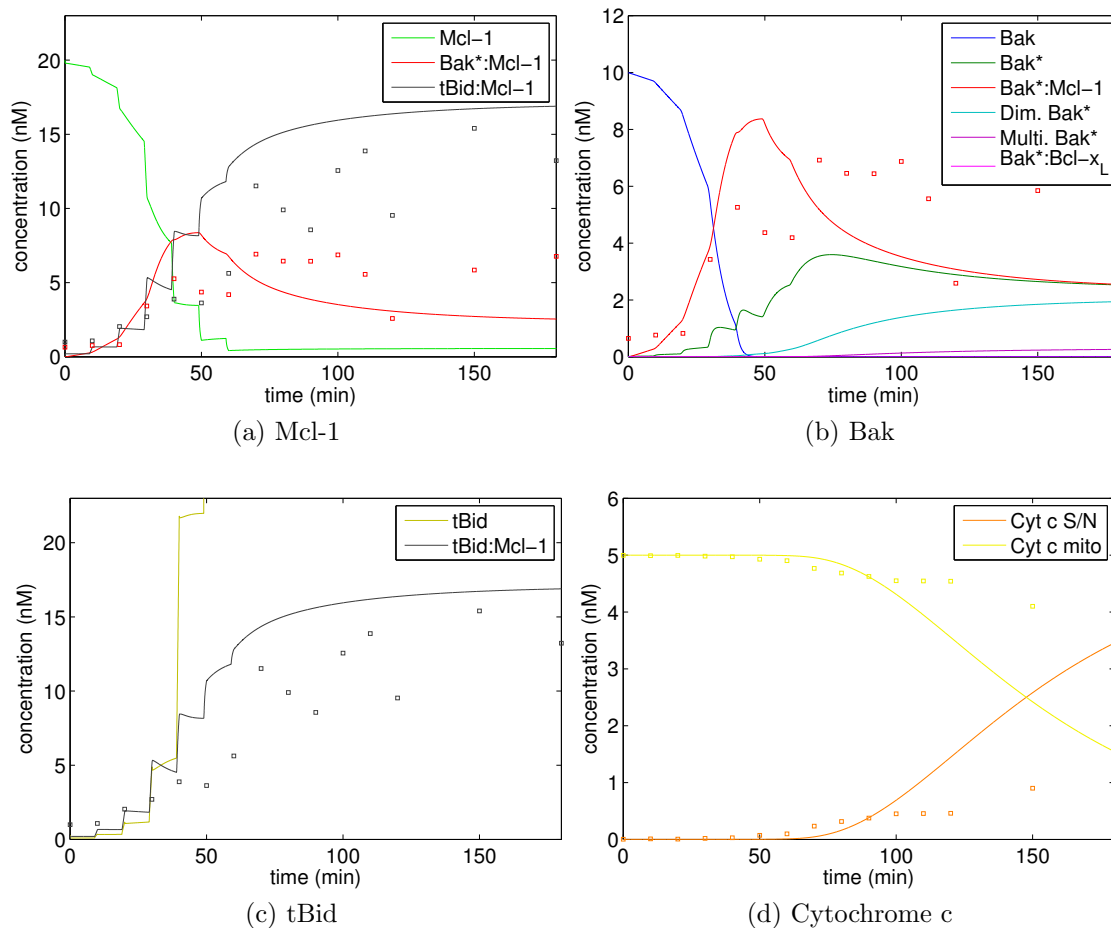


Figure 4.5: Direct activation of Bak via tBid stimulation. Dynamic simulation of BH3-only spike-in experiment using available Biacore-measured parameters. The remaining unknown parameters are fitted using non-linear least squares ( $R^2 = 0.11$ ). Scale in (c) has been truncated to focus on tBid:Mcl-1 complex. The curves represent model simulations, the points represent available MLM data points.

## 4.4.2 Scaled use of binding data

A naive use of Biacore-measured kinetic rates may be inappropriate because the proteins measured are not the exact proteins used in the experiments and most of the interactions occur on or near the membrane which may affect the kinetics. To account for these factors we scale the measured association and dissociation rates by a common factor. In addition to the parameters estimated in Section 4.4.1, a forward scale factor,  $D_f$ , and reverse scale factor,  $D_r$ , are estimated such that, for measured rates:  $v_i = 10^{D_f} v_i^+ - 10^{D_r} v_i^-$ , for each reaction with measured data ( $i \in \{2, 3, 8, 9\}$ ). The initial parameter estimates for  $D_f$  and  $D_r$  are set at 0 and are allowed to vary over 6 orders of magnitude:  $D_f, D_r \in [-3, 3]$ . Again, the Bak deactivation rate is fixed at  $k_{1d} = 10^{-6}$  and unknown initial estimates are set at  $10^{-4}$ .

The direct activation model is fitted to the MLM experiment data ( $R^2 = 0.16$ ). Thus, scaling the Biacore-measured kinetic rates slightly improves the fit of the model to the data. The measured forward rates are multiplied by a factor of  $10^{-0.17}$  and the reverse rates by  $10^{1.1}$ . Given the above-mentioned problem of early tBid:Mcl-1 complex formation it is not surprising a better fit is obtained by a *reduction* in the forward reaction rate and an increase in the reverse reaction rates. Figure 4.6 and Figure 4.7 illustrate the simulated experiment using these fitted kinetic parameters and the direct activation model. The formation of the tBid:Mcl-1 complex has indeed been delayed. However, under tBIM stimulation the transient Bak:Mcl-1 complex appears to dissociate too quickly and under tBid stimulation the transient Bak:Mcl-1 complex peaks at approximately  $t = 30$ mins, which does not match the data.

The indirect activation model is fitted to the MLM experiment data ( $R^2 = 0.16$ , simulation not shown). By scaling the forward rates by  $10^{-1.3}$  and the reverse rates by  $10^{-0.57}$  a significant improvement in the quality of the fit to data is obtained, compared with the initial, ‘naive’ attempt. The levels of the Bak:Mcl-1 complex are too low and the Bak homo-dimerisation takes place too early and cytochrome c is released before observed. The Bak\* : Bcl-x<sub>L</sub> complex steadily dissociates throughout the experiment, and this appears to contribute to the early formation of Bak homo-dimers.

The heuristic introduction of these scale factors lacks any solid theoretical moti-

vation and inspection of Figure 4.6 and Figure 4.7 does not demonstrate a convincing reproduction of what is observed *in vitro* – even if the imprecision of the quantification process is considered.

### 4.4.3 Relative use of binding data

The most sparse way to make use of the available binding data is to assume that only the relative rates for the association and dissociation of tBid:Mcl-1 and tBIM:Mcl-1 and tBid:Bcl-x<sub>L</sub> and tBIM:Bcl-x<sub>L</sub> have meaning. We also assume that on- and off-rates for Bak:Mcl-1 and tBid:Mcl-1 cannot be compared, for example, because one interaction is membrane associated while the other is not. Therefore, *all* kinetic parameters are estimated except for  $k_{3a,tbid}$ ,  $k_{3d,tbid}$ ,  $k_{9a,tbid}$  and  $k_{9d,tbid}$ , whose values are determined by their measured ratio to  $k_{3a,tbim}$ , *etc.* Again, the Bak deactivation rate is fixed at  $k_{1d} = 10^{-6}$  and unknown initial estimates are set at  $10^{-4}$ .

The direct activation model is fitted to the MLM experiment data ( $R^2 = 0.54$ ). Figure 4.8 and Figure 4.9 illustrate the simulated experiment using these fitted kinetic parameters and the direct activation model. Comparison of these figures to those in Section 4.4.2 shows an obvious improvement in fit for both tBid and tBIM stimulation. With tBIM stimulation there is significant cytochrome c release, whilst with tBid stimulation its release is less significant, though, still predicted to occur. This is a result of cytochrome c release being modelled as irreversible. Though this is a reasonable assumption to make, the inevitability of MOMP and cytochrome c release is a flaw in the current model and suggests a more detailed (perhaps stochastic) implementation of membrane pore formation may be required.

The indirect activation model is fitted to the MLM experiment data ( $R^2 = 0.45$ ). Figure 4.10 and Figure 4.11 illustrate the simulated experiment using these fitted kinetic parameters and the indirect activation model. Even with the extra degrees of freedom the indirect model struggles to mimic experimentally observed behaviour. The failure to mimic the observed timing of the Bak:Mcl-1 complex under both tBIM and tBid stimulation reflects the difficulty the indirect model has in finding a balance between Bak auto-activation following BH3-only stimulation and Bak sequestration by Bcl-x<sub>L</sub>, preventing MOMP occurring by default. This suggests the indirect model is in some way less ‘stable’ or ‘robust’ to changes in the relevant kinetic parameters.

### Direct activation model, tBIM stimulation, scaled use of binding data

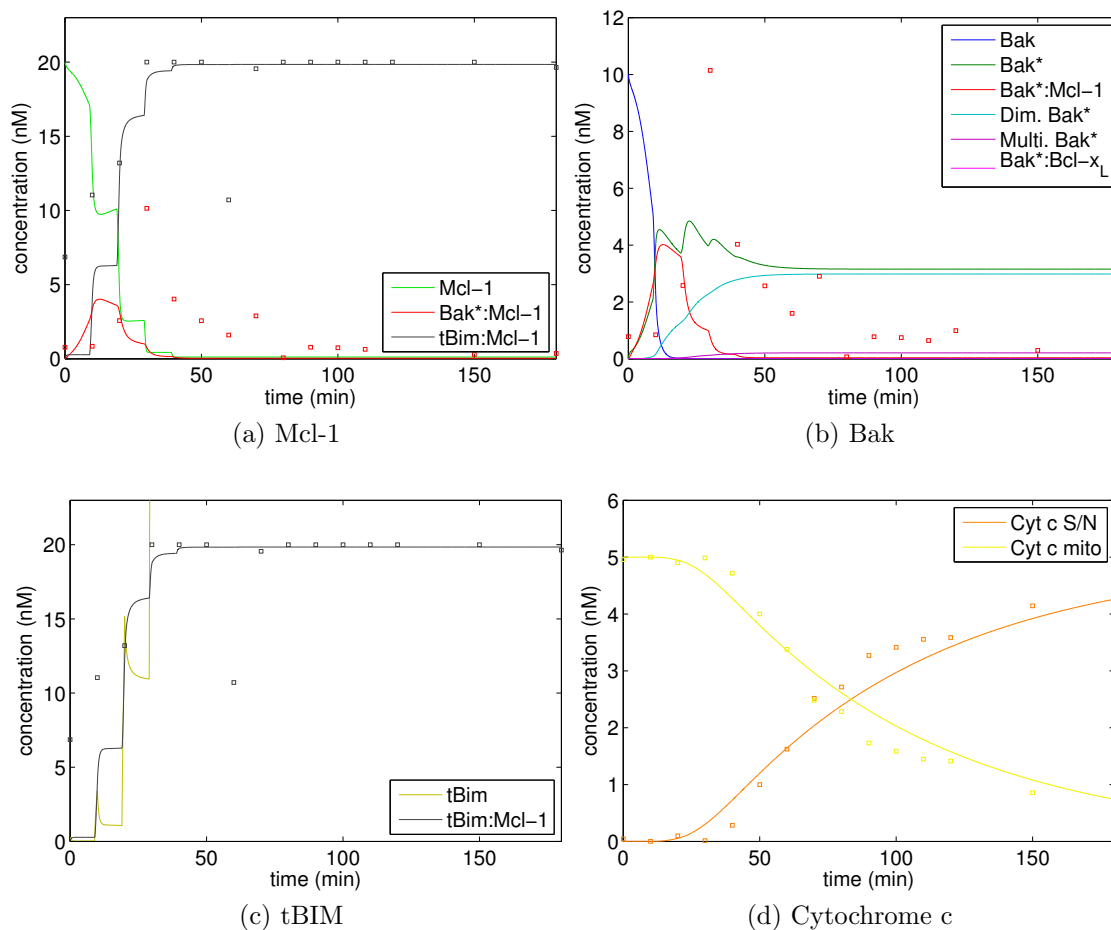


Figure 4.6: Direct activation of Bak via tBIM stimulation. Simulation of BH3-only spike-in experiment using scaled Biacore-measured parameters. The remaining unknown parameters are fitted using non-linear least squares ( $R^2 = 0.15$ ). Scale in (c) has been truncated to focus on tBIM:Mcl-1 complex. The curves represent model simulations, the points represent available MLM data points.

Direct activation model, tBid stimulation, scaled use of binding data

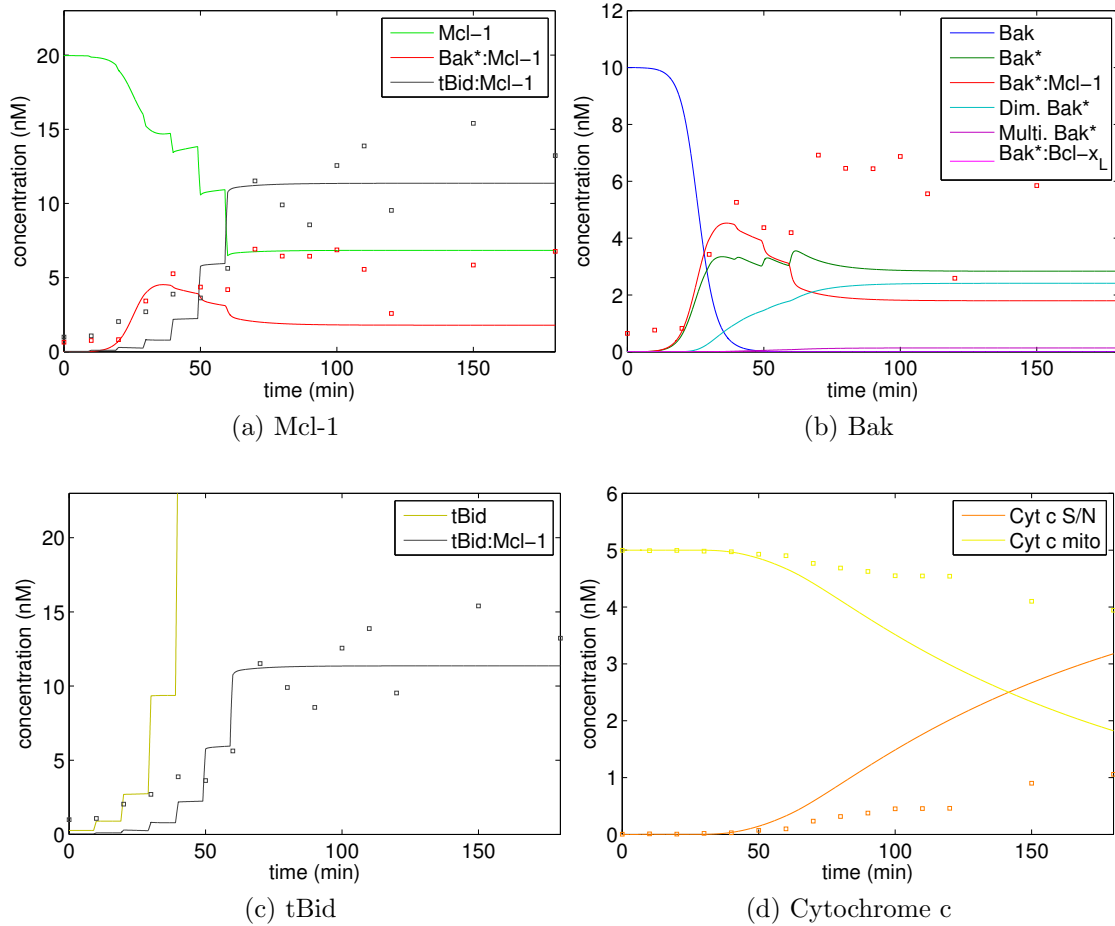


Figure 4.7: Direct activation of Bak via tBid stimulation. Simulation of BH3-only spike-in experiment using scaled Biacore-measured parameters. The remaining unknown parameters are fitted using non-linear least squares ( $R^2 = 0.15$ ). Scale in (c) has been truncated to focus on tBid:Mcl-1 complex. The curves represent model simulations, the points represent available MLM data points.

### Direct activation model, tBIM stimulation, relative use of binding data

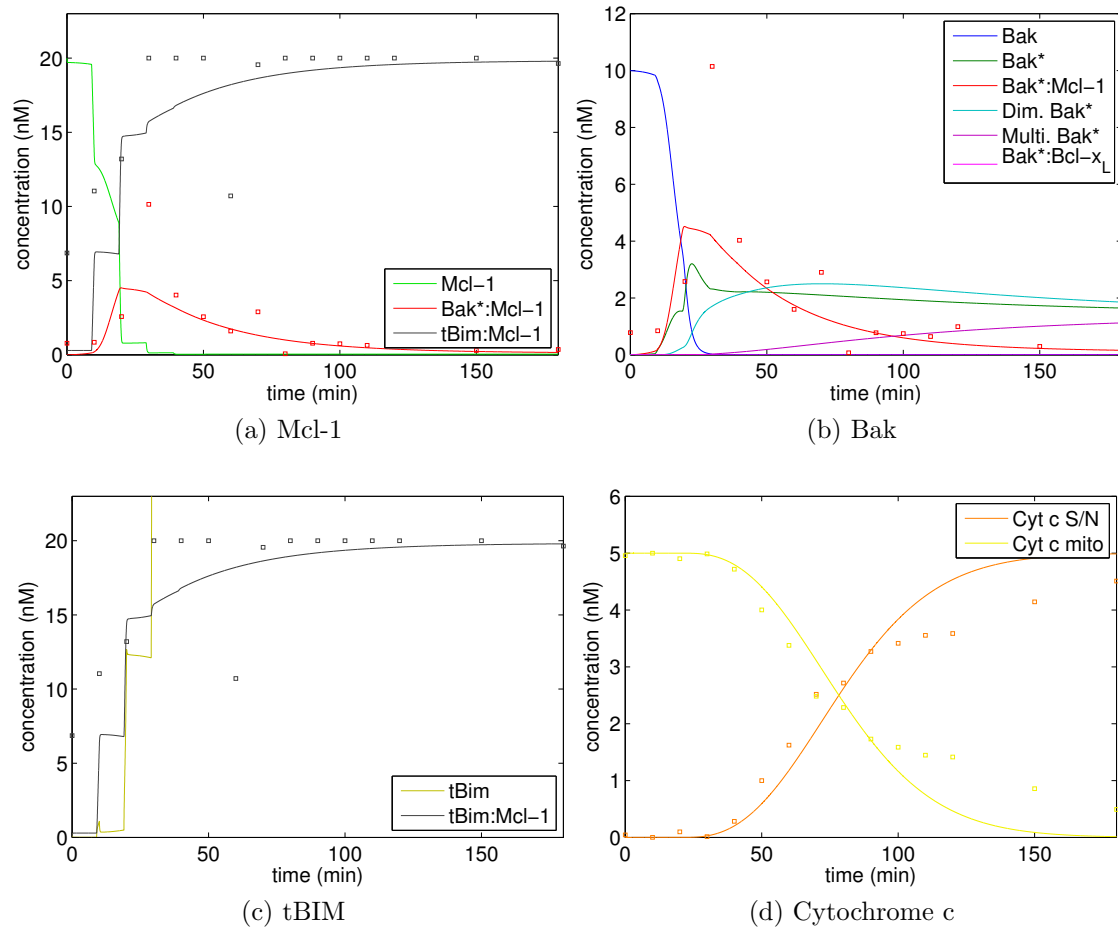


Figure 4.8: Direct activation of Bak. Dynamic simulation of BH3-only spike-in experiment using available Biacore-measured parameters. The remaining unknown parameters are fitted using non-linear least squares ( $R^2 = 0.54$ ). Scale in (c) has been truncated to focus on tBIM:Mcl-1 complex. The curves represent model simulations, the points represent available MLM data points.

### Direct activation model, tBid stimulation, relative use of binding data

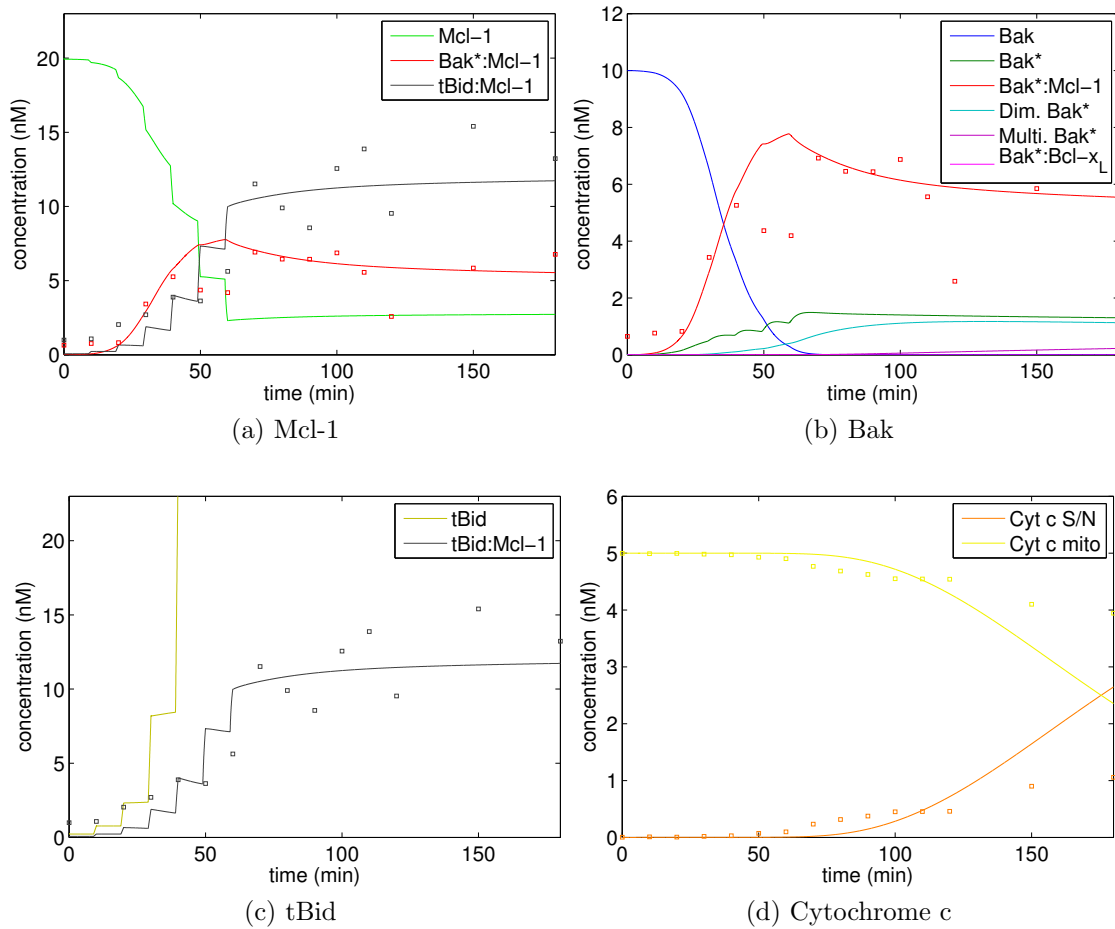


Figure 4.9: Direct activation of Bak. Dynamic simulation of BH3-only spike-in experiment using available Biacore-measured parameters. The remaining unknown parameters are fitted using non-linear least squares ( $R^2 = 0.54$ ). Scale in (c) has been truncated to focus on tBid:Mcl-1 complex. The curves represent model simulations, the points represent available MLM data points.

Indirect activation model, tBIM stimulation, relative use of binding data

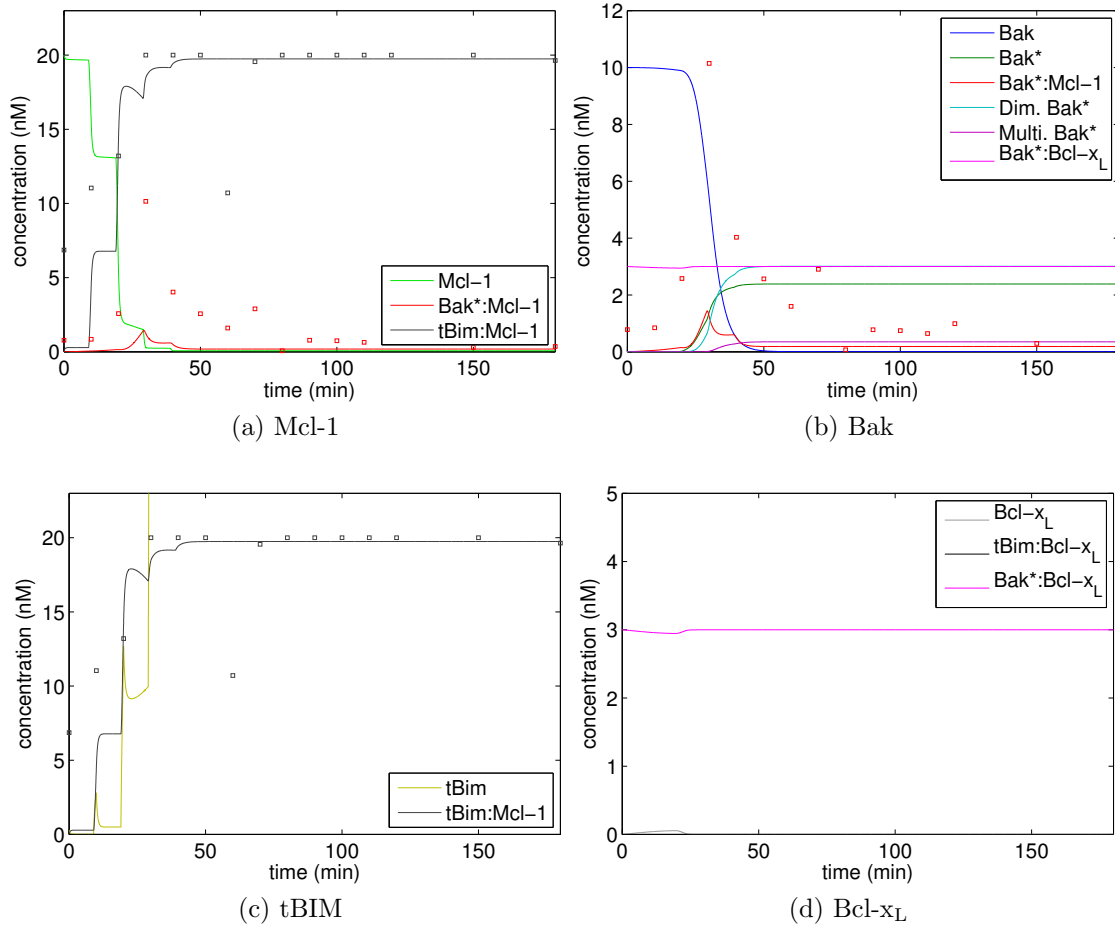


Figure 4.10: Indirect activation of Bak under tBIM stimulation. Simulation of BH3-only spike-in experiment using available Biacore-measured parameters. The remaining unknown parameters are fitted using non-linear least squares ( $R^2 = 0.45$ ). Scale in (c) has been truncated to focus on tBIM:Mcl-1 complex. The curves represent model simulations, the points represent available MLM data points.

Indirect activation model, tBid stimulation, relative use of binding data

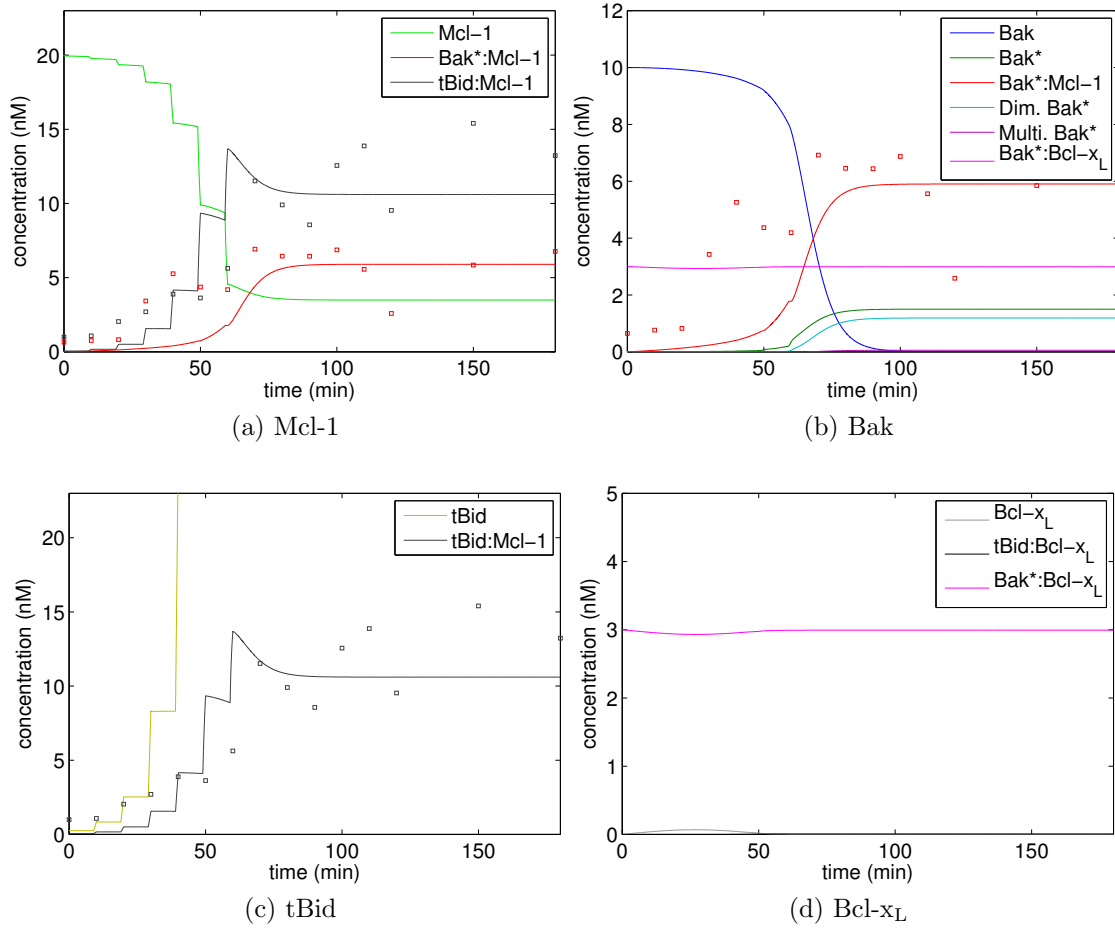


Figure 4.11: Indirect activation of Bak under tBid stimulation. Simulation of BH3-only spike-in experiment using available Biacore-measured parameters. The remaining unknown parameters are fitted using non-linear least squares ( $R^2 = 0.45$ ). Scale in (c) has been truncated to focus on tBid:Mcl-1 complex. The curves represent model simulations, the points represent available MLM data points.

#### 4.4.4 Molecular transport

Finally, rather than an *ad hoc* adjustment of experimentally determined kinetic rates, Section 3.3.3 derived an adjustment to the rate constants applicable when reactions involve solution- and membrane-associated proteins. The following reactions rates are adjusted accordingly:

$$\begin{aligned} k'_{1a} &= \frac{10^6 D k_{1a}}{10^6 D + \hat{B} k_{1a}}, \\ k'_{2a} &= \frac{10^6 D k_{2a}}{10^6 D + \hat{B} k_{2a}}, & k'_{2d} &= \frac{10^6 D k_{2d}}{10^6 D + \hat{B} k_{2d}}, \\ k'_{9a} &= \frac{10^6 D k_{9a}}{10^6 D + X k_{9a}}, & k'_{9d} &= \frac{10^6 D k_{9d}}{10^6 D + X k_{9d}}. \end{aligned} \tag{4.4.1}$$

This allows the experimentally determined kinetic rates to be incorporated in a fashion which accounts for mass-transport effects. The diffusion parameter,  $D$ , is allowed to vary between  $D = 10^{-4}$  and  $D = 10^{-9}$ , with an initial estimate of  $D = 10^{-6}$ , and is fitted with the above-described usages. Figure 4.12 demonstrates the effect the diffusion rate has on a direct activation model.

Table 4.4 lists the goodness-of-fit for each of the above described methods of integrating Biacore binding data with MLM experiment data on both a direct and indirect activation model. The effect on the goodness-of-fit by including a diffusion term is listed.

For each of the preceding corrections described in Section 4.4.1, Section 4.4.2 and Section 4.4.3, the modelling of diffusion effects does not significantly affect the quality of the fit to experimental data. In the tBid signalling case, diffusion slows the formation of the Bak:Mcl-1 complex, which in turn, increases the rate of tBid:Mcl-1 complex formation. (Figure 4.12). Since qualitatively or quantitatively the diffusion-limited models do not appear to provide any advantage in modelling the Bcl-2 family interactions they are neglected from later analysis. The issues in using Biacore-measured kinetic reaction rates do not appear to be a result of mass-transport effects.

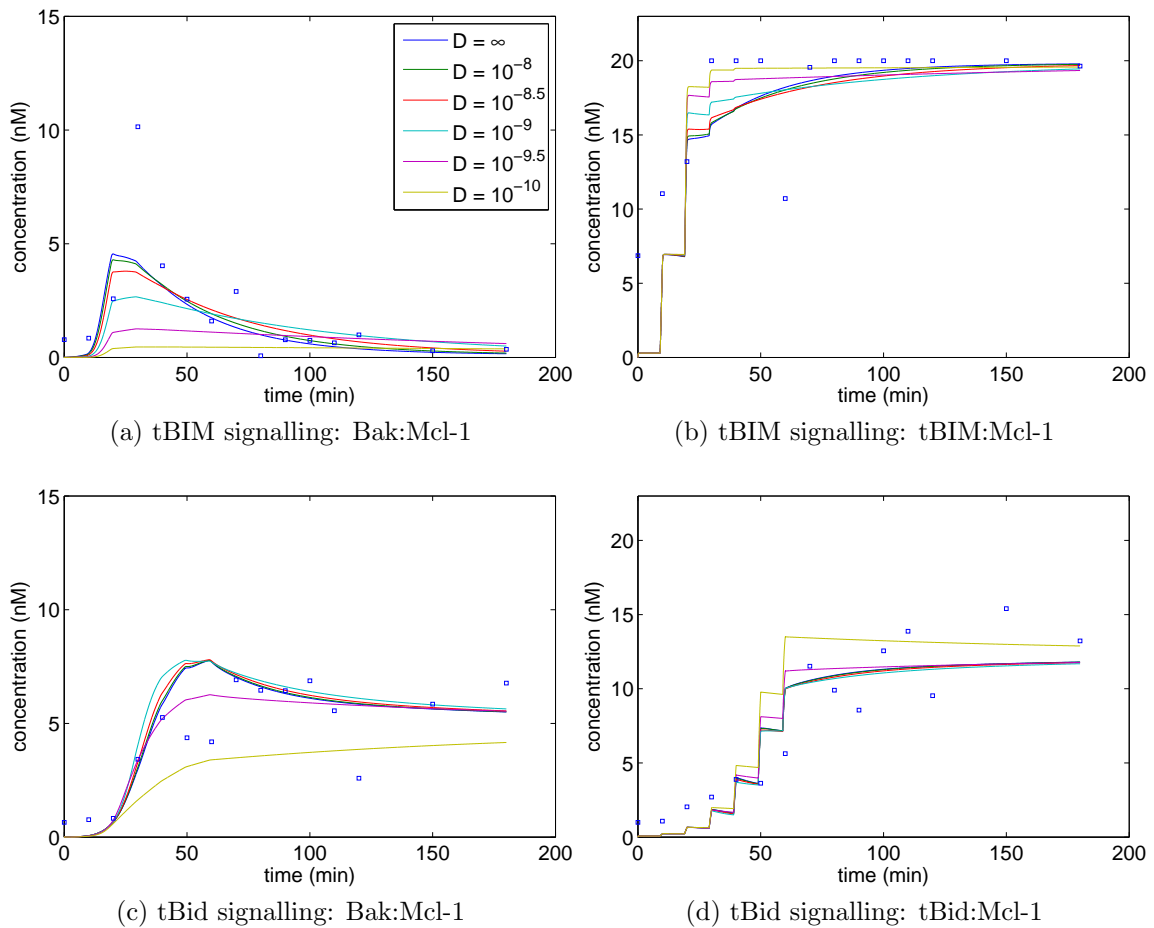


Figure 4.12: Effect of diffusion-limited mass-transport on a direct activation model using tBIM and tBid stimulation. Using fitted kinetic parameters listed in Table 4.6 and a range of diffusion constants. The curves represent simulated concentrations, the points represent densitometry data. Curves in all plots (a)-(d) are identified using the legend in plot (a).

<i>Transport</i>	<i>Binding data</i>	<i>n</i>	<i>R</i> <sup>2</sup>	tBid			tBIM		
				tBid:Mcl-1	Bak*:Mcl-1	tBIM:Mcl-1	Bak*:Mcl-1	tBIM:Mcl-1	Diffusion <i>D</i>
Reaction-limited	Naive	7	0.11	0.18	-0.17	0.37	0.37	-	
	Scaled	9	0.15	0.77	-1.02	0.35	-0.44	-	
	Relative	11	0.54	0.79	0.51	0.42	0.5	-	
Diffusion-limited	Naive	8	0.3	0.42	0.24	0.42	0.25	$1 \times 10^{-9}$	
	Scaled	10	0.27	0.4	0.12	0.35	0.37	$1.05 \times 10^{-8}$	
	Relative	12	0.55	0.8	0.59	0.42	0.5	$5.25 \times 10^{-8}$	

Table 4.4: Goodness-of-fit for direct activation model under various binding and transport assumptions. Non-linear least squares fit. The optimisation problem was solved iteratively using the trust-region reflective algorithm. From log-uniform, random initial parameter estimates within a biologically realistic parameter range ( $10^{-6}$  to  $10^{-1}$ ) the optimisation was performed. For each fitting procedure, 200 initial estimates were sampled. *n* is the number of free parameters fitted.

<i>Transport</i>	<i>Binding data</i>	<i>n</i>	<i>R</i> <sup>2</sup>	tBid			tBIM		
				tBid:Mcl-1	Bak*:Mcl-1	tBIM:Mcl-1	Bak*:Mcl-1	tBIM:Mcl-1	Diffusion <i>D</i>
Reaction-limited	Naive	5	-0.09	-0.06	0	0.37	0.12	-	
	Scaled	7	0.17	0.27	-1.7	0.02	-0.5	-	
	Relative	13	0.45	0.57	0.01	0.38	-0.28	-	
Diffusion-limited	Naive	6	0.03	0.01	0.11	0.37	0.28	$8.91 \times 10^{-5}$	
	Scaled	8	0.21	0.72	-1.4	0.41	-0.4	$3.80 \times 10^{-7}$	
	Relative	14	0.13	0.56	0.11	0.39	-0.29	$3.24 \times 10^{-8}$	

Table 4.5: Goodness-of-fit for indirect activation model under various binding and transport assumptions. Non-linear least squares fit. The optimisation problem was solved iteratively using the trust-region reflective algorithm. From log-uniform, random initial parameter estimates within a biologically realistic parameter range ( $10^{-6}$  to  $10^{-1}$ ) the optimisation was performed. For each fitting procedure, 200 initial estimates were sampled. *n* is the number of free parameters fitted.

#### 4.4.5 Discussion

Given the superior fit obtained by using the binding data in a relative fashion, all later analysis of both the direct and indirect models will use this assumption and the kinetic parameters listed in Table 4.6. Of course, it is not at all surprising that a ‘better’ fit to data will be obtained as the number of parameters to be estimated is increased. However, given the stated deficiencies in the models determined in Section 4.4.1 and Section 4.4.2, a minimal use of measured binding data is necessary. We are ensuring that our models are *consistent* with the binding data but are not constrained by them.

This demonstrates the danger in utilising experimentally determined kinetic rates without regard to their applicability to the present situation. It is not only the absolute value of the measured rates that needed scaling, but their values relative to each other. Thus, care is needed to make effective use of experimentally determined kinetic reaction rates.

In addition to the methods employed above to utilise the kinetic binding data, another approach would be to use the data simply for model validation. This would involve performing the fitting procedure completely unconstrained and then comparing the fitted parameters to the Biacore binding data. This has the benefit of providing independent estimates of important binding parameters which, if consistent with the Biacore data, would provide support that the binding data do indeed represent binding on- and off-rates as they occur *in vitro*. Such an approach is worth pursuing in future incarnations of this analysis. Further, the models built here are ultimately based on a number of stated hypotheses about what interactions are relevant to the MLM experiments. It is possible then that these models are missing relevant interactions, in which case the *structure* or *topology* of the models built would need to be changed.

Comparing the quality of fit for both the direct and indirect model to available experimental data shows, regardless of the inclusion of diffusion effects or use of kinetic binding data, that the direct model is more able to accurately model the timing experiment in the MLM system. The  $R^2$  values reported are not adjusted by the number of parameters fitted but inspection of Table 4.4 and Table 4.5 shows that this is unlikely to affect our findings.

Does this mean that the direct activation of Bak via BH3-only interaction is necessary in order to model MLM experiments? A key difference between the direct and indirect model simulations is the timing of formation of the Bak:Mcl-1 complex. As stated in Section 4.4.3, the inclusion of a direct activating mechanism appears to enable a more dynamic response to BH3-only stimulation thereby producing a model more reflective of the MLM experimental data. The proceeding chapter explores this comparison further.

<i>Reaction</i>	$J_i$	Direct		Indirect	
		On-rate	Off-rate	On-rate	Off-rate
Direct activation (tBid)	1	$k_{1a} = 7.41 \times 10^{-6}$	$k_{1d} = 1 \times 10^{-6}$	-	$k_{1d} = 1 \times 10^{-6}$
Direct activation (tBIM)	1	$k_{1a} = 2.69 \times 10^{-4}$	$k_{1d} = 1 \times 10^{-6}$	-	$k_{1d} = 1 \times 10^{-6}$
Bak:Mcl-1 complex	2	$k_{2a} = 7.94 \times 10^{-4}$	$k_{2d} = 5.25 \times 10^{-4}$	$k_{2a} = 9.55 \times 10^{-3}$	$k_{2d} = 8.51 \times 10^{-3}$
tBid:Mcl-1 complex	3	$k_{3a} = 2.4 \times 10^{-2}$	$k_{3d} = 1.58 \times 10^0$	$k_{3a} = 1.48 \times 10^{-2}$	$k_{3d} = 5.75 \times 10^{-1}$
tBIM:Mcl-1 complex	3	$k_{3a} = 9.55 \times 10^{-3}$	$k_{3d} = 6.31 \times 10^{-3}$	$k_{3a} = 5.89 \times 10^{-3}$	$k_{3d} = 2.29 \times 10^{-3}$
Bak homo-dimerisation	4	$k_{4a} = 3.98 \times 10^{-4}$	$k_{4d} = 5.75 \times 10^{-4}$	$k_{4a} = 5.01 \times 10^{-2}$	$k_{4d} = 9.55 \times 10^{-2}$
Bak auto-activation	5	$k_{5a} = 1.66 \times 10^{-3}$	-	$k_{5a} = 2.00 \times 10^{-3}$	-
Bak multimerisation	6	$k_{6a} = 3.09 \times 10^{-5}$	$k_{6d} = 4.79 \times 10^{-5}$	$k_{6a} = 7.94 \times 10^{-4}$	$k_{6d} = 2.04 \times 10^{-2}$
Cytochrome c release	7	$k_{7a} = 1 \times 10^{-3}$	-	$k_{7a} = 1 \times 10^{-3}$	-
Bak:Bcl-x <sub>L</sub> complex	8	-	-	$k_{8a} = 9.12 \times 10^{-2}$	$k_{8d} = 2.24 \times 10^{-5}$
tBid:Bcl-x <sub>L</sub> complex	9	-	-	$k_{9a} = 4.27 \times 10^{-6}$	$k_{9d} = 8.71 \times 10^{-3}$
tBIM:Bcl-x <sub>L</sub> complex	9	-	-	$k_{9a} = 1.07 \times 10^{-5}$	$k_{9d} = 1.07 \times 10^{-3}$

Table 4.6: Kinetic parameters determined by considering densitometry data and Biacore binding data.

Some reaction rates estimated in Table 4.6 are unknown to experiment (though see the recently published data in [18]). In particular the rate of Bak activation through interaction with tBid or tBIM. The relative value of these rates compared with Bak:Mcl-1 complex association and tBid/tBIM:Mcl-1 complex formation is of biological interest. Successfully using the fitted values for these activation rates in future experiments to predict the timing of cytochrome c release, *etc*, would provide a validation of our model and information about the activity of the BH3-only proteins being tested. This is addressed in Chapter 5. Outside of model validation, the relative value of these kinetic rate parameters can be used to predict the outcome of future MLM experiments using the same stock of protein.

The sparsity of experimental data makes these estimates difficult to assess. Only one instance of the modelled experiment was performed with the same stock of tBid and tBIM meaning that no information about the *variability* between repeat MLM experiments was obtained. It is known that different stocks of BH3-only have different efficacies in activating Bak and this will affect the outcome of the experiments and the kinetic parameter estimates. In the future perhaps a procedure to calibrate the model for different stocks of BH3-only can be developed but this was not explored in the present work.

## 4.5 Conclusion

This chapter examined modelling one experiment in the MLM system. In Section 4.1 the timing experiment was described. An important step in modelling the experiment is determining the unknown kinetic parameters. Section 4.2 describes the details of the parameter estimation and simulation methods used. In Section 4.4 we investigated the best way to incorporate the Biacore binding data and densitometry data into the model. Once this was determined, comparing the fits of direct and indirect model showed that the model including direct activation was more responsive to different BH3-only stimulus and provided a better overall fit to the experiment. Section 4.4.5 highlighted that our model can be used to determine the relative value of kinetic parameters which have yet to be determined experimentally.

# Chapter 5

## Exploring apoptosis *in silico*

The previous chapter dealt with fitting to and predicting experiments from the MLM system. This chapter analyses these fitted models and the kinetic model more generally.

### 5.1 On the role of auto-activation

To investigate the differences between the direct and indirect activation models a ‘hybrid’ activation model, which includes both mechanisms, is built. Both the direct activation parameter  $k_{1a}$  and the Bcl-x<sub>L</sub> interaction parameters ( $k_{8a}$ ,  $k_{8d}$ ,  $k_{9a}$  and  $k_{9d}$ ) are allowed to be non-zero. This helps determine if the differences between the direct and indirect models are a result of the direct activation pathway or the presence/absence of endogenous Bak\*:Bcl-x<sub>L</sub> complexes.

Using the parameters determined by a non-linear least square fitting procedure ( $R^2 = 0.52$ , simulation not shown), we investigate the importance of the direct activation mechanism in the hybrid model. For the hybrid model we compute the total concentration of Bak which is activated via direct activation ( $\Gamma_d$ ) and via auto-activation ( $\Gamma_a$ ):

$$\Gamma_d = \int_0^S k_{1a}B(t)T(t) dt, \quad \Gamma_a = \int_0^S k_{5a}B(t)\hat{B}(t) dt, \quad (5.1.1)$$

where  $S$  is the time of experiment in seconds and  $B$ ,  $\hat{B}$  and  $T$  represent concentration

of Bak, Bak\* and Act in nano-molar, respectively.

Simulations of the MLM experiment with the hybrid model, using (5.1.1), show approximately 99% of Bak is directly activated under tBid stimulus and approximately 99% is directly activated under tBIM stimulation. This suggests that the direct activation is needed to match the observed tBid:Mcl-1 and Bak:Mcl-1 complex formation under tBid stimulation. Indeed, Figure 5.1 demonstrates the detrimental effect removing this pathway from the model has on the fit to data, whilst also demonstrating the minimal effect removing the auto-activation pathway has. In this simulated MLM experiment, with tBid stimulation, the direct pathway is necessary to model the timing of Bak activation and the formation of the Bak:Mcl-1 complex.

We have demonstrated that only by including direct activation can we model this particular MLM experiment. The inclusion of endogenous Bcl-x<sub>L</sub> has little effect on our ability to model the experiment. Of course, this result is specific to the models implemented and the experiments modelled.

## 5.2 On the role of bistability

Previous studies have discussed the role bistability or hysteresis effects play in the control of apoptosis by the Bcl-2 family proteins [48, 54, 55, 47, 49]. These studies demonstrate that deterministic models based on the direct activation hypothesis have the capacity to exhibit bistable behaviour. This bistability is shown to be bolstered by a positive feedback loop caused by Bak auto-activation. The presence of a *robust* (with respect to parameter variation) bistable switch is identified as a biologically plausible control mechanism for the intrinsic apoptotic pathway.

In contrast to those studies, the present models are not designed to model Bcl-2 interactions *in vivo* but rather are designed to mimic behaviour in MLM experiments. Importantly, these experiments represent *isolated* systems – energy and material is not allowed to flow freely into and out of the environment. A closed system is clearly unable to capture a living system in its entirety. It can be proven mathematically that closed biochemical systems, given sufficient time, approach a unique thermodynamic equilibrium. In contrast, open systems are able to achieve a *non-equilibrium steady state* which is not necessarily unique. In these settings bistability is therefore not a consideration [78].

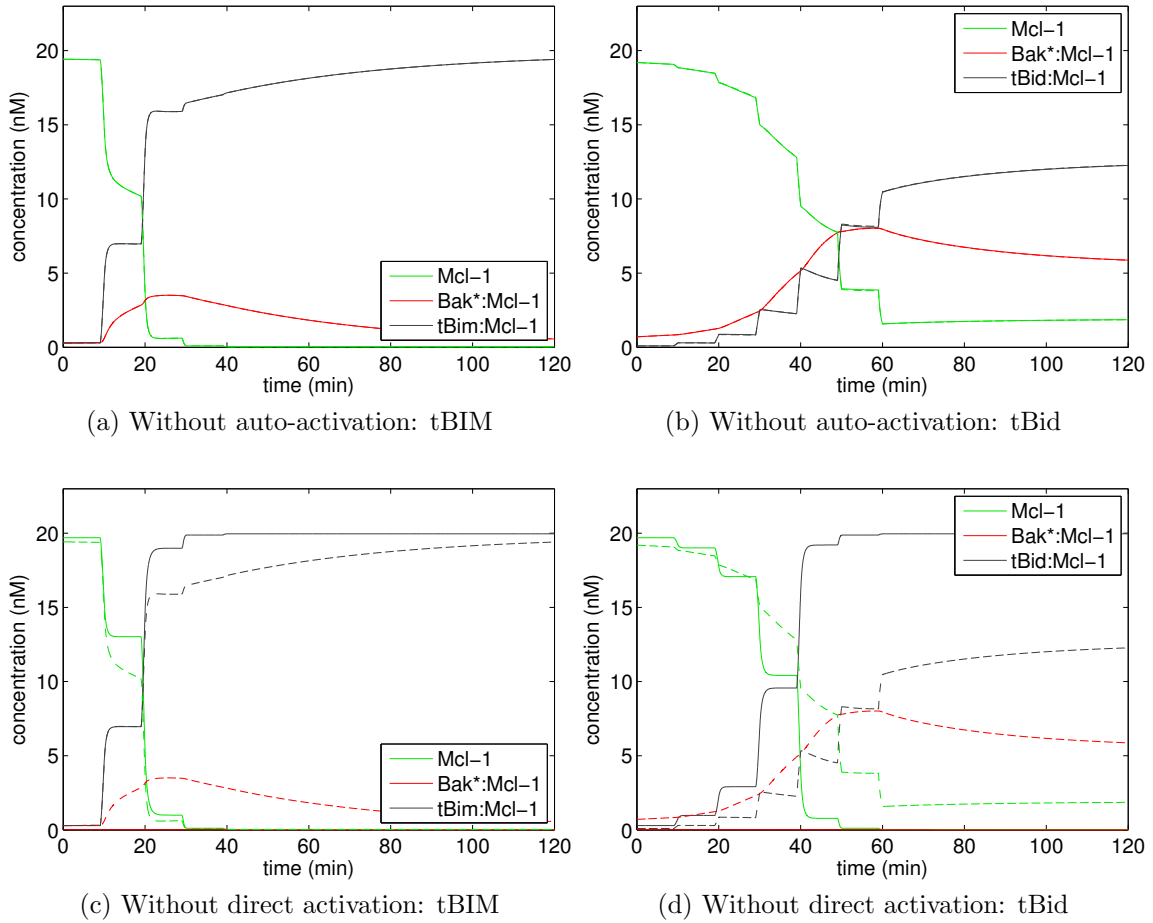
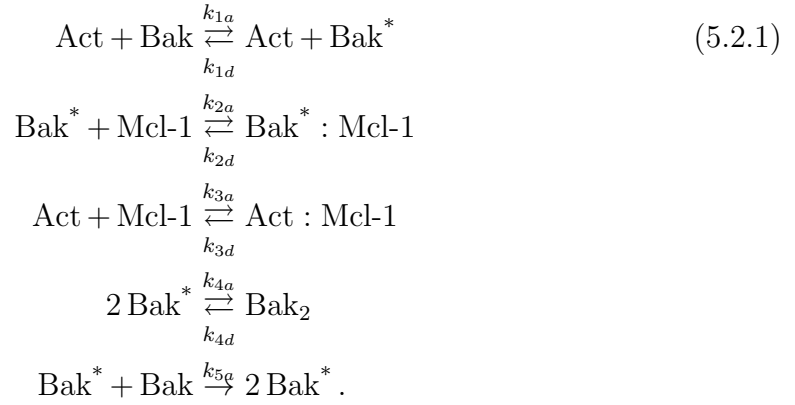


Figure 5.1: Alternative direct activation model, including endogenous Bcl-x<sub>L</sub>. The role of the direct activation pathway ( $k_{1a} = 0$ ) and the auto-activation pathway ( $k_{5a} = 0$ ) is demonstrated by removing each of them separately. Dotted lines represent the complete ‘hybrid’ model concentrations. Solid lines represent reduced model concentrations. For clarity only species involving Mcl-1 are shown.

### 5.2.1 Bifurcation analysis of a reduced fitted model

However, to compare the fitted model we have constructed to those used in other studies, the possibility of bistability in a modified, open model, which contains protein production and degradation terms is examined. Bifurcation analysis is performed on a simplified model which includes production and degradation but does not include Bcl-x<sub>L</sub>. We have argued that auto-activation as a result of endogenous BH3 disruption of the Bak\* : Bcl-x<sub>L</sub> complex does not play a dominant role in our experiments. The simplified reactions we study are



Reactions involving Bcl-x<sub>L</sub> are removed and, since they do not affect the dynamics of the remainder of the reactants, Cyt-c<sub>C</sub> and Cyt-c<sub>M</sub> are also removed. The Bak dimers are changed from tetramers to homodimers. Since cytochrome c is not a part of the model, a non-negligible concentration of Bak<sub>2</sub> is taken as the indicator of commitment to apoptosis.

As before, let  $\mathbf{x} = (B, A, M, \hat{B}, \hat{B}_2, \hat{A}_M, \hat{M})$  be the state vector. The variable names are listed on page 44. A constant production,  $\mathbf{p} = (p_1, p_2, p_3, 0, 0, 0, 0)^T$ , and first-order degradation at rate  $u$  is added by including in each rate expression:

$$\frac{dx_i}{dt} = \mathbf{S}_{bcl2,i} \cdot \mathbf{J}_{bcl2}(\mathbf{x}) + p_i - ux_i.$$

Note that only the production rates for Bak, the activating BH3-only and Mcl-1 – the uncomplexed proteins – are non-zero.

The reduced set of equations is

$$S_{bcl2} = \begin{pmatrix} -1 & 0 & 0 & 0 & -1 \\ 0 & 0 & -1 & 0 & 0 \\ 0 & -1 & -1 & 0 & 0 \\ 0 & 0 & 0 & 1 & 0 \\ 1 & -1 & 0 & -2 & 1 \\ 0 & 0 & 1 & 0 & 0 \\ 0 & 1 & 0 & 0 & 0 \end{pmatrix}. \quad (5.2.2)$$

The reaction-rate vector is

$$\mathbf{J}_{bcl2} = \begin{pmatrix} k_{1a}BA - k_{1d}\hat{B} \\ k_{2a}M\hat{B} - k_{2d}\hat{M} \\ k_{3a}AM - k_{3d}\hat{A}_M \\ k_{4a}\hat{B}^2 - k_{4d}\hat{B}_2 \\ k_{5a}\hat{B}B \end{pmatrix}. \quad (5.2.3)$$

We investigate bistability numerically. The bifurcation software AUTO [45] is used to discover steady-states of the model when the activator production rate is varied – this is presumed to be the trigger for apoptosis *in vivo*. Kinetic parameters are taken from those fitted in Chapter 4, provided in Table 4.6. The degradation rate is set to  $10^{-4}$  and the production rates are set to  $p_1 = 10^{-4}$ ,  $p_2 = 2 \times 10^{-4}$  and  $p_3 = 8 \times 10^{-3}$ . Figure 5.2 demonstrates that, for both tBid and tBIM stimulation, the model does not exhibit bistability. This supports the argument that bistability is not a requisite feature of a Bcl-2 family model to regulate cytochrome c release. The continuation also demonstrates that tBIM acts as a better instigator of apoptosis as it takes a lower production rate of tBIM compared with tBid to produce a persistent Bak<sub>2</sub> complex. This is expected given the kinetic parameters used.

Next we ask the question if it is the topology of the model which excludes the possibility of bistability or if it is our choice in parameters. Figure 5.3 demonstrates that the model is indeed capable of acting as a bistable switch for a set of nearby kinetic parameter values.

Once these parameter values are found, the ‘robustness’ to other parameter vari-

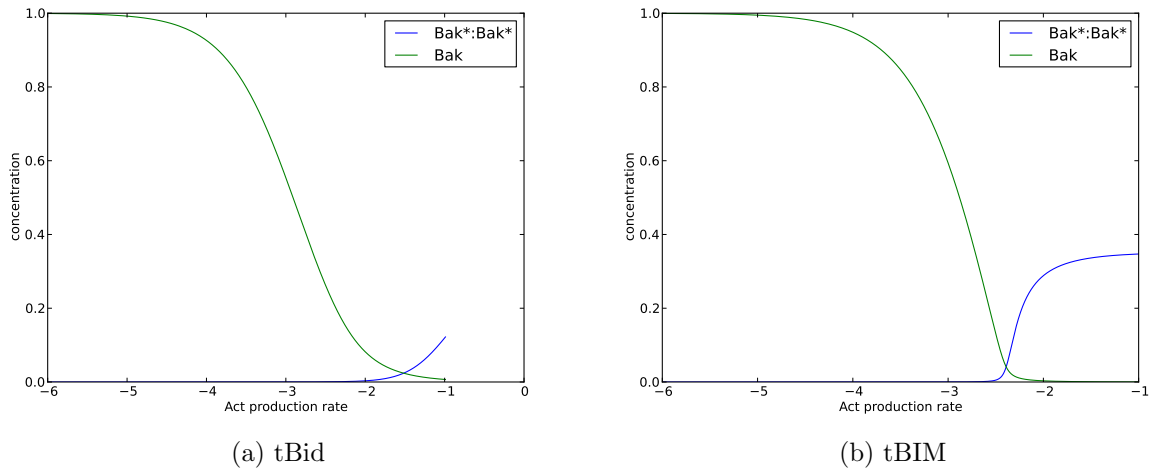


Figure 5.2: Production rate of activator ( $p_2$ ) is varied and the steady-state concentration of Bak and Bak\* homodimer is observed. Kinetic parameters are those listed for the direct activation model on page 44, obtained from fitting to MLM experiment. The production rate  $p_2$  is plotted on a  $\log_{10}$ -scale.

ations can be determined. A two parameter continuation is shown in Figure 5.4, in which the size of the  $p_2$  bistability region is plotted as a function of the value of the production rate of Bak ( $p_1$ ). Note that only for a small range of  $p_1$  values is the bistability a reversible process. For a wider range of values the bistable mechanism acts as an essentially irreversible switch – the commitment to apoptosis is difficult to undo.

## 5.2.2 Robustness of bistability

The concept of robustness of bistability can be explored further. Instead of picking a particular parameter set from experimental data we can randomly sample the parameter space and answer questions about bistability in the system more generally. Since the kinetic parameters vary over several orders of magnitude, a set of 1000 kinetic parameter values was chosen from a log-uniform distribution between the values  $10^{-6}$  and  $10^{-1}$ . The production rates were the same as those in the above analyses. On each parameter set continuation was performed, again using the activator production rate  $p_2$  as the continuation parameter.

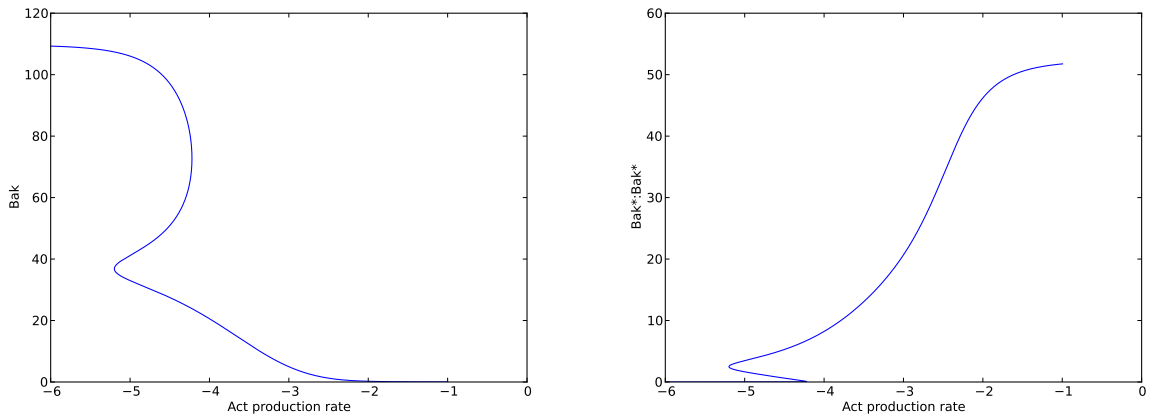


Figure 5.3: Production rate of activator ( $p_2$ ) is varied and the steady-state concentration of Bak and Bak\* homodimer is observed. Kinetic parameters are as follows:  $k_{1a} = 5 * 10^{-3}$ ,  $k_{1d} = 10^{-4}$ ,  $k_{2a} = 5 * 10^{-3}$ ,  $k_{2d} = 10^{-3}$ ,  $k_{3a} = 10^{-3}$ ,  $k_{3d} = 10^{-3}$ ,  $k_{4a} = 2 * 10^{-4}$ ,  $k_{4d} = 2 * 10^{-2}$ ,  $k_{5a} = 2 * 10^{-4}$ .

In the reduced model 20.7% of the parameter sets exhibited bistability manifested by the presence of saddle node bifurcations.<sup>1</sup> Interestingly if for each parameter set the parameter for the Bak activation rate ( $k_{1a}$ ) is set equal to zero and the continuation analysis is performed again only, 1% exhibit bistability. Removing the direct activation pathway from the model creates an indirect activation model and, in a sense, then provides a comparison between the direct and indirect mechanisms. In this case the direct model is more robust to parameter variation than the indirect model. This is the finding of [54] so it is not surprising to find it recapitulated here for a similar model.

For the reduced, direct model, Figure 5.5 shows the distribution of  $p_2$  values at which bifurcations occurred. Only the irreversible bistable parameter sets (which contain only one limit point) are shown. A similar plot for the reversible bistable parameter sets could also be produced, showing the distribution of the size (in terms of orders of magnitude) of the bistable region, however the reversible bistable

<sup>1</sup>A saddle node bifurcation occurs at a given continuation parameter value  $s^*$  and fixed point value  $x^*$  when to the left/right of  $s^*$  there are no fixed points and to the right/left of  $s^*$  there are two fixed points – one stable and one unstable. For example, Figure 5.3 shows two such bifurcation points, which delimit the bistable region.

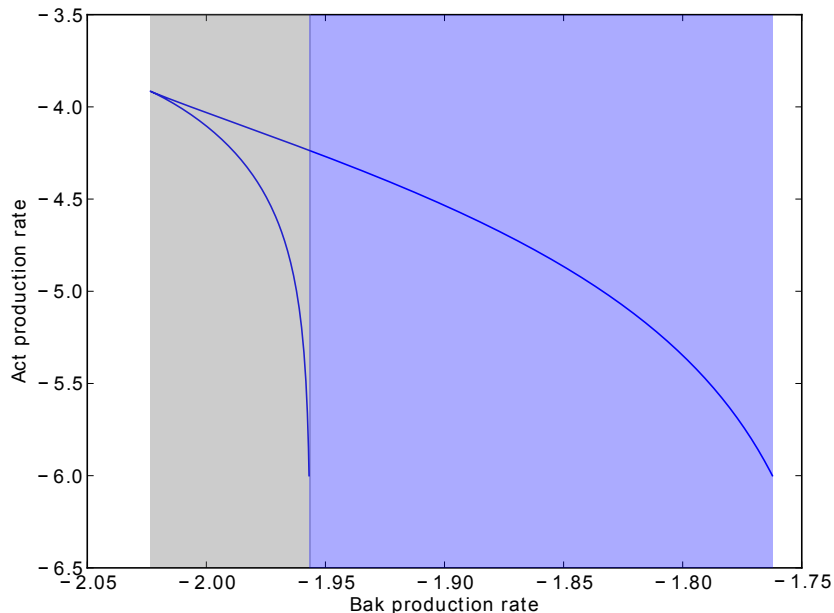


Figure 5.4: Two parameter continuation of reduced model using kinetic parameters from Figure 5.3. Curves represent saddle node bifurcations and enclose a bistable region. The shaded grey box represents values of Bak production rate ( $p_1$ ) which produce reversible bistability when activator production rate ( $p_2$ ) is varied. The shaded blue region represents values of  $p_1$  in which the bistability is essentially irreversible – once the Bak dimer is formed  $p_2$  would have to be reduced to very small values (less than  $10^{-6}$ ) to reverse to process. White regions represent values of  $p_1$  in which no bistability is present.

parameter sets were too few ( $n = 17$ ) to produce an informative histogram. The relative rarity of reversible bistable parameters is perhaps not surprising given the size of the reversible and irreversible regions shown in Figure 5.4, although in that figure it was a production rate that was varied, not the kinetic parameters.

### 5.2.3 Discussion

Though bistability remains a possibility within our model, it does not play a role in the MLM experiments herein performed and likely does not play a role in a model *in vivo* system based on the same determined parameters. This suggests that control of MOMP is possible without resorting to a bistable switch. Indeed, certain

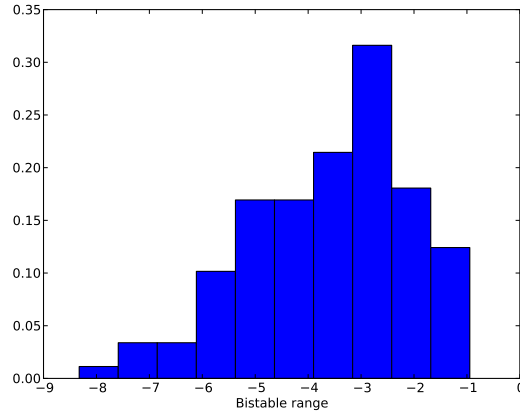


Figure 5.5: Histogram of  $p_2$  bifurcation values from set of randomly sampled parameters. Only sets exhibiting irreversible activation are shown. Mean = -3.62, Std = 1.50.

requisite features of the developed bistable systems (*e.g* [47]) may be biologically unrealistic, and this raises doubts as to their relevance *in vivo*. These features are the reversibility of Bak activation and the significant role of Bak auto-activation. Neither of these are known to occur on a relevant timescale compared to the other interactions being considered.

There is also the possibility that studying what happens at dynamical equilibrium is not reflective of what happens *in vivo*. Indeed, in their study on the ‘snap-action’ response of the apoptotic pathway Albeck *et al* [58] write that, given all the other processes occurring prior to and following cytochrome *c* release, cellular decisions may have been made long before any dynamical steady states are reached and that bistability may not be needed for a signal transduction system to commit to a decision. Bistability in the specific sense studied in this chapter is an attractive concept in systems biology for its ability to act as a robust biological switch between two candidate cell states and for its dynamical simplicity. It is not necessarily the only means by which a cell can make the decision to commit to apoptosis, however.

## 5.3 Sensitivity analysis

In addition to investigating the robustness of bistability in the model we also study the robustness or sensitivity of the simulations to parametric variation. As outlined in Section 2.2.3, we will use the sensitivity metric employed in [42]. The metric gives a measure of the proportional response of a given species concentration throughout a simulation to a proportional perturbation in one of the kinetic parameters. The sensitivities are then unitless quantities. A species with low sensitivity can be described as robust.

### 5.3.1 Local analysis

Figure 5.6 shows the robustness of the hybrid model presented in Section 5.1 for tBid and tBIM stimulation respectively. A notable difference is observed between the overall sensitivities of tBid stimulation compared with tBIM. For instance, under tBid stimulation the cytosolic concentration of cytochrome c and of the multimerised Bak shows remarkable sensitivity to most parameters, in particular  $k_{2a}$  or the association rate of the Bak : Mcl-1 complex. Since under tBid stimulation the concentration of cytochrome c release is small (see for example Figure 4.9) the *proportional* change is naturally going to be more sensitive to changes in absolute concentrations. However, the sensitivity to  $k_{2a}$  remains striking. In this instance, more than any other parameter, the association rate of Bak:Mcl1 exerts control over whether cytochrome c is released from the mitochondrial membrane. This is an insight which can be tested experimentally. If the formation of the Bak:Mcl-1 complex plays a large role in the release of cytochrome c then, with tBid stimulation, even small changes in the endogenous levels of Bak or the added levels of Mcl-1 should have a large effect on cyt c release timing.

In contrast, under tBIM stimulation, when the unperturbed system predicts cytochrome c release, the sensitivity of cytochrome c release is greatly diminished. In particular, the sensitivity to the parameter  $k_{2a}$  no longer stands out. For this set of parameter values, given tBIM's activation strength, cytochrome c release is inevitable and perturbing the parameter values slightly is unlikely to change this outcome. Converse to the above prediction, with tBIM stimulation our analysis

suggests that varying the concentration of endogenous Bak or added Mcl-1 should have less of an effect on the timing of cytochrome c release.

The two figures taken together show that under different types of BH3 stimulation different complexes play different levels of importance in the regulation of MOMP. This complicates our understanding of Bcl-2 induced apoptosis. Sensitivity analysis can provide insight into the mechanisms which are relevant and under which situations they arise. Interestingly, [42] report that the most downstream parts of the model are quite robust – indicating strong overall robustness of the pathway. This is in contrast to our findings which suggest that the most downstream components of the model (cytochrome c release) can be some of the *least* robust. Perhaps this is because of the minimal role auto-activation appears to be playing in the simulations and the lack of bistability in the system, since feedback loops can play a stabilising role in the dynamics.

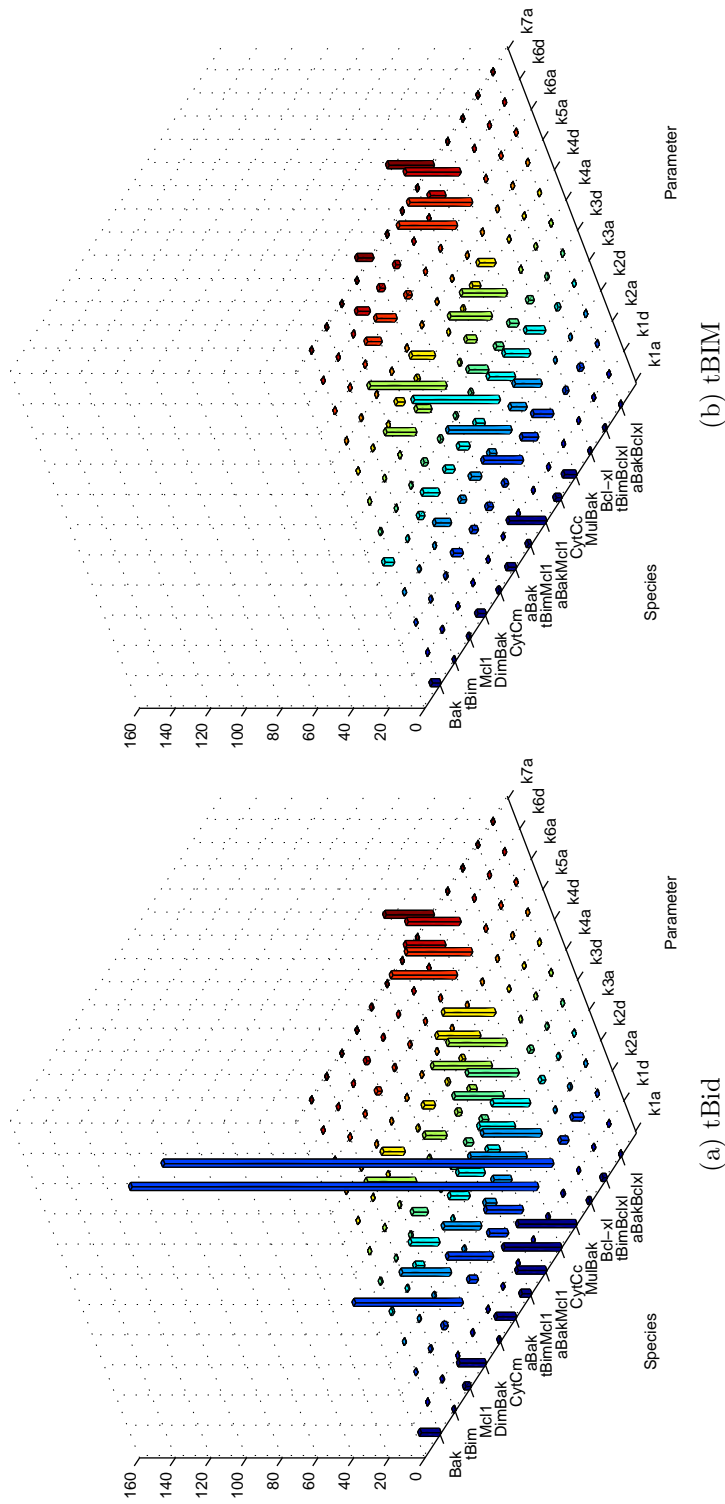


Figure 5.6: Local sensitivity analysis for hybrid model with (a) tBid and (b) tBIM stimulation. Height of each column represents the ‘sensitivity’ of each indicated species as a result of perturbing the indicated parameter by 10%. Initial concentrations and timing of tBid stimulation are taken from the timing experiment modelled in Section 4.4.

### 5.3.2 Global analysis

We can again consider the robustness of the model more generally if we sample the parameter space as with the bifurcation analysis. Figure 5.7 shows the mean sensitivity of each species and parameter pair for a set of 2000 randomly sampled sets chosen from a log-uniform distribution between  $10^{-6}$  and  $10^{-1}$ . Some obtained sensitivities are very large in magnitude and some very small, to the point that the plot must be shown on a log scale. The most sensitive species are again cytochrome c and the dimerised Bak, as in the ‘local’ sensitivity analysis above. This suggests that in general our model does not provide robust regulation of apoptosis. Of course, as noted, there can be marked differences in the dynamics for a model with and without production and degradation rates. In the present simulations, without the possibility of dynamical phenomena such as bistability, we should not expect the system to operate in a robust fashion. It is interesting to note the parameters which cause the largest variation in the model are the association rate of Bak:Mcl1 complex (as before) and the dissociation rate of the Act:Mcl1 complex. Future MLM experiments can test the hypothesis that these parameters have a large influence on whether cytochrome c is released in a timely fashion or not. On the other hand, the parameter having least effect on the simulations is sensibly the rate of cytochrome c release in the presence of Bak dimers ( $k_{7a}$ ). This is expected, given that the release of cytochrome c does not effect the rest of the model.

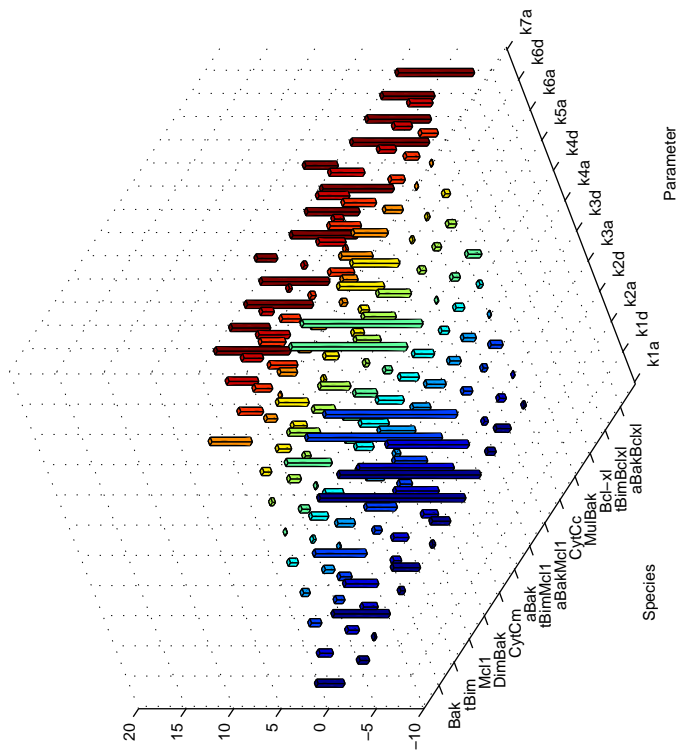


Figure 5.7: ‘Global’ sensitivity analysis for hybrid model, where 2000 log-uniform randomly selected kinetic parameters are selected between  $10^{-1}$  and  $10^{-6}$ . Initial concentrations and timing of BH3-only stimulation are taken from the timing experiment modelled in Section 4.4. The mean sensitivities are here shown for each species and parameter. Some parameters are *very* sensitive, some are *very* insensitive so the y-axis has a log scale.

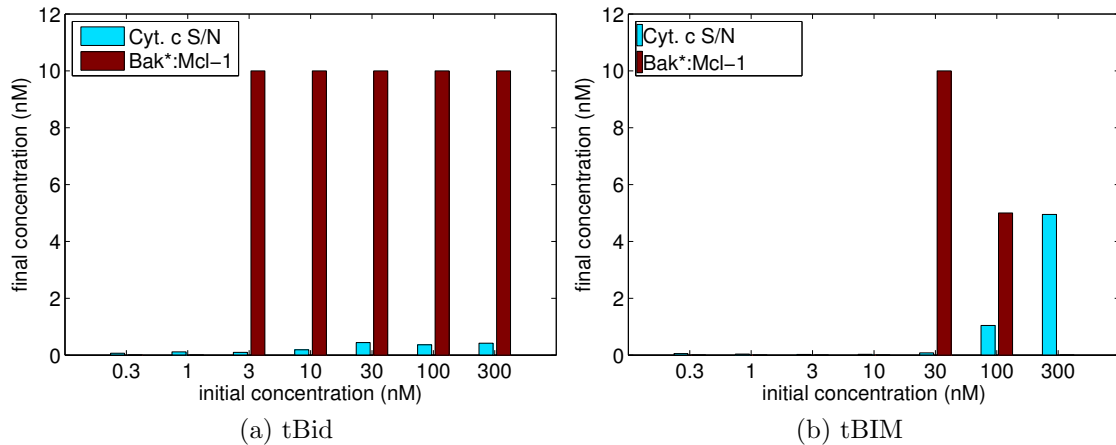


Figure 5.8: MLM experiments demonstrating Mcl-1 blocking tBid from releasing cytochrome c and Mcl-1 not blocking tBIM from releasing cytochrome c. See western blot data in Figure 1.6. Each column represents a separate mitochondrial incubation in which 20nM Mcl-1 and the specified level of BH3-only stimulus is spiked-in to the system. Unlike the timing experiment in Figure 4.1, samples are all taken following two hours incubation.

## 5.4 Modelling other experiments

This section uses the fitted model to predict the outcome of another experiment performed with the MLM system. Here, the direct and indirect models are used to predict cytochrome c release in the experiment outlined in Figure 5.8.

The experiments demonstrate that tBid stimulation is not able to produce significant cytochrome c release in the presence of Mcl-1, whereas tBIM is able to. Binding data indeed suggest that tBIM binds more strongly with Mcl-1 than tBid, and therefore can disrupt the Bak:Mcl-1 complex. Plots are interpreted qualitatively: the Bak:Mcl-1 complex is present or is not present and either cytochrome c has been released or has not. The western blot on which this data is based is illustrated in Figure 1.6.

### Model predictions

The direct and indirect models specified in Table 4.6 are used to predict the concentration of Bak\*:Mcl-1 and multimerised Bak following two hours incubation as

per the experiment (Figure 5.9 and Figure 5.10). Multimer Bak is used as a surrogate for cytochrome c release since cytochrome c release is, in the current models, inevitable regardless of the concentration of BH3-only stimulus.

Over the range of concentrations tested, a clear Bak<sup>\*</sup>:Mcl-1 complex and minimal Bak multimerisation is predicted with the direct model and tBid stimulation. With increasing tBIM stimulation the model predicts increasing and subsequently decreasing Bak<sup>\*</sup>:Mcl-1 concentration and slowly increasing Bak multimerisation. This is in contrast with the discrete drop in Bak:Mcl-1 concentration and release of cytochrome c in observed experimentally between 3nM and 10nM tBIM. Given the stoichiometry one might expect this threshold to exist between 10nM and 30nM – the threshold between excess Mcl-1, able to sequester all activated Bak, and insufficient Mcl-1, unable to sequester all activated Bak. The reason for this discrepancy is unknown.<sup>2</sup>

The indirect model, equally, fails to account for this release of cytochrome c with 10nM, but not 3nM, of tBIM. With tBid stimulation the indirect model also fails to predict a strong Bak:Mcl-1 complex for most input tBid concentrations, as is observed. The predictions take a similar form for both tBid and tBIM stimulation – in contrast with both experiment and the direct model predictions. In this sense, the indirect model exhibits considerably less control over the regulation of cytochrome c release. Perhaps this is because, assuming indirect activation only, the rate of activation depends only on the auto-activation rate and not on the activation potencies of the BH3-only proteins.

Both the direct and indirect models lack the ability to fully reproduce what is observed in this experiment, especially the discrete change in behaviour when the spike in concentration of tBid or tBIM is increased past a threshold. The direct model could be described as more responsive to different BH3-only stimulation compared to the indirect model, and is therefore more realistic. The direct activation pathway appears to be necessary to produce significantly different results for different BH3-only proteins and suggests that differing rates of direct activation are a key factor in whether cytochrome c release is observed or not.

An important shortcoming of the model is that, by treating Bak activation as irreversible in simulations, eventually all Bak is activated and, regardless of how little

---

<sup>2</sup>Dr. Ruth Kluck, WEHI. Personal communication

activator protein is added, after sufficient time cytochrome c release is predicted. This is in contrast with the experiments presented here in which minimal BH3-only stimulation resulted in no cytochrome c release. Making Bak activation reversible may remedy this deficiency of both models.

## 5.5 Conclusion

This chapter analysed various features of the model we have built of the Bcl-2 pathway. A hybrid model containing both endogenous Bcl-x<sub>L</sub> and direct activation was constructed to test the role played by both direct and auto-activation. Bistability was investigated using both the fitted kinetic parameters and a set of randomly chosen parameters. Bistability was found to not play a role in either the direct or indirect fitted models. The kinetic models, however, are capable of exhibiting bistability. Bistability is more commonly observed in the direct model compared to the indirect model. Sensitivity analysis was performed using the fitted kinetic parameters and globally by sampling the kinetic parameter space. From this an experimentally verifiable prediction was made. The outcome of a separate MLM experiment was predicted using the fitted direct and indirect models. While the model including direct activation made more consistent predictions to the data, both models failed to capture qualitatively its behaviour. The direct activation rate, determined by the form of BH3-only stimulation, was found to be a key factor in controlling cytochrome c release.

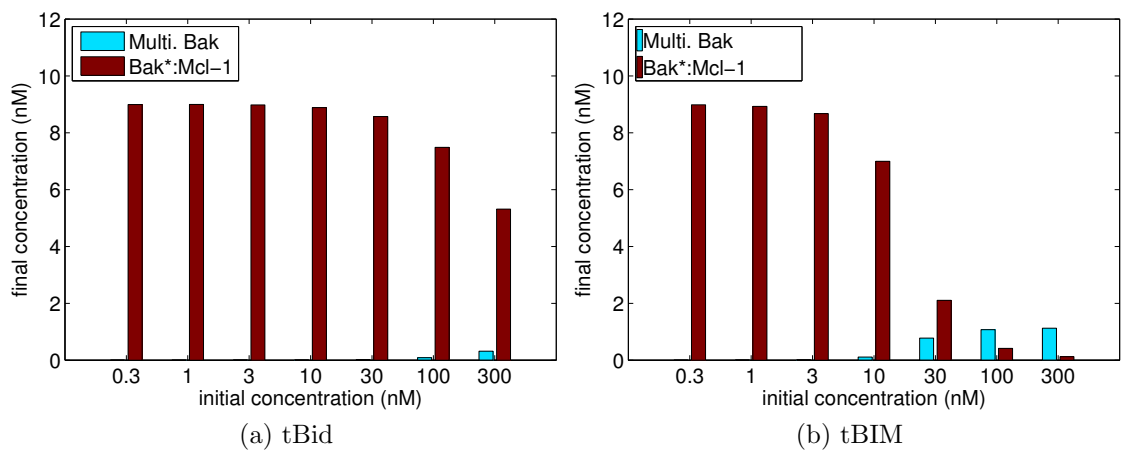


Figure 5.9: Direct model prediction of second MLM experiment. Each column represents a separate experiment in which 20nM Mcl-1 and the specified level of BH3-only stimulus is spiked-in to the system. Samples are taken following two hours incubation.

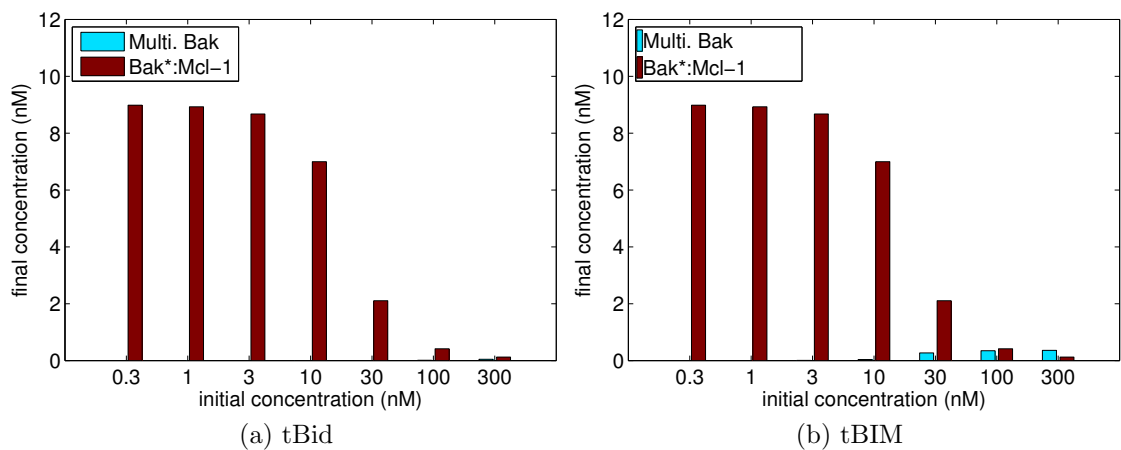


Figure 5.10: Indirect model prediction of second MLM experiment. Each column represents a separate experiment in which 20nM Mcl-1 and the specified level of BH3-only stimulus is spiked-in to the system. Samples are taken following two hours incubation.

# Chapter 6

## Conclusion

### 6.1 Principal findings

This thesis developed a mass-action kinetic model of a subset of the Bcl-2 family of proteins relevant to understanding a simplified experimental system. The principal aim of the experiments was to observe under what circumstances the Bak:Mcl-1 complex both formed and was disrupted. Sensitivity analysis revealed that under specific forms of BH3-only stimulation the Bak:Mcl-1 association rate was a decisive parameter in controlling the rate of cytochrome c release. This indicates that when the Bak:Mcl-1 complex is formed and disrupted indeed plays an important role in apoptosis regulation. The framework constructed in this thesis provides the means to investigate similar questions for other protein complexes and under different BH3-only stimulation, including candidate anti-cancer BH3-only mimetics.

The model was also constructed to address more general questions. Before any analysis was performed, however, significant care was taken to ensure that the model conformed with present knowledge of the Bcl-2 family and observed behaviour of the MLM model system. How binding data obtained from an SPR based Biacore machine could be utilised in our models was investigated. Binding data was used in a comparative sense only, ensuring that our models were consistent with the data but not significantly constrained by it. Mass transport considerations were considered briefly and modelling diffusion-limited interactions, at least in the way implemented, were decided to not be useful.

Once confident that the model reproduced key behaviour in a particular MLM timing experiment, aspects of apoptosis regulation could be investigated. Considerable scientific effort has been spent determining whether or not the direct activation of the pro-apoptotic protein Bak plays a role in the intrinsic death pathway. In calibrating our model to the MLM timing experiment the direct activation mechanism was found to be a necessary component of the model, indicating that direct activation indeed plays an important role in apoptosis regulation. Our modelling also suggests that the principal mechanism by which different forms of BH3-only stimulation elicit different responses from the cell is through the direct activation of Bak.

The role of bistability in the MLM experiments and in apoptosis more generally was addressed. Using kinetic parameters found by fitting to a MLM timing experiment bistability was not found to occur in an augmented system which included production and degradation rates. Confirming findings of previous bistability studies, however, other regions of the model's parameter space did indeed exhibit bistability. As in previous studies, bistability was more prevalent in the direct model compared with an indirect model. We suggest that bistability does not play a significant role in the modelled Bcl-2 family interactions.

## 6.2 Significance

This work represents the first effort to construct a strictly biologically constrained model of the intrinsic apoptosis pathway, constrained both in terms of the kinetic parameters used and in terms of the behaviours it exhibits. This provides a more realistic model which means we can have more faith in any conclusions drawn from it. Combining the 'direct' and 'indirect' activation models allows us to compare the relative importance each mechanism plays in the MLM system and hence in apoptosis more generally. Sensitivity analysis allowed us to identify important interactions in the model, which can lead to experimentally verifiable predictions.

Dynamical properties of the model such as bistability have been thoroughly investigated in previous studies. Contrary to these studies, based on our models, we do not suggest that bistability plays any significant role in the Bcl-2 mediated apoptosis pathway.

The necessarily simplified explanations biologists consider when studying a complex family of protein interactions may be inadequate to understand apoptosis regulation. The truth may lie outside what can be easily determined experimentally and a reliable computational model may be needed to fully comprehend the behaviour of the Bcl-2 family of proteins. This thesis has laid the foundation for future models which can realise this goal. Understanding the specific role protein complexes play in the Bcl-2 family will contribute to making targeted anti-cancer drug therapies more specific and effective.

### 6.3 Challenges

A number of challenges presented themselves in the course of this project. Obtaining experimental MLM data takes a considerable amount of time and effort. This involves preparing the stocks of Bcl-2 protein, performing the experiments and the subsequent densitometry analysis. This means that the amount of data available for our models was limited. Since no repeat experiments were performed with the same stock of BH3-only protein, no indication of the variability and hence no confidence intervals for our parameter estimates could be obtained. Different stocks of BH3-only proteins have different Bak activating efficiencies, and this makes extrapolating our parameter estimates and model conclusions difficult. Indeed, the difficulty encountered when trying to extrapolate our models to predict the outcome of a second MLM experiment reflect the need for a large amount of data to be available to have confidence in the accuracy of the models built.

Our modelling efforts commenced after the experimental design and protocols for working in the MLM system had been established. Initially, the design of the experiments and methods of quantification was not chosen with mathematical modelling in mind which made creating our model more difficult, necessitating, for instance, the arguments detailed in Section 4.1.1. These difficulties highlight the value in working with biologists from the beginning of a project to ensure the aims and expectations of the mathematical modelling are compatible with the aims and possibilities of the experimental work, to ensure that the experimental data will be useful to the modellers and that the results from the modelling are useful to the biologists.

These challenges are an inherent part of the developing, interdisciplinary field

of mathematical biology. However, establishing mathematics as a valuable tool in biological research and providing inspiration for novel mathematics makes these challenges worth overcoming.

## 6.4 Future work

A number of possible extensions to the current work present themselves. To simplify the analysis and programming difficulty a reduced dimension model was analysed in AUTO when investigating bistability. While the reduced model still provides useful results it would be interesting to compare the reduced to a full model.

Constructing a mathematical model of a biological system allows us perform experiments *in silico* which have not yet been, or are unable to be, performed *in vitro*. The MLM experiments here worked exclusively with tBid and tBIM. Through simulation is it a straightforward matter to investigate what happens in similar experiments with different forms of BH3-only stimulation and propose experiments which would provide the most biological insight. The model could be extended to include not just the MLM system but the intrinsic apoptosis pathway more generally, by including additional Bcl-2 proteins. This is an important application of any mathematical model which was not fully explored in this thesis.

Enhancements to the realism of the model could also be made. The induction of MOMP may require very few dimerised Bak molecules on the outer membrane in which case stochastic effects may play an important role in apoptosis regulation. Stochastic reaction dynamics or a cellular automaton model may be more appropriate in this case and it would be interesting to see the difference between our deterministic model and a stochastic equivalent.

Finally, since a lot, but not all, of the modelled interactions occur on the mitochondrial membrane, it would be useful to consider in more detail mass-transport effects. This could be achieved by implementing a multi-compartment model which separated the concentrations and kinetic rates into two compartments – membrane associated and cytosolic.

## 6.5 Concluding comments

The complexity of biological systems is in some sense incongruous with the abstractions and generalisations which mathematics builds on. General principles or laws in biology are hard to come by. Nonetheless, as advances in technology continue to allow more and more biological phenomena to be quantified, mathematical modelling will continue to play an ever increasing role in our understanding of living systems. This thesis represents one such attempt to extract, from a biological world of immense intricacy, a precise mathematical framework, in an area of significant and immediate scientific interest, programmed cell death.



# Bibliography

- [1] L. Gonick and M. Wheelis, *The cartoon guide to genetics*. New York: Harper-Perennial, 1991.
- [2] J. Kerr, A. Wyllie, and A. Currie, “Apoptosis: A Basic Biological Phenomenon with Wide-ranging Implications in Tissue Kinetics,” *Br J Cancer*, vol. 26, pp. 239–257, August 1972.
- [3] G. Werlen, B. Hausmann, D. Naeher, and E. Palmer, “Signaling Life and Death in the Thymus: Timing Is Everything,” *Science*, vol. 299, no. 5614, pp. 1859–1863, 2003.
- [4] D. Green, *Means to an End: Apoptosis and Other Cell Death Mechanisms*. New York: Cold Spring Harbor Laboratory Press, 2011.
- [5] K. Eguchi, “Apoptosis in Autoimmune Diseases,” *Internal Medicine*, vol. 40, April 2001.
- [6] D. R. Green and G. Evan, “A matter of life and death,” *Cancer Cell*, vol. 1, pp. 19–30, February 2002.
- [7] J. Lee, J. Abrahamson, and A. Bernstein, “DNA damage, oncogenesis and the p53 tumour-suppressor gene,” *Mutat Res.*, vol. 307, pp. 573–581, June 1994.
- [8] J. Teodoro and P. Branton, “Regulation of apoptosis by viral gene products,” *J. Virol.*, vol. 71, no. 3, pp. 1739–1746, 1997.
- [9] J. M. Adams and S. Cory, “The Bcl-2 apoptotic switch in cancer development and therapy,” *Oncogene*, vol. 26, pp. 1324–1337, February 2007.

- [10] Y. Tsujimoto, L. Finger, J. Yunis, P. Nowell, and C. Croce, "Cloning of the chromosome breakpoint of neoplastic B cells with the t(14;18) chromosome translocation," *Science*, vol. 226, no. 4678, pp. 1097–1099, 1984.
- [11] D. Vaux, S. Cory, and J. Adams, "Bcl-2 gene promotes haemopoietic cell survival and cooperates with c-myc to immortalize pre-B cells," *Nature*, vol. 335, no. 6189, pp. 440–442, 1988.
- [12] G. Dewson and R. M. Kluck, "Mechanisms by which Bak and Bax permeabilise mitochondria during apoptosis," *J Cell Sci*, vol. 122, no. 16, pp. 2801–2808, 2009.
- [13] T. Lindsten, A. J. Ross, A. King, W.-X. Zong, J. C. Rathmell, H. A. Shiels, E. Ulrich, K. G. Waymire, P. Mahar, K. Frauwirth, Y. Chen, M. Wei, V. M. Eng, D. M. Adelman, M. Simon, A. Ma, J. A. Golden, G. Evan, S. J. Korsmeyer, G. R. MacGregor, and C. B. Thompson, "The Combined Functions of Proapoptotic Bcl-2 Family Members Bak and Bax Are Essential for Normal Development of Multiple Tissues," *Molecular Cell*, vol. 6, no. 6, pp. 1389–1399, 2000.
- [14] G. Dewson, T. Kratina, H. W. Sim, H. Puthalakath, J. M. Adams, P. M. Colman, and R. M. Kluck, "To Trigger Apoptosis, Bak Exposes Its BH3 Domain and Homodimerizes via BH3:Groove Interactions," *Molecular Cell*, vol. 30, no. 3, pp. 369–380, 2008.
- [15] T. Oltersdorf, S. W. Elmore, A. R. Shoemaker, R. C. Armstrong, D. J. Augeri, B. A. Belli, M. Bruncko, T. L. Deckwerth, J. Dinges, P. J. Hajduk, M. K. Joseph, S. Kitada, S. J. Korsmeyer, A. R. Kunzer, A. Letai, C. Li, M. J. Mitten, D. G. Nettesheim, S. Ng, P. M. Nimmer, J. M. O'Connor, A. Oleksijew, A. M. Petros, J. C. Reed, W. Shen, S. K. Tahir, C. B. Thompson, K. J. Tomaselli, B. Wang, M. D. Wendt, H. Zhang, S. W. Fesik, and S. H. Rosenberg, "An inhibitor of bcl-2 family proteins induces regression of solid tumours," *Nature*, vol. 435, pp. 677–681, May 2005.

- [16] J. E. Chipuk and D. R. Green, “How do BCL-2 proteins induce mitochondrial outer membrane permeabilization?,” *Trends in Cell Biology*, vol. 18, no. 4, pp. 157–164, 2008.
- [17] D. Westphal, G. Dewson, P. E. Czabotar, and R. M. Kluck, “Molecular biology of Bax and Bak activation and action,” *Biochimica et Biophysica Acta*, vol. 1813, no. 4, pp. 521–531, 2011.
- [18] H. Dai, A. Smith, X. W. Meng, P. a. Schneider, Y.-P. Pang, and S. H. Kaufmann, “Transient binding of an activator BH3 domain to the Bak BH3-binding groove initiates Bak oligomerization.,” *The Journal of cell biology*, vol. 194, pp. 39–48, July 2011.
- [19] Y.-P. Pang, H. Dai, A. Smith, X. W. Meng, P. a. Schneider, and S. H. Kaufmann, “Bak Conformational Changes Induced by Ligand Binding: Insight into BH3 Domain Binding and Bak Homo-Oligomerization.,” *Scientific reports*, vol. 2, p. 257, Jan. 2012.
- [20] F. Llambi, T. Moldoveanu, S. W. G. Tait, L. Bouchier-Hayes, J. Temirov, L. L. McCormick, C. P. Dillon, and D. R. Green, “A unified model of mammalian BCL-2 protein family interactions at the mitochondria.,” *Molecular cell*, vol. 44, pp. 517–31, Nov. 2011.
- [21] L. J. Pagliari, T. Kuwana, C. Bonzon, D. D. Newmeyer, S. Tu, H. M. Beere, and D. R. Green, “The multidomain proapoptotic molecules Bax and Bak are directly activated by heat,” *Proceedings of the National Academy of Sciences of the United States of America*, vol. 102, no. 50, pp. 17975–17980, 2005.
- [22] C. Tan, P. J. Dlugosz, J. Peng, Z. Zhang, S. M. Lapolla, S. M. Plafker, D. W. Andrews, and J. Lin, “Auto-activation of the Apoptosis Protein Bax Increases Mitochondrial Membrane Permeability and Is Inhibited by Bcl-2,” *Journal of Biological Chemistry*, vol. 281, no. 21, pp. 14764–14775, 2006.
- [23] R. T. Uren, G. Dewson, L. Chen, S. C. Coyne, D. C. Huang, J. M. Adams, and R. M. Kluck, “Mitochondrial permeabilization relies on BH3 ligands engaging multiple prosurvival Bcl-2 relatives, not Bak,” *The Journal of Cell Biology*, vol. 177, no. 2, pp. 277–287, 2007.

- [24] J. L. Richens, R. A. Urbanowicz, E. A. M. Lunt, R. Metcalf, J. Corne, L. Fairclough, and P. O’Shea, “Systems biology coupled with label-free high-throughput detection as a novel approach for diagnosis of chronic obstructive pulmonary disease,” *Respir Res*, vol. 10, p. 29, Jan 2009.
- [25] D. G. Myszka, “Improving biosensor analysis,” *J Mol Recognit*, vol. 12, pp. 279–84, Jan 1999.
- [26] C. C. Lin and L. A. Segel, *Mathematics Applied to Deterministic Problems in the Natural Sciences*. SIAM, 1 ed., 1988.
- [27] J. Murray, *Mathematical biology: I. An introduction*. Springer, 2005.
- [28] T. Wilhelm, “The smallest chemical reaction system with bistability,” *BMC Systems Biology*, vol. 3, no. 1, p. 90, 2009.
- [29] S. H. Strogatz, *Nonlinear Dynamics And Chaos: With Applications To Physics, Biology, Chemistry, And Engineering (Studies in nonlinearity)*. Studies in nonlinearity, Perseus Books Group, 1 ed., January 1994.
- [30] R. Heinrich, *The Regulation of Cellular Systems*. New York: Chapman and Hall, 1996.
- [31] G. de Vries, T. Hillen, M. Lewis, J. Muller, and B. Schonfisch, *A Course in Mathematical Biology: Quantitative Modeling with Mathematical and Computational Methods*. SIAM, 2006.
- [32] C. Guldberg and P. Waage, “Concerning Chemical Affinity,” *Erdmann’s Journal für Practische Chemie*, vol. 127, pp. 69–114, 1879.
- [33] F. Horn and R. Jackson, “General Mass Action Kinetics,” *Arch. Rational Mech. Anal.*, vol. 47, no. 2, pp. 81–116, 1972.
- [34] G. Schreiber, “Kinetic studies of protein-protein interactions,” *Current Opinion in Structural Biology*, vol. 12, no. 1, pp. 41 – 47, 2002.
- [35] G. Schreiber, G. Haran, and H. X. Zhou, “Fundamental aspects of protein-protein association kinetics,” *Chemical Reviews*, vol. 109, pp. 839–860, March 2009.

- [36] M. Gavutis, E. Jaks, P. Lamken, and J. Piehler, “Determination of the Two-Dimensional Interaction Rate Constants of a Cytokine Receptor Complex,” *Biophysical Journal*, vol. 90, no. 9, pp. 3345–3355, 2006.
- [37] B. Goldstein, D. Coombs, X. He, A. R. Pineda, and C. Wofsy, “The influence of transport on the kinetics of binding to surface receptors: application to cells and BIAcore,” *J. Mol. Recognit.*, vol. 12, pp. 293–299, 1999.
- [38] H. Duessmann, M. Rehm, C. G. Concannon, S. Anguissola, M. Wuerstle, S. Kacmar, P. Vller, H. J. Huber, and J. H. M. Prehn, “Single-cell quantification of Bax activation and mathematical modelling suggest pore formation on minimal mitochondrial Bax accumulation,” *Cell Death Differ*, vol. 17, pp. 278–290, 2010.
- [39] D. J. Wilkinson, *Stochastic Modelling for Systems Biology (Chapman & Hall/CRC Mathematical & Computational Biology)*. Chapman & Hall, 1 ed., April 2006.
- [40] D. T. Gillespie, “Stochastic simulation of chemical kinetics,” *Annual Review of Physical Chemistry*, vol. 58, no. 1, pp. 35–55, 2007.
- [41] B. P. Ingalls and H. M. Sauro, “Sensitivity analysis of stoichiometric networks: an extension of metabolic control analysis to non-equilibrium trajectories,” *Journal of Theoretical Biology*, vol. 222, pp. 23–36, 2003.
- [42] M. Bentele, I. Lavrik, M. Ulrich, S. Ster, D. Heermann, H. Kalthoff, P. Kramer, and R. Eils, “Mathematical modeling reveals threshold mechanism in CD95-induced apoptosis,” *The Journal of Cell Biology*, vol. 166, no. 6, pp. 839–851, 2004.
- [43] R. Krüger and R. Heinrich, “Model reduction and analysis of robustness for the wnt/beta-catenin signal transduction pathway,” *Genome Inform*, vol. 15, no. 1, pp. 138–148, 2004.
- [44] R. LeVeque, *Finite difference methods for ordinary and partial differential equations*. Siam, 2007.

- [45] E. J. Doedel, A. R. Champneys, T. F. Fairgrieve, Y. A. Kuznetsov, B. Sandstede, and X. Wang, “AUTO 2007p: Continuation And Bifurcation Software For Ordinary Differential Equations (with HomCont),” 2007.
- [46] W. Govaerts, “Numerical bifurcation analysis for ODEs,” *Journal of Computational and Applied Mathematics*, vol. 125, pp. 57–68, Dec. 2000.
- [47] C. Chen, J. Cui, H. Lu, R. Wang, S. Zhang, and P. Shen, “Modeling of the Role of a Bax-Activation Switch in the Mitochondrial Apoptosis Decision,” *Biophysical Journal*, vol. 92, no. 12, pp. 4304–4315, 2007.
- [48] E. Bagci, Y. Vodovotz, T. Billiar, G. Ermentrout, and I. Bahar, “Bistability in Apoptosis: Roles of Bax, Bcl-2, and Mitochondrial Permeability Transition Pores,” *Biophysical Journal*, vol. 90, no. 5, pp. 1546–1559, 2006.
- [49] J. Cui, C. Chen, H. Lu, T. Sun, and P. Shen, “Two independent positive feedbacks and bistability in the bcl-2 apoptotic switch,” *PLoS ONE*, vol. 3, p. e1469, 01 2008.
- [50] K. L. Ho and H. a. Harrington, “Bistability in apoptosis by receptor clustering.,” *PLoS computational biology*, vol. 6, p. e1000956, Jan. 2010.
- [51] S. M. Sen, E. Z. Bagci, and M. C. Camurdan, “Bistability analysis of an apoptosis model in the presence of nitric oxide.,” *Bulletin of mathematical biology*, vol. 73, pp. 1952–68, Aug. 2011.
- [52] G. Craciun and M. Feinberg, “Multiple equilibria in complex chemical reaction networks: Ii. the species-reaction graph,” *SIAM Journal of Applied Mathematics*, vol. 66, no. 4, pp. 1321–1338, 2006.
- [53] G. Craciun and M. Feinberg, “Multiple equilibria in complex chemical reaction networks: I. the injectivity property,” *SIAM Journal on Applied Mathematics*, vol. 65, pp. 1526–1546, 2005.
- [54] C. Chen, J. Cui, W. Zhang, and P. Shen, “Robustness analysis identifies the plausible model of the bcl-2 apoptotic switch,” *FEBS Letters*, vol. 581, no. 26, pp. 5143 – 5150, 2007.

- [55] T. Eissing, F. Allgoewer, and E. Bullinger, “Robustness properties of apoptosis models with respect to parameter variations and intrinsic noise.,” *Syst Biol (Stevenage)*, vol. 152, no. 4, pp. 221–8, 2005.
- [56] A. Eldar, R. Dorfman, D. Weiss, H. Ashe, B.-Z. Shilo, and N. Barkai, “Robustness of the bmp morphogen gradient in drosophila embryonic patterning,” *Nature*, vol. 419, pp. 304–308, Sep 2002. 10.1038/nature01061.
- [57] J. Stelling, U. Sauer, Z. Szallasi, F. J. D. III, and J. Doyle, “Robustness of cellular functions,” *Cell*, vol. 118, no. 6, pp. 675 – 685, 2004.
- [58] J. G. Albeck, J. M. Burke, S. L. Spencer, D. A. Lauffenburger, and P. K. Sorger, “Modeling a snap-action, variable-delay switch controlling extrinsic cell death,” *PLoS Biol*, vol. 6, p. e299, 12 2008.
- [59] H. Huber, M. Laussmann, J. Prehn, and M. Rehm, “Diffusion is capable of translating anisotropic apoptosis initiation into a homogeneous execution of cell death,” *BMC Systems Biology*, vol. 4, no. 1, p. 9, 2010.
- [60] H. J. Huber, H. Duesmann, J. Wenus, S. M. Kilbride, and J. H. Prehn, “Mathematical modelling of the mitochondrial apoptosis pathway,” *Biochimica et Biophysica Acta (BBA) - Molecular Cell Research*, vol. 1813, no. 4, pp. 608 – 615, 2011. Mitochondria: The Deadly Organelle.
- [61] S. L. Spencer and P. K. Sorger, “Measuring and Modeling Apoptosis in Single Cells,” *Cell*, vol. 144, pp. 926–939, Mar. 2011.
- [62] L. Michaelis and M. L. Menten, “Die kinetik der invertinwirkung,” *Biochem. Z*, vol. 49, no. 333-369, p. 352, 1913.
- [63] A. Asthagiri and D. Lauffenburger, “A Computational Study of Feedback Effects on Signal Dynamics in a Mitogen-Activated Protein Kinase (MAPK) Pathway Model,” *Biotechnology Progress*, vol. 17, no. 2, pp. 227–239, 2001.
- [64] T. Kuwana, M. R. Mackey, G. Perkins, M. H. Ellisman, M. Latterich, R. Schneiter, D. R. Green, and D. D. Newmeyer, “Bid, bax, and lipids cooperate to form supramolecular openings in the outer mitochondrial membrane,” *Cell*, vol. 111, no. 3, pp. 331 – 342, 2002.

- [65] M. Saito, S. J. Korsmeyer, and P. H. Schlesinger, “BAX-dependent transport of cytochrome c reconstituted in pure liposomes,” *Nature Cell Biology*, vol. 2, pp. 553–555, 2000.
- [66] D. A. Lauffenburger and J. J. Linderman, *Receptors: Models for Binding, Trafficking, and Signaling*. New York: Oxford University Press, January 1996.
- [67] O. Dushek, R. Das, and D. Coombs, “A Role for Rebinding in Rapid and Reliable R Cell Responses to Antigen,” *PLoS Comput Biol*, vol. 5, no. 11, 2009.
- [68] Z. Li, M. R. Osborne, and T. Prvan, “Parameter estimation of ordinary differential equations,” *IMA J Numer Anal*, vol. 25, no. 2, pp. 264–285, 2005.
- [69] Y. Bard, *Nonlinear parameter estimation*. Academic Press, New York, 1974.
- [70] J. J. More and D. C. Sorensen, “Computing a trust region step,” *SIAM Journal on Scientific and Statistical Computing*, vol. 4, no. 3, pp. 553–572, 1983.
- [71] J. Moré, “The levenberg-marquardt algorithm: Implementation and theory,” in *Numerical Analysis* (G. A. Watson, ed.), vol. 630 of *Lecture Notes in Mathematics*, ch. 10, pp. 105–116, Springer Berlin Heidelberg, 1978.
- [72] K. Levenberg, “A Method for the Solution of Certain Problems in Least-Squares,” *Quarterly Applied Math*, vol. 2, pp. 164–168, 1944.
- [73] S. B. Childs and M. R. Osborne, “Fitting solutions of ordinary differential equations to observed data,” tech. rep., College Station, TX, USA, 1995.
- [74] U. Nowak and P. Deuffhard, “Numerical identification of selected rate constants in large chemical reaction systems,” *Applied Numerical Mathematics*, vol. 1, no. 1, pp. 59 – 75, 1985.
- [75] T. Coleman and Y. Li, “An Interior, Trust Region Approach for Nonlinear Minimization Subject to Bounds,” *SIAM Journal on Optimization*, vol. 6, pp. 418–445, 1996.
- [76] L. Shampine and M. Reichelt, “The MATLAB ODE Suite,” *SIAM Journal on Scientific Computing*, vol. 18, pp. 1–22, 1997.

- [77] D. A. Beard and H. Qian, *Chemical Biophysics: Quantitative Analysis of Cellular Systems (Cambridge Texts in Biomedical Engineering)*. Cambridge University Press, 1 ed., July 2008.
- [78] H. Qian and D. A. Beard, “Thermodynamics of stoichiometric biochemical networks in living systems far from equilibrium,” *Biophysical Chemistry*, vol. 114, no. 2-3, pp. 213 – 220, 2005.